UNIVERSITÀ DEGLI STUDI DI MILANO

DIPARTIMENTO DI SCIENZE BIOMEDICHE PER LA SALUTE

CORSO DI DOTTORATO IN RICERCA BIOMEDICA INTEGRATA

XXXIII CICLO

CT- AND MRI-DERIVED BIOMARKERS FOR CARDIOVASCULAR DISEASE

Tutor:

Chiarissimo Prof. Francesco SARDANELLI

Co-tutor:

Prof. Francesco SECCHI

Tesi di dottorato di:

Caterina Beatrice MONTI

R11879

Anno Accademico 2019/2020

TABLE OF CONTENTS

ABSTRACT

Cardiac computed tomography (CT) and magnetic resonance imaging (CMR) have shown potential in providing new insights concerning different cardiovascular pathologies. More recently, the focus of such studies has shifted from a simple qualitative evaluation of imaging, to a more objective approach, which includes the assessment of quantitative biomarkers. In particular, late gadolinium enhancement (LGE), myocardial strain and extracellular volume fraction (ECV) could be used to aim for a more tailored approach to the study of different diseases. The main applications for LGE discussed in this study include the definition of a more appropriate gadolinium-based contrast dosage for the assessment of myocardial infarction at CMR, and the appraisal of LGE patterns and roles in patients with Tetralogy of Fallot (ToF), the most common cyanogen congenital heart defect. The analysis of myocardial strain focused on the detection of subclinical contractility anomalies in patients with ToF, and with myocarditis, aiming for a quantitative approach which could help highlight early cardiac disease before myocardial function is irreversibly altered. The study of ECV, conversely, focused on the early detection of subclinical cardiotoxicity stemming from anthracycline treatment for breast cancer. Overall, the use of such quantitative biomarkers in imaging studies could help pave the way for a more tailored patient treatment, and towards personalized medicine.

INTRODUCTION

Cardiac magnetic resonance (CMR) and computed tomography (CT) are the two main second-level imaging modalities that find a great number of applications in the study of the heart: from screening low-risk patients for coronary artery disease, to a thorough non-invasive tissue characterization in patients with overt cardiac pathology [1].

While both CMR and CT allow a volumetric imaging visualization, each technique yields its own advantages and drawbacks. In particular, while CMR does not imply the use of ionizing radiations, allows an accurate evaluation of cardiac volumes and function along with a more in-depth tissue characterization [2], it is contraindicated in those with certain implantable devices [3]. Moreover, during recent years the use of gadolinium-based contrast agents (GBCAs), which is necessary for some vital CMR applications, has been linked to potential adverse effects such as nephrogenic systemic fibrosis [4] and the presence of brain gadolinium depositions of unknown clinical significance [5]. On the other hand, while CT does employ ionizing radiations, the radiation dose involved in examinations has been decreasing steadily throughout the latest years [6]. Moreover, CT examinations require less time than CMR, meaning that sedation is not mandatory in younger children, and CT yields a higher spatial resolution which allows the assessment of smaller structures such as the coronary arteries [7]. Therefore, at present CMR is mostly utilized in the assessment of structural cardiomyopathies and myocardial volumes and function, while CT is a mainstay in the evaluation of coronary artery disease.

Therefore, the aim of this thesis is to review potential technical features and applications of different biomarkers deriving from CMR or CT according to a historical pattern, starting from the less recent and more well-established late gadolinium enhancement (LGE), then assessing myocardial strain, ending with the most novel, namely extracellular volume (ECV) fraction analysis at both CMR and CT.

LATE GADOLINIUM ENHANCEMENT

The assessment of myocardial LGE is a well-established CMR application which can help detect localized fibrosis [8]. The concept of LGE is based on the fact that extracellular contrast agents, such as those most used for CMR, tend to remain longer in tissues which present an expansion of the extracellular compartment, which is typical of fibrosis or inflammation [9].

The main CMR sequences used for the evaluation of LGE are bright-blood, inversion recovery (IR) or phase-sensitive inversion-recovery (PSIR) acquisitions [10]. Images are then acquired after 10 to 30 minutes after the injection of a GBCA, so that the GBCA is expected to have washed-out from healthy tissues, and to only be present in pathological areas [11]. Such sequences allow the nulling of signal coming from the myocardium which appears black, whereas the areas presenting LGE and the blood pool are represented in white/light-grey, as in **Figure 1**. GBCA doses used for LGE acquisitions varied widely, with a general consensus aiming at concentrations between 0.10 and 0.20 mmol/kg of GBCA.

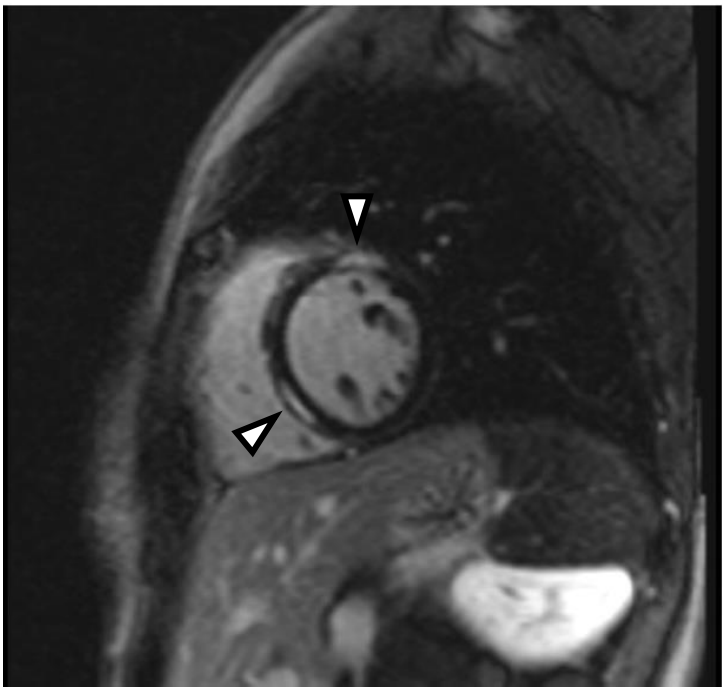

Figure 1 *Inversion recovery sequence for the visualization of late gadolinium enhancement (white arrowheads)*

The assessment of LGE can be qualitative, or it can be performed quantitatively, the former method being most common in current clinical applications as it may prove less time-consuming and cumbersome to physicians [12]. For instance, the Lake Louise Criteria for diagnosing myocarditis at CMR include a visual appraisal of LGE as a potential marker of fibrosis or inflammation of the myocardium [13]. A quantitative approach to LGE assessment is mostly used for research purposes, as it requires the segmentation of both endocardium and epicardium over a variable number of images (usually around 15). Nevertheless, the quantification of LGE as both absolute value and percentage over the myocardial mass has shown a strong correlation to fibrosis or other microscopical tissue changes observed at histology, thus validating the technique [14]. Moreover, a meta-analysis from 2016 observed that quantitative LGE exhibited a substantial prognostic value for adverse events in patients with hypertrophic cardiomyopathy [15]. Another international, multi-institutional work observed that LGE could help identify high-risk patients among those with dilated cardiomyopathy [16]. In fact, LGE may indicate the presence of scar tissue, which can facilitate the onset of arrhythmias, that yield an increased risk of adverse events, especially in patients who already present with cardiac pathologies [17].

Thus, LGE may be regarded as a CMR biomarker indicating potential unfavorable prognosis, and its assessment both qualitative and quantitative, may help a timely identification of patients at higher risk, providing the opportunity to have a window for the prevention of adverse events.

The aim of this section of the thesis is to review both technical and clinical applications of LGE imaging, with particular focus on the ideal concentration of GBCA to perform imaging in patients with chronic myocardial infarction, and on a review of the potential of LGE in patients with Tetralogy of Fallot (ToF).

Image quality of late gadolinium enhancement in cardiac magnetic resonance with different doses of contrast material in patients with chronic myocardial infarction

(from Monti CB, Codari M, Cozzi A, Alì M, Saggiante L, Sardanelli F, Secchi F - *European Radiology Experimental* 2020)

Background

Coronary heart disease is one of the main causes of morbidity and mortality, especially in developed countries, where it causes around 20% of all deaths [18]. The most common presentation of coronary heart disease is myocardial infarction, which is defined as the occurrence of necrosis in the setting of myocardial ischemia [19].

Contrast-enhanced CMR is a multi-parametric, multi-planar imaging technique, which represents the current non-invasive standard of care for assessing cardiac volumes, function and tissue characterization through LGE [20,21]. The importance of LGE may be found, among other reasons, in its prognostic potential [22]. Given its capability to monitor cardiac conditions, contrast-enhanced CMR may be useful in the evaluation of patients with chronic myocardial infarction, especially when the latter is transmural and of greater clinical relevance [23,24]. Moreover, automatic scar quantification is growing in popularity due to the increase in numbers of examinations and the development of increasingly more reliable methods [25]. Scar recognition is most often based on image characteristics of the scarred area, such as signal- (SNR) and contrast-to-noise ratio (CNR) [26].

However, especially in the latest years, concerns about the safety of GBCAs have arisen. In addition to the well-known issue of nephrogenic systemic fibrosis [27], gadolinium deposits of yet unknown clinical relevance have been shown in the brain of patients, adults and children, who underwent repeated GBCA-enhanced magnetic resonance examinations [28,29]. This led to a

growing attention concerning the possibility to reduce GBCA doses such examinations, provided that scar quality is not hindered.

Patients with chronic myocardial infarction hence represent a population where GBCA dose reduction would lead to a lower chance of contrast-related adverse events. At present, GBCA doses used in these patients are variable among countries and centres, usually between 0.1 (single dose) and 0.2 (double dose) mmol/kg [30]. While in some countries, such as Japan, the single dose is recommended, in most cases there are no specific indications [31]. All doses seem to provide diagnostic quality to examinations, albeit a reduction in scar visualization corresponding to a lower contrast dosage might, for instance, hinder post-processing applications.

The purpose of our study was to analyse image quality of the scar tissue in CMR examinations performed with different GBCA doses in patients with chronic transmural myocardial infarction, to investigate the impact of gadolinium dose variation on the visibility of myocardial LGE quantified as SNR and CNR.

Methods

Ethical statement and study design

The local Ethics Committee approved this study (Ethics Committee of IRCCS Ospedale San Raffaele; protocol code "Cardioretro Ricerca Spontanea"; approved on September 14th, 2017 and amended on July 18th, 2019). This study was supported by local research funds of IRCCS Policlinico San Donato, a clinical research hospital partially funded by the Italian Ministry of Health. This research received no specific grant from funding agencies in the public, commercial, or non-profit sector. Due to the retrospective nature of this study, specific informed consent was waived.

Study population

All patients who had undergone a contrast-enhanced CMR examination with administration of gadobutrol (Gadovist, Bayer Healthcare, Leverkusen, Germany), at our institution between March 2014 (the introduction of our newer magnetic resonance unit) and May 2018, and who were

diagnosed with chronic myocardial infraction from clinical findings and CMR, were included in our study. Exclusion criteria were the presence of oedema, indicating acute phase of infarction, presence of relevant artifacts which rendered differentiation of the myocardial scar difficult, and non-transmural, thin infarcts which were either only subendocardial (≤50% of wall thickness) or too small (scar ≤10% of the myocardium), as such conditions do not allow the calculation of SNR and CNR of the scarred region [32]. Moreover, in patients with subendocardial infarction, image contrast may vary according to acquisition timing, and thus this may provide data that are not compatible with those of transmural scars [33].

Patients were then divided into three subgroups, depending on the contrast dose they were administered during their CMR: the first group (A) received 0.10 mmol/kg, the second (B) 0.15 mmol/kg, and the third (C) 0.20 mmol/kg. These different doses were mainly due to choices of the physicians in charge for the examination during the study period, not related to specific patient's condition.

Image acquisition

All subjects were imaged using one 1.5 T whole-body magnetic resonance unit (Magnetom Aera, Siemens Healthineers, Erlangen, Germany) with 45 mT/m gradient power and an 18-channel surface phased-array coil. The examined patient was laying supine and the coil was placed over the thorax. All images were acquired with breath-holding and ECG gating.

The imaging protocol of all patients included cine and LGE sequences.

Cine images were acquired in multiple short- and long-axis planes using an ECG-triggered bright-blood steady-state free-precession pulse sequence.

LGE images were acquired after intravenous administration of 0.10, 0.15, or 0.20 mmol/kg of gadobutrol (Gadovist, Bayer Healthcare, Leverkusen, Germany), and were performed using a 2D segmented inversion-recovery fast gradient-echo sequence covering the entire left ventricle. Earlier exams utilized higher contrast doses, which were then lowered over time. Nevertheless, the sequence

for LGE imaging remained the same. The time of echo was 3.33 milliseconds, while the time of repetition was adapted to patients' heart rates, and inversion time was progressively modified from 260 to 330 milliseconds, to blacken cardiac muscle; flip angle was 25°, slice thickness 8 mm, and pixel size 3.6 mm^2. LGE images were reconstructed using magnitude reconstruction. From the R wave of the electrocardiogram, a delay period was used to ensure that image acquisition occurred in mid-diastole, when the heart is relatively motionless, therefore reducing motion artifacts. Data were acquired every other heartbeat, although in tachycardic patients, data were acquired every third heartbeat, while in bradycardic patients and in patients with difficulties in breath holding acquisition was performed every heartbeat. Timing between contrast administration and acquisition of delayed enhancement scans was tailored to the contrast dose that was utilized in each case, according to literature recommendations [31].

Image analysis

Image analysis was performed using QMass 7.6 (Medis Medical Imaging Systems, Leiden, The Netherlands). The epicardial contour of the left ventricle was manually traced for all short-axis slices at end-diastolic and end-systolic phase in cine sequences. Afterwards, a blood-thresholding technique (Mass-K mode) was applied to automatically segment myocardium and blood pool. The software then calculated end-diastolic and end-systolic volumes, both indexed and non-indexed to body surface area, myocardial mass, stroke volume and ejection fraction.

For LGE quantification, manual segmentation of endocardium and epicardium of the left ventricle was performed in inversion recovery sequences after contrast agent injection. Then the software automatically detected the myocardial scar as being 6-standard deviations above average myocardial intensity [34]. Manual corrections were made when the software erroneously detected additional scarred areas, or when it failed to properly detect the scar. LGE was quantified as percentage over the whole myocardium. Two regions of interest were automatically placed in the scarred and healthy myocardium. An example of LGE segmentation is shown in **Figure 2**.

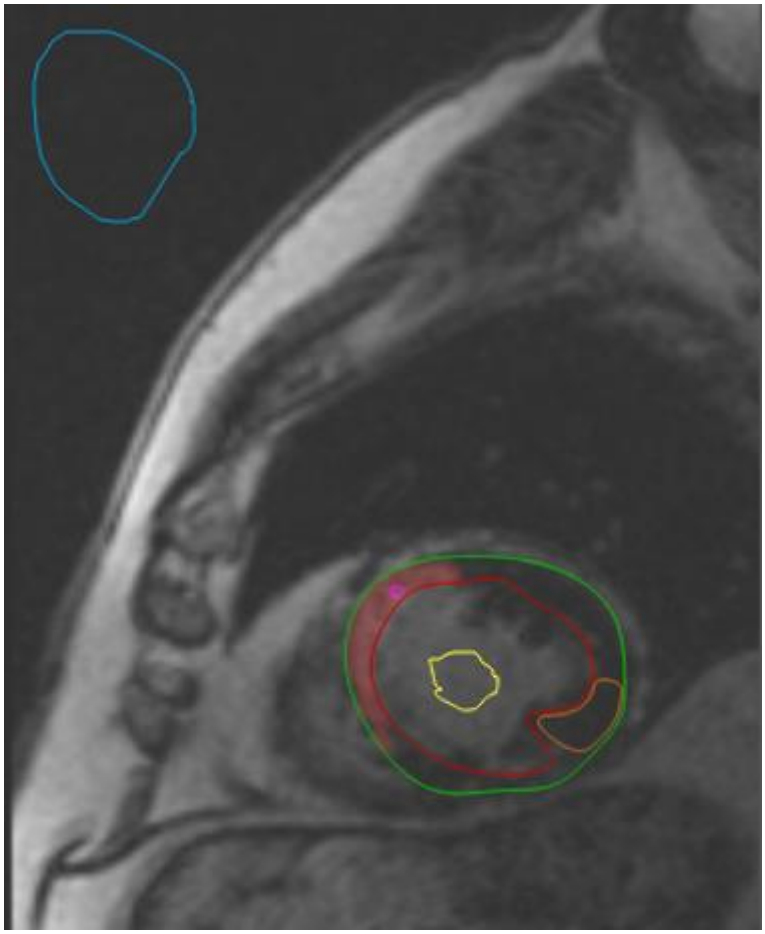

Figure 2 *Figure showing segmentation of the scarred myocardium in a 49-year-old male patient. Scarred myocardium is shown in red and is automatically segmented at 6 standard deviations above average signal intensity. Regions of interest placement is also depicted: those in the scarred (pink) and healthy (orange) myocardium are automatically placed during scar segmentation, while the ones in the blood pool (yellow) and air (blue) are manually placed on the same image.*

SNR and CNR were calculated using data provided by automatic LGE quantification, namely intensities from the two ROIs automatically placed in the scarred and healthy myocardium, and two additional ROIs traced in the left ventricular blood pool and in the background air. SNR was calculated as $SNR = 0.655 \cdot \frac{signal\ intensity}{SD_{background}}$ according to a study by Kaufman et al. [35], while CNR was calculated as $CNR_{1/2} = \frac{|signal\ intensity_1 - signal\ intensity_2|}{SD_{background}}$. SNR was calculated on the scar tissue (SNR_{scar}), while CNR was calculated between scar tissue and remote myocardium ($CNR_{scar-rem}$), and

between scar tissue and blood ($CNR_{scar-blood}$). Timings between contrast injection and acquisition of LGE sequences were also reported.

Subjective image quality was also analysed, using a 4-point Likert scale, defining score as follows: 0: non diagnostic; 1: diagnostic exam, sufficient quality; 2: diagnostic exam, good quality; 3: diagnostic exam, excellent quality. The quality definition was based on the visual contrast differences between blood pool signal and LGE.

Statistical analysis

Data were reported as median and interquartile range (IQR). Differences between groups were appraised with Kruskal-Wallis test for numerical variables, and post-hoc tests when a significant difference was appraised by Kruskal-Wallis test, or Fisher χ^2 tests for non-numerical variables.

Statistical analysis was performed with MATLAB R2018b (Mathworks, Natick, MA, US), and p values ≤ 0.05 were considered statistically significant.

Results

Study population

Out of 124 patients who had undergone contrast enhanced CMR at our institution, with gadobutrol as GBCA, 79 were included. The flowchart of exclusion is shown in **Figure 3**. Out of the 79 included patients, 22 belonged to the group being administered 0.10 mmol/kg of gadobutrol (group A), 26 to the group being administered 0.15 mmol/kg of gadobutrol (group B), and 31 to the last group, which was administered 0.20 mmol/kg of gadobutrol (group C). There were no significant differences in either age or sex among the three groups ($p \geq 0.300$). Groups demographics are summarized in **Table 1**.

The median acquisition time of LGE sequences was 9 min (IQR 8–13 minutes) for group A, 14 min (IQR 9–17 minutes) for group B, and 17 min (IQR 14–20 minutes) for group C. Acquisition time showed a significant difference ($p < 0.001$) among groups; in particular, it did not differ between

group A and group B ($p = 0.105$), but was shorter in group B than group C ($p < 0.018$), and shorter in group A than in group C ($p < 0.001$).

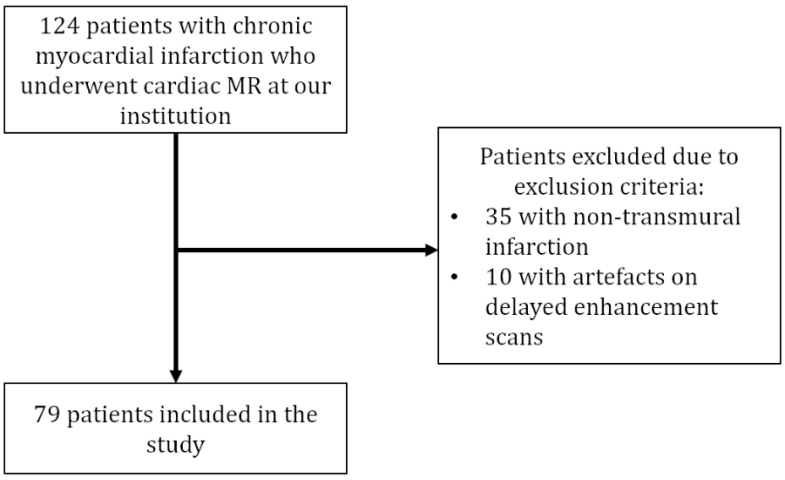

Figure 3 *Study flowchart. Out of 124 initially retrieved patients, 35 were excluded due to their infarction not being transmural and 10 due to artifacts on late gadolinium enhancement scans regardless of the size of their infarction.*

	Group A	**Group B**	**Group C**	***p***
Number	22	26	31	–
Age (years)	68 (58–71)	62 (51–72)	60 (51–68)	0.300
Males (%)	95	92	90	0.811
LV EDVi (ml/m2)	94 (75–118)	93 (73–107)	100 (80–126)	0.319
LV ESVi (ml/m2)	58 (31–77)	56 (46–74)	63 (46–87)	0.472
LV SV (ml)	66 (46–78)	69 (60–86)	70 (62–83)	0.410
LV EF (%)	38 (28–46)	38 (31–47)	37 (30–45)	0.800
LV Mi (g/m2)	89 (81–116)	91 (77–114)	92 (77–102)	0.961
LGE (%)	32.5 (21.7–38.1)	30.9 (23.0–42.4)	31.1 (25.5–44.0)	0.594

Table 1 *Demographics, left ventricular function and volume and scar data from the three study subgroups. EDVi End-diastolic volume indexed to body surface area, EF Ejection fraction, ESVi End-systolic volume indexed to body surface area, LGE Percentage of scar represented as late gadolinium enhancement over the myocardial mass, Mi Myocardial mass index, SV Stroke volume. Kruskal-Wallis test was used.*

Cardiac morphology and function

Left ventricular volumetric and functional data are reported in Table 1, along with myocardial scar burden quantified as percentage of scar tissue volume over the whole left ventricular volume. There were no significant differences in volumetric, functional or scar data.

Image quality

Images of LGE in patients belonging to the three different groups are shown in **Figure 4**.

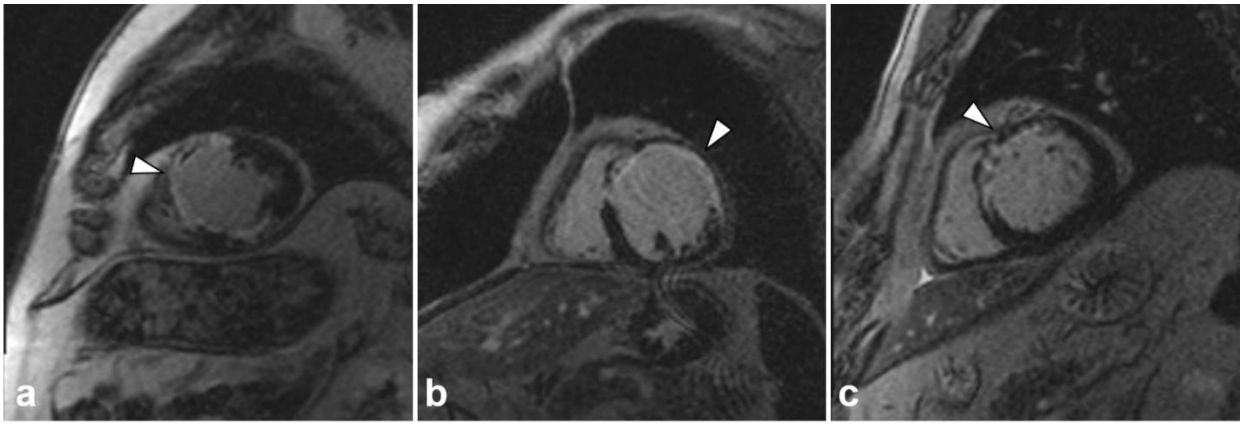

Figure 4 *Inversion recovery sequences for late gadolinium enhancement performed using 0.10 (A), 0.15 (B), or 0.20 (C) mmol/kg of gadobutrol, in male patients of 76, 54 and 49 years of age, respectively, matched for percentage infarct size.*

SNR_{scar} was 46.4 (IQR 40.3–65.1) in group A, 70.1 (IQR 52.2–111.5) in group B, and 72.1 (IQR 59.4–100.0) in group C. There was a significant difference in SNR_{scar} among groups ($p = 0.002$), in particular SNR_{scar} in group A was lower than both that of group B ($p = 0.013$) and group C ($p = 0.002$), while there was no significant difference in SNR_{scar} between group B and group C ($p = 0.884$).

$CNR_{scar-rem}$ was 62.9 (IQR 52.2–87.4) in group A, 96.5 (IQR 73.1–152.8) in group B, and 103.9 (IQR 83.9–132.0) in group C. There was a significant difference in $CNR_{scar-rem}$ among groups ($p < 0.001$), in particular $CNR_{scar-rem}$ in group A was significantly lower than both that of group B ($p = 0.008$) and group C ($p = 0.001$), while there was no significant difference in $CNR_{scar-rem}$ between group B and group C ($p = 0.871$).

$CNR_{scar-blood}$ was 25.5 (IQR 14.4–35.0) in group A, 32.7 (IQR 17.9–60.8) in group B, and 29.6 (IQR 18.2–53.5) in group C. There were no significant differences in $CNR_{scar-blood}$ among groups ($p \geq 0.335$).

Box plots of SNR_{scar}, $CNR_{scar-rem}$ and $CNR_{scar-blood}$ across the three groups are depicted in **Figure 5**, data are reported in **Table 2**.

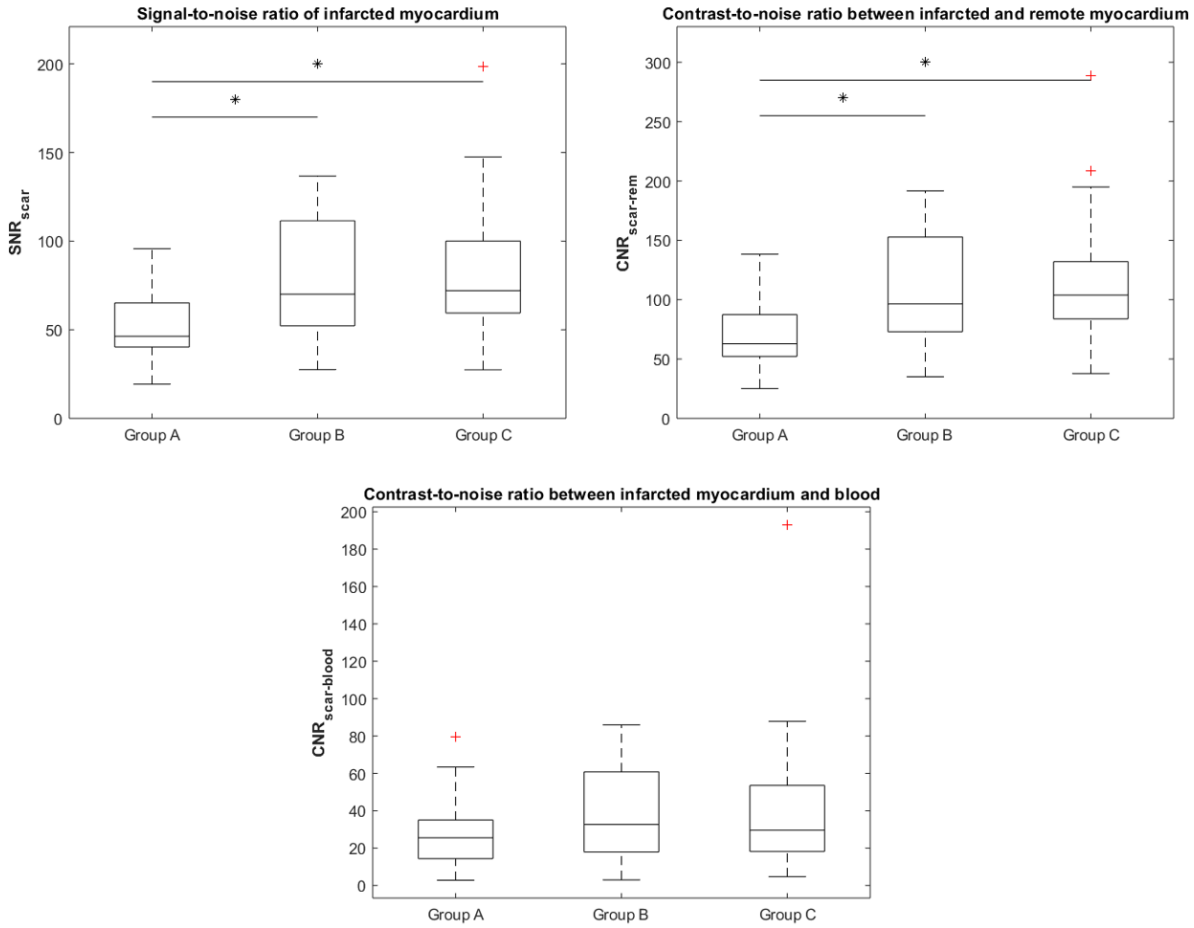

Figure 5 *Box plots of signal-to-noise ratio of the scarred myocardium (SNRscar), contrast-to-noise ratio between infarcted and remote myocardium (CNRscar-rem), and contrast-to-noise ratio between infarcted myocardium and blood (CNRscar-blood) in the three groups being administered 0.10 (group A), 0.15 (group B) and 0.20 (group C) mmol/kg of gadobutrol. Significant differences between groups are indicated with an asterisk (*), red crosses (+) indicate outliers. In particular, SNRscar was lower in group A (46.4 IQR 40.3–65.1) than in both group B (70.1 IQR 52.2–111.5, P = 0.013) and group C (72.1 IQR 59.4–100.0, P = 0.002), and CNRscar-rem is lower in group A (62.9 IQR 52.2–87.4) than in both group B (96.5 IQR 73.1–152.8, P = 0.008) and group C (103.9 IQR 83.9–132.0, P = 0.001). There were no other significant differences in SNRscar, CNRscar-rem or CNRscar–blood (P > 0.335).*

Concerning subjective image quality, no exams were non-diagnostic (Likert score 0), 7 exams displayed sufficient quality (Likert score 1), 24 exams good quality (Likert score 2), and 48 exams excellent quality (Likert score 3). In group A, 4 exams displayed sufficient quality, 7 good quality and 11 excellent quality. In group B, 3 exams displayed sufficient quality, 7 good quality and 16 excellent quality. In group C, 10 exams displayed good quality and 21 excellent quality. There were no significant differences in subjective image quality among groups (p = 0.250).

	Group A	**Group B**	**Group C**	***p* value (global)**	***p* value (A *versus* B)**	***p* value (B *versus* C)**	***p* value (A *versus* C)**
SNR_{inf}	46.4 (40.3–65.1)	70.1 (52.2–111.5)	72.1 (59.4–100.0)	0.002*	0.013*	0.884	0.002*
$CNR_{scar-rem}$	62.9 (52.2–87.4)	96.5 (73.1–152.8)	103.9 (83.9–132.0)	< 0.001*	0.008*	0.871	0.001*
$CNR_{scar-blood}$	25.5 (14.4–35.0)	32.7 (17.9–60.8)	29.6 (18.2–53.5)	0.335	–	–	–

Table 2 *Image quality and differences among the three groups according to the dose of gadobutrol used for late gadolinium enhancement. Group A received 0.10 mmol/kg, group B 0.15 mmol/kg, and group C 0.20 mmol/kg of gadobutrol. CNRscar-blood Contrast-to-noise ratio between myocardial scar and blood, CNRscar-rem Contrast-to-noise ratio between scarred and remote healthy myocardium, SNRinf Signal-to-noise ratio of the myocardial scar. Kruskal-Wallis and Fisher 2 test were used. * indicates statistical significance*

Discussion

The issue of GBCA dose reduction has become crucial in the last few years [36]. Among patients who undergo contrast-enhanced CMR, one of the main groups is represented by patients with chronic myocardial infarction, especially when the infarct is transmural and of greater clinical relevance [37]. In this study we wished to ascertain whether lower GBCA doses resulted in lower scar image quality, or if there was room for dose reduction while preserving scar visibility. Even lower GBCA doses guarantee diagnostic quality, however especially given the rise of automatic post-processing methods, it may be important to preserve the highest possible scar discernment to ensure images can be utilized for such purposes. In fact, the quantification of LGE using standard deviations may be influenced by SNR and CNR, as lower SNR and CNR may signify that background noise has a higher

impact on intrinsic signal intensity variations, and this may lead to less accurate scar detection, for instance using standard deviations-related systems.

Acquisition time was optimal in all groups, never exceeding 30 min as recommended by the literature [38]. Moreover, the differences in acquisition timings reflect the recommendations to obtain adequate image contrast according to the dose of contrast agent used [31]. Among our study groups, there were no significant differences in demographics or volumetric or functional left ventricle data and scar percentage over the whole myocardium. This would imply that none of these variables should have influenced the results of our research.

Concerning scar visibility, a lower SNR_{scar} (see **Table 2**) in group A than in both group B and group C could be due to the fact that a 0.10 mmol/kg GBCA dose was not sufficient to enhance the scarred myocardium in the same way as the two other doses, even though timing was appropriate for LGE (median 9 min, IQR 8–13 min) [11]. This hypothesis is also supported by a lower $CNR_{scar\text{-}rem}$ (see **Table 2**) in group A than in both group B and group C. $CNR_{scar\text{-}blood}$ showed no differences (see **Table 2**) between group A and group B, in accordance with our hypothesis, since both the scarred myocardium and blood are enhanced by the same contrast dose and are still enhanced at the time of LGE acquisition. SNR_{scar} was not significantly different between group B and group C, neither did $CNR_{scar\text{-}rem}$ and $CNR_{scar\text{-}blood}$, suggesting that image quality between the two doses of 0.15 mmol/kg and 0.20 mmol/kg of gadobutrol is comparable.

Our results concerning SNR and CNR were not always similar to those obtained by other authors using the same doses of gadobutrol. At 0.10 mmol/kg, our SNR_{blood} was lower than that obtained for by De Cobelli et al. [39] using gadobutrol 0.10 mmol/kg on a group of patients with mixed pathologies exhibiting LGE. Our $CNR_{scar\text{-}rem}$ was on average slightly lower than theirs but overlapping to a certain degree due to the wide range of distributions; conversely our $CNR_{scar\text{-}blood}$ was higher. Their method of calculating SNR was equal to ours expect for the lack of the 0.655 adjusting factor which would indeed lower our SNR compared to theirs. Their method of calculating CNR was equal to ours.

Concerning 0.15 mmol/kg, both $CNR_{scar\text{-}rem}$ and $CNR_{scar\text{-}blood}$ were higher than those obtained by Durmus et al. [40] utilizing gadobutrol at 0.15 mmol/kg with a 15-min delay to LGE scan. Durmus et al. used the same method for calculating CNR as our study. However, we should consider that our study only included transmural infarctions, while these authors did not exclude patients by scar size. Concerning the comparison of objective image quality parameters, while studies have assessed the differences between different contrast agents at different doses [41,42], to our knowledge none have yet compared different gadobutrol doses.

This study has some limitations, the first being its retrospective design. Results refer to the specific sequence for LGE used at our centre, and to gadobutrol. However, fast inversion-recovery gradient-echo sequences are widely used in clinical practice, and our timings for LGE are aligned to recommendations [38]. On the other hand, gadobutrol is commonly used in CMR [30], it has a double concentration (1.0 M) in comparison with all other vascular/interstitial GBCAs and exhibits an r1-relaxivity relatively higher. However, the double molarity should not impact on LGE findings (obtained after about 10 min after injection), especially concerning SNR and $CNR_{scar\text{-}rem}$, as observed by Wildgruber et al. [42], while the clearance of each single GBCA might impact on $CNR_{scar\text{-}blood}$. Conversely, since the relatively higher relaxivity of gadobutrol may have positively impacted objective image quality of LGE imaging, as also reported by Schlosser et al. [43], the results obtained for gadobutrol may not be generalizable to GBCAs with a lower relaxivity. Another potential limitation could be posed by the variability of the placement of the regions of interest in the different areas. Nevertheless, the two regions of interest in scarred and healthy myocardium, which were the ones that could carry more issues, were automatically placed by the scar quantification software, and the ones in the air and the blood pool, which were hand-drawn, brought less difficulties. One further limitation, related to the retrospective nature of the study, is represented by the method used for SNR and CNR calculation. In fact, with the only availability of LGE sequences for the assessment of such parameters, the lone viable method for SNR and CNR calculation depended on the use of ROIs

placed on the desired structures and background. However, this method has shown to provide the highest variability on SNR in a study by Dietrich et al. [44]. An ideal method for SNR and CNR calculation would perhaps be the one presented by Holtackers et al. [45], who utilized subsequent acquisitions of the same sequence using different inversion times. Nevertheless, we utilized the same sequence for all patients, thus variations in SNR and CNR should be of a systematic nature, thus preserving statistical significance of the observed differences.

In conclusion, results from our study suggest that, while 0.10 mmol/kg of gadobutrol provides inferior scar image quality of CMI than 0.15 and 0.20 mmol/kg, the last two dosages seem to provide similar LGE. In view of a global trend of standardization and reduction of GBCA doses, 0.15 mmol/kg of gadobutrol could be suggested instead of 0.20 mmol/kg, with no hindrance to image quality. Further studies should be conducted to evaluate whether lower GBCA dosages provide a high enough scar quality for clinical evaluations. This would pave the way for further GBCA dose reduction which may impact on image quality, but not on diagnostic utility of CMR examinations.

Late gadolinium enhancement in patients with Tetralogy of Fallot: a systematic review

(under review)

Background

ToF is the most common cyanotic congenital heart defect, which occurs in 5 per 10,000 live births and represents 5–7% of all congenital heart defects [46]. In patients with ToF, accurate follow-up with dedicated cardiac imaging is vital to identify structural or functional cardiac modifications that may require specific therapy or additional surgery [47,48].

CMR is one of the main imaging techniques used for the follow-up evaluation of ToF patients, due to the absence of ionising radiation exposure and its capability to accurately assess the anatomy and function of the left and right heart along with providing non-invasive information on the main vessels [49,50]. CMR should be performed in the first evaluation of ToF immediately after its diagnosis, for the assessment of pulmonary regurgitation, as mentioned in the criteria for pulmonary valve replacement [51], and in general for follow-up after surgical correction, appraising further or residual lesions. According to the 2018 AHA/ACC Guideline for the Management of Adults With Congenital Heart Disease [52], CMR bears class Ib evidence for ToF patients' follow-up. The most common sequences used for the CMR evaluation of ToF patients are unenhanced cine sequences of the heart for morpho-functional assessment, phase-contrast sequences for flow evaluation, and unenhanced three-dimensional whole heart sequences for anatomy assessment [53,54].

In addition, the study of myocardial fibrosis is considered to have an incoming role in the assessment of ToF patients [55]. LGE imaging is a specific CMR application consisting in a T1-weighted inversion recovery turbo fast low-angle shot acquisition, obtained from 5 to 20 minutes after the injection of paramagnetic gadolinium-based contrast, which shows areas of fibrosis in the myocardium. The assessment of myocardial fibrosis through LGE imaging is well-accepted in a

number of cardiac diseases, including cardiomyopathies [56] and myocarditis [57], where it has been shown to yield a clinically relevant prognostic value.

Different studies have come to different conclusions concerning the clinical role of LGE findings in ToF patients [55,58], and there seems to be no definite agreement. Thus, a better definition of the role of LGE in ToF patients may be useful for identifying indications for performing LGE acquisitions and reach a shared interpretation of related findings, which might pave the way for more tailored patient management.

Therefore, the aim of this study is to review the literature concerning myocardial LGE in ToF patients, with regards to its prevalence, characteristics, and clinical relevance.

Methods

In November 2019, a systematic search was performed on MEDLINE (PubMed, https://www.ncbi.nlm.nih.gov/pubmed/), EMBASE (Elsevier), the Cochrane Library (Cochrane Database of Systematic Reviews) and the Cochrane Central Register of Controlled Trials for articles that performed CMR with LGE in ToF. A controlled vocabulary (medical subject headings in PubMed and EMBASE thesaurus keywords in EMBASE) was used. The search string was ('congenital heart disease'/exp OR 'congenital cardiac disease' OR 'congenital cardiac distress' OR 'congenital heart disease' OR 'congenital heart distress' OR 'congenital heart failure' OR 'heart congenital disease' OR 'heart disease, congenital' OR 'neonatal cardiopathy' OR 'truncus arteriosus, persistent' OR 'congenital heart malformation'/exp OR 'congenital heart anomaly' OR 'congenital heart defect' OR 'congenital heart malformation' OR 'heart anomaly' OR 'heart congenital anomaly' OR 'heart congenital defect' OR 'heart congenital malformation' OR 'heart defects, congenital' OR 'heart malformation') AND ('late gadolinium enhancement'/exp OR 'late gadolinium enhancement' OR 'delayed enhancement magnetic resonance imaging'/exp OR 'delayed enhancement magnetic resonance imaging' OR lge OR 'image enhancement'/exp OR 'enhancement, image' OR 'image enhancement') AND ([article]/lim OR [article in press]/lim OR [conference paper]/lim OR

[editorial]/lim OR [letter]/lim OR [review]/lim) AND [humans]/lim AND [english]/lim AND [abstracts]/lim).

The search was limited to original studies published in English, with available abstract. No publication date limits were applied. First article screening was performed by two independent readers (BLINDED and BLINDED, with 2 and 3 years of experience in cardiac imaging), considering only title and abstract. After downloading eligible articles, the full text was read for complete assessment. Finally, references of included articles were manually searched to check for further eligible studies. Only original articles that evaluated LGE in ToF were finally included and analysed.

Data extraction

Data extraction was performed independently by one reader among the two who performed the literature search (BLINDED). Extracted data were subsequently checked by the second reader who performed the literature search (BLINDED). For each analysed article, year of publication, study design, number of acquired subjects, age and sex, type of surgical repair, age at repair and time from the procedure were retrieved. Technical parameters for LGE acquisition, such as MR unit, magnetic field strength, sequence, type and dose of gadolinium-based contrast agent and timing for LGE acquisition were retrieved. Cardiac volumes and functions of right (RV) and left ventricle (LV) were obtained, namely including end-diastolic and end-systolic volumes indexed to patients' body surface area, stroke volume, and ejection fraction, if available.

For each study, LGE location, characteristics and clinical significance were retrieved and reported.

Results

Study selection

From a total of 261 retrieved studies, 54 papers were first selected. Then, both reviewers evaluated the full text of each work, and 40 articles were excluded as they did not assess LGE in ToF patients,

resulting in 14 remaining articles. One article not initially retrieved by the search string was found from the references of included works leading to 15 included articles [55,58–71]. Study selection is reported in **Figure 6**.

Figure 6 *Study selection process for article inclusion in the systematic review. MR: magnetic resonance; LGE: late gadolinium enhancement; CHD: congenital heart disease; ToF: tetralogy of Fallot*

Study characteristics

The included studies [55,58–71] accounted for a total of 1133 patients. Such works were published between 2005 and 2019. Study design was prospective in 10 works [55,58–62,67–70] and retrospective in 5 [63–66,71]. Study populations ranged from 14 [67] to 237 [64] patients. Average patients' age ranged from 10.2 years [70] to 39 years [66]. Three studies [55,64,70] included mainly only paediatric patients, whereas the others [58–63,65–69,71] included mixed, and mostly adult populations. The percentage of male subjects in each study varied from 43% [59] to 66% [64].

Regarding the surgical procedure performed in ToF patients, 13 studies [55,58,59,61–66,68–71] contained information about the surgical intent. In 733 patients reported in 12 studies [55,58,59,64–

66,68–72], surgery had a curative intent. Surgery was palliative in 197 patients reported in 11 studies [55,58,59,62,64–66,68–71], while surgical aim was not specified for the remaining 936 patients. Nine studies [55,59,63–66,68,69,71] specifically described the surgical procedures performed. The most used procedure was the transannular patch, a curative technique, in 513 patients, followed by the non-transannular patch, in 33 patients. The most used palliative technique resulted to be the RV-pulmonary artery conduit in 97 patients. Average time from surgery to CMR ranged from 9.2 [70] to 33.5 [66] years. Demographics and other data for the included studies are reported in **Table 3**. Technical parameters involved in CMR acquisition and contrast-enhanced evaluations are reported in **Table 4.** Volumetric and functional parameters of the RV and LV are reported in **Table 5**.

Late gadolinium enhancement features

Among all ToF patients, 1003 described in 15 studies [55,58–71] presented RV LGE, with a prevalence ranging from 41% [60] to 100% [55,58,62,64,67,69].

When expressly mentioned, LGE was located in the RV outflow tract in 558 patients [58,59,61,62,65–70], at ventricular insertion points in 565 patients [55,60,62,63,65,67–71], in the ventricular septal defect patch in 321 patients [55,58,59,62,67,69,70]. Other less common LGE sites included the free wall [55,59,61,63,65,66,70], mostly anterior in 145 patients [55,59,61,63,65,66,70], or inferior in 77 patients [55,59,61,65,66,70], in the interventricular septum in 69 patients [55,59,60,63,67], in the trabecular and moderator band in 37 patients [55,59,62,70]. The distribution of LGE at different sites is depicted in **Figure 7.** Examples of LGE at different locations are displayed in **Figure 8**.

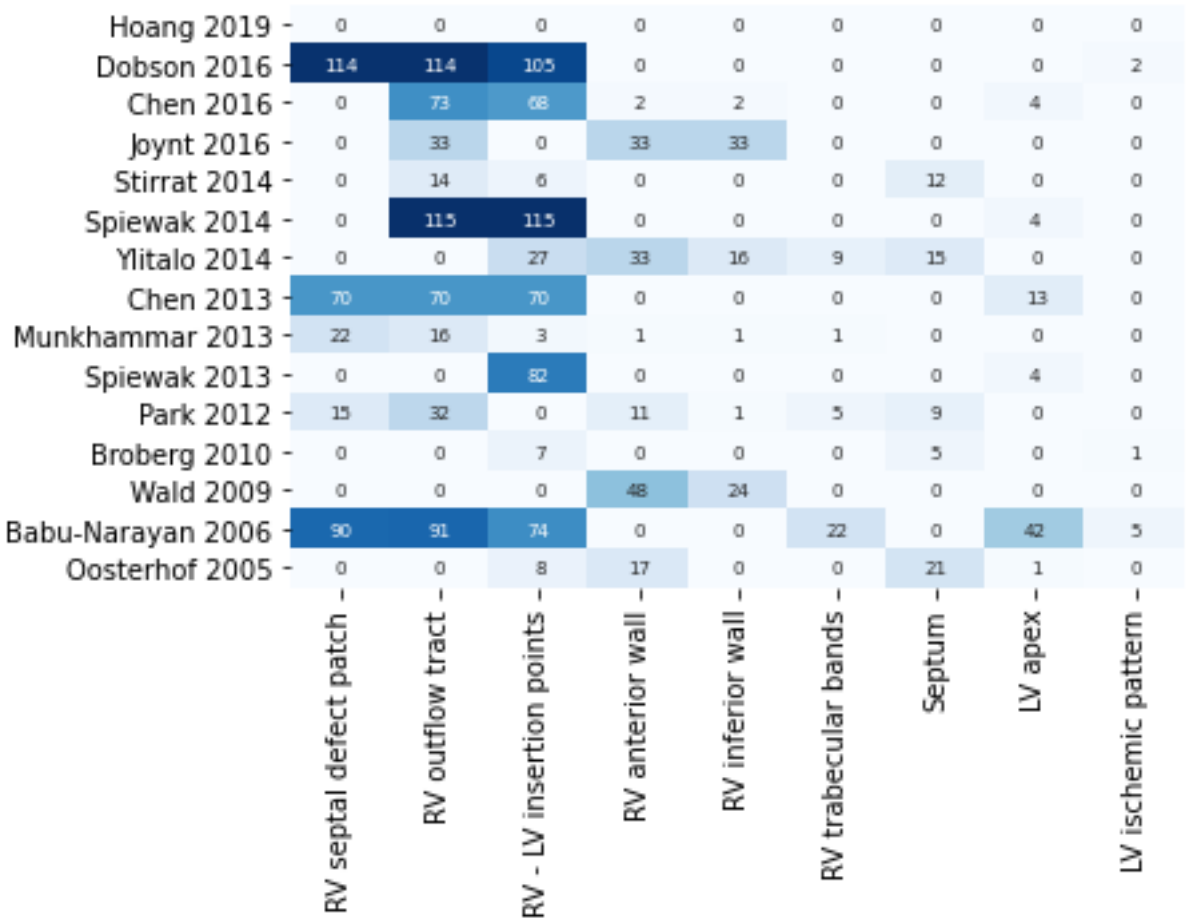

Figure 7 *Distribution of late gadolinium enhancement among patients in different sites of the right (RV) and left ventricle (LV)*

Concerning the LV, nine studies [58–62,68,69,71] described LV LGE in 196 patients. LGE was observed in the LV apex in 68 patients [62,63,68,69,71], while 8 patients [58,60,62] displayed an ischemic pattern of LGE, in the inferior or lateral wall.

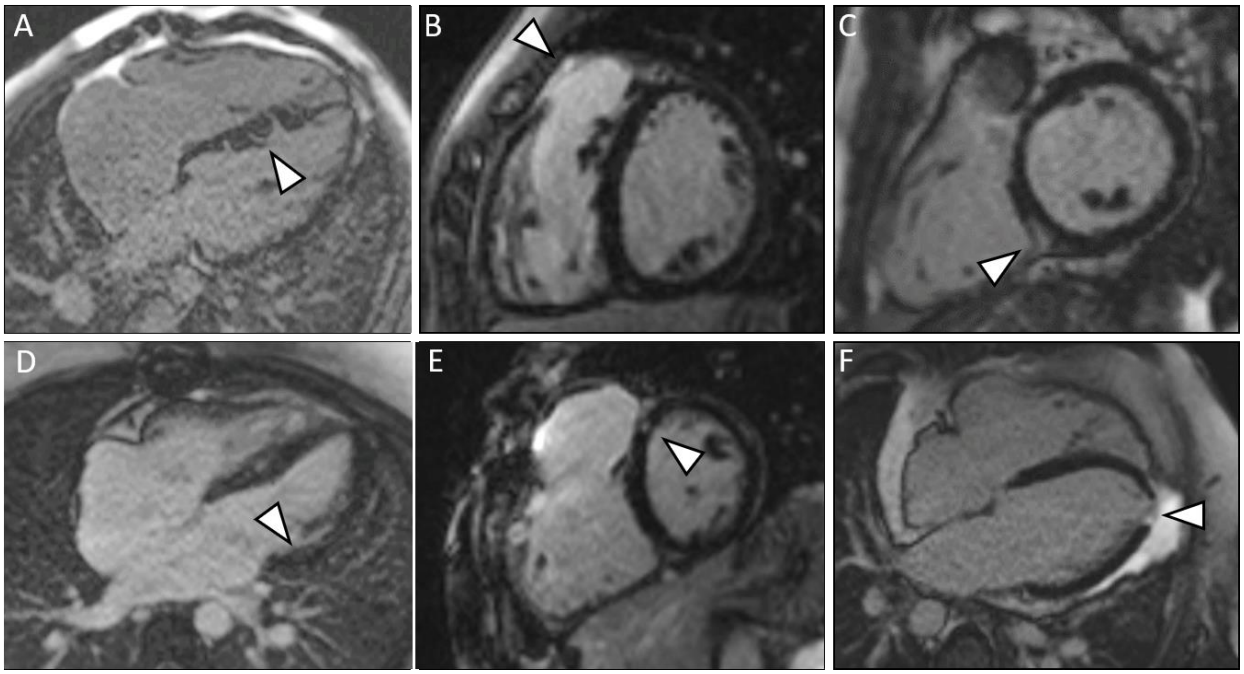

Figure 8 *Depictions of late gadolinium enhancement in tetralogy of Fallot patients, indicated by white arrowheads, at different sites. A: ventricular septal defect patch; B: right ventricular (RV) outflow tract; C: RV-left ventricle (LV) inferior insertion point; D: LV lateral wall; E: superior insertion point; F: LV apex*

Late gadolinium enhancement and demographic data

Higher age and late time of surgical repair were independent factors predicting LGE [55]. The identification of RV LGE in the RV outflow tract or closed to the interventricular septal defect patch [55,62,70] was reported to be correlated with previous surgical procedure. Even the presence of LV LGE in the apex is related to surgery, from a transapical approach to the heart [55].

LGE was also found outside surgical sites in the RV, as in trabecular or moderator band, potentially related to multiple factors. Possible causes included a foetal pattern of congenital anomalies that can be associated with ToF, such as hypoplastic left heart syndrome or truncus arteriosus [55], preoperative cyanosis related to the low-oxygen blood, intra-operative procedures [70], peri and post-operative ischemic insults [62], hypoxia before surgery [55] and peri-operative complications [62].

Late gadolinium enhancement and cardiac function

Seven studies [55,58,60–64] assessed the relationship between RV LGE and cardiac volumes and function. In particular, three works [55,60,63] identified a positive correlation between RV LGE and RV dilation. Two studies [58,62] described an association of RV LGE with lower RV stroke volume and systolic impairment, while four studies [60–62,64] observed a negative correlation between RV LGE and RV ejection fraction. Broberg et al. [60] observed that the degree of LGE in ToF correlated with ventricular enlargement and impaired ventricular function.

Correlations between LGE and clinical variables are reported in **Table 6**.

Late gadolinium enhancement and arrhythmias

Two studies evaluated the correlation between LGE and arrhythmias [59,62]. Park et al. [59] observed that a fragmented QRS correlated with higher values of RV LGE. Also Babu-Narayan et al. [62] reported that RV LGE was a predictor of arrhythmias. Correlations between LGE and clinical variables are reported in **Table 6**.

Late gadolinium enhancement and serum biomarkers

Three studies [55,64,69] appraised the correlations between LGE and different serum biomarkers. Ylitalo et al. [55] found a positive correlation between LGE and N-terminal prohormone of brain natriuretic peptide, a biomarker of heart failure. Hoang et al. [64] revealed a correlation between LGE and genetic variants of hypoxia-inducible factor 1a, that promotes transformation of endothelial and smooth muscle cells into fibroblasts. Chen et al. [69] observed a significant correlation between elevated circulating carboxy-terminal pro-peptide of procollagen type I, a serum biomarker of collagen type I, identifying a profibrotic state in ToF patients. Correlations between LGE and clinical variables are reported in **Table 6**.

	Design	N	Males (n)	Age (years)	Time from surgery (years)	Curative surgery (n)	Palliative surgery (n)	RV LGE prevalence (%)	LV LGE prevalence (%)
Hoang 2019	R	237	157	12.3 (8.7–16.2)	11	200	37	100	
Dobson 2016	P	114	64	29.5 (17.5–64.2)	27.5	68	46	100	94
Chen 2016	R	84	47	23.3 (16.3–32.8)	20.4	60	20	94	
Joynt 2016	R	47	26	39.1 ± 12.5	33.5 ± 9.3	47	0	70	
Stirrat 2014	P	14	6	32.2 ± 11.9	30.3 ± 11.9			100	
Spiewak 2014	P	146	88	26.4 ± 8.2	21.6 ± 6.4	82	14	94	3
Ylitalo 2014	P	40	25	13.1 ± 3.2	11.8 ± 2.9	23	16	100	
Chen 2013	P	70	39	24.8 (21.3–30.8)	20. 7 (17.6–26.2)	70	0	100	19
Munkhammar 2013	P	27	14	10.2 ± 2.6	9.2 ± 2.7	27	0	59	
Spiewak 2013	R	122	74	24.2 (20.3–30.9)	20.1 (16.4–25.0)	69	12	67	3
Park 2012	P	37	16	30 (23.3–40)	22.9 (19.9–28.8)	32	3	95	0
Broberg 2010	P	17	8	34.1 ± 11.7				41	70
Wald 2009	P	62	34	19.7 (4.2–67.2)	22 (7.7–41.6)	40	13	77	0
Babu-Narayan 2006	P	92	56	32.2 ± 11	27 (19–33)		36	100	53
Oosterhof 2005	R	24	16	25 ± 8.4	21 ± 6.7	15		88	4

Table 3 *Patients demographical data, including timing from surgery, surgery type and prevalence of late gadolinium enhancement (LGE) in the right (RV) and left ventricle (LV)*

	MR unit	Field strength (T)	Contrast agent type	Contrast dose (mmol/kg)	LGE delay (min)	Slice thickness (mm)	TE (ms)	TR (ms)	Flip angle (°)
Hoang 2019	Siemens MAGNETOM Avanto	1.5	Gadopentetate dimeglumine	0.4	10	1.5 - 2.5			75 - 90
Dobson 2016	Siemens MAGNETOM Avanto	1.5	Gadobutrol	0.15	10-15	10	1.4	3.5	50
Chen 2016	Philips Achieva	1.5	Gadopentetate dimeglumine	0.15	20	8	2.5	8	12
Joynt 2016	Philips Intera Achieva or Ingenia	1.5	Gadoteridol/Gadopentetate dimeglumine	0.2	12-15				
Stirrat 2014	Siemens MAGNETOM TRIO	3	Gadobutrol	0.2	10	6	1.5	3	50
Spiewak 2014	Siemens MAGNETOM Avanto	1.5	Gadobutrol	0.2	10-15				
Ylitalo 2014	Philips Achieva	1.5	Gadoterate meglumine	0.2	10	7	1.628	3.239	
Chen 2013	Siemens MAGNETOM Sonata	1.5	Gadopentetate dimeglumine	0.2	10				
Munkhammar 2013	Philips Intera CV	1.5	Gadobenate dimeglumine/Gadopentetate dimeglumine	0.2	10-20	8	1.58	3.14	
Spiewak 2013	Siemens MAGNETOM Avanto	1.5	Gadobutrol	0.2	10-15	8	1.2	2.2 - 3.6	64 - 79
Park 2012	Philips Achieva	1.5	Gadopentetate dimeglumine	0.15	5-15	6	1.4	4.6	
Broberg 2010	Philips Achieva or Intera	1.5 - 3	Gadopentetate dimeglumine	0.15	10-20	8			
Wald 2009	GE Signa Horizon	1.5	Gadopentetate dimeglumine	0.2	10-20				
Babu-Narayan 2006	Siemens MAGNETOM Sonata	1.5	Gadopentetate dimeglumine	0.1	5	7			
Oosterhof 2005	Philips NT15 Gyroscan	1.5	Gadopentetate dimeglumine	0.2	10-15	5	1.36	4.53	15

Table 4 *Technical data for cardiac magnetic resonance (CMR) in the included studies. LGE: late gadolinium enhancement; TE: time of echo; TR: time of repetition*

	RV EDVi (ml/m^2)	RV ESVi (ml/m^2)	RV SV (ml)	RV EF (%)	LV EDVi (ml/m^2)	LV ESV
Hoang 2019	112.0 (89.7-140.0)			58.8 (52.8-63.8)		
Dobson 2016	125 (100-152)	64 (49.75-83)		48 (43-54)	80.5 (72-93)	32
Chen 2016	153.8 ± 47.8	83.3 ± 39.6		47.4 ± 9.5	89.3 ± 17.6	41.
Joynt 2016				48.0 ± 7.1		
Stirrat 2014	117.0 ± 41.5	55.2 ± 26.3		53.9 ± 9.2	68.6 ± 21.9	25.
Spiewak 2014	160.4 ± 47.4	88.1 ± 35.8	72.3 ± 19.2	46.1 ± 8.1	88.8 ± 20.2	38.
Ylitalo 2014	115 ± 26.5			50.1 ± 8.6	75.3 ± 15.1	
Chen 2013	99 (81-124)	55 (47-77)		40.4 ± 7.4	61 (53-68)	55
Munkhammar 2013	134 ± 50	67± 33		56 ± 5		
Spiewak 2013	159.8 ± 48.3	87.9 ± 37.2		46.2 ± 8.7	90.0 ± 19.2	38.
Park 2012	131 (111-157)	84 (69-103)		37 (30-43)	78 (65-94)	36
Broberg 2010						
Wald 2009	139 (77-372)	67 (22-282)		50 (24-71)	84 (59-176)	34
Babu-Narayan 2006	126 (110-142)	55 (48-68)		56 ± 9		2
Oosterhof 2005	158 ± 47	86 ± 36		46 ± 9		

Table 5 *Morpho-functional data of the right (RV) and left ventricle (LV) for the included studies. EDVi: end-diastolic volume indexed to body surface area; ESVi: end-systolic volume indexed to body surface area; SV: stroke volume; EF: ejection fraction*

Name	LGE location	Cardiac function	Serum biomarkers	Arrhythm
Hoang 2019	RV	RV EF (-)	hypoxia-inducible factor 1a (+)	
Dobson 2016	RV	RV EF (-)		
	LV	LV ESVi (+)		
Chen 2016				
Joynt 2016				
Stirrat 2014				
Spiewak 2014				
Ylitalo 2014	RV	pulmonary regurgitation (+), RV EDV (+)	NT-proBNP (+)	
Chen 2013	RV		PICP (+)	
Munkhammar 2013				
Spiewak 2013	RV	RV EF (-)		
Park 2012	RV			fragmented
Broberg 2010	RV	RV EDVi (+) and EF (-)		
Wald 2009	RV	RV EF (-)		
Babu-Narayan 2006	RV	RV EDV (+)		
Oosterhof 2005	RV	RV ESVi (+) and EF (-)		arrhythmi

Table 6 *Correlations between late gadolinium enhancement (LGE) in the right (RV) or left ventricle (LV) with clinical parameters. EF: ejection fraction; ESVi: end-systolic indexed volume; EDV: end-diastolic volume; EDVi: end-diastolic indexed volume; NT-proBNP: N-terminal prohormone of brain natriuretic peptide; PICP: carboxy-terminal pro-peptide of procollagen type I*

MYOCARDIAL STRAIN

The analysis of myocardial strain provides a noninvasive method for assessing cardiac contractility [73]. At first, strain was assessed through echocardiography, a real-time technique which allows the performance of different measurements throughout the whole cardiac cycle [74]. Nevertheless, echocardiography bears two important limitations, the first being the high dependance of its result on the experience of the reader performing the examination, and the second being that in some patients, especially obese patients or those with breathing or chest movement difficulties, who are also more prone to cardiac disease, an appropriate acoustic window for imaging may not be always achievable [75].

More recently, CMR has been proposed for strain calculations via different methods. The first method proposed for CMR strain assessment was feature tagging, which requires the acquisition of specific imaging sequences and is based on the creation of spectral peaks in the Fourier domain during the modulation of images [76]. While this methods yields accurate results for myocardial strain, comparable to those of echocardiography and highly reproducible, the need for dedicated sequences may prove time consuming and hinder the use of this application in a clinical setting [77]. For this reason, a novel method for strain calculation, feature tracking (FT) was introduced, allowing to estimate strain directly from cine acquisitions, which are a routine part of virtually every CMR examination. FT myocardial strain has since shown a high concordance with data obtained from feature tagging and echocardiography, and has thus become a more commonly used mean for assessing strain without the need for additional sequences or complex processing [78].

The study of myocardial strain was performed in countless patients with a number of different pathologies, and the main results deriving from this approach seem to indicate that strain might be a biomarker of subclinical cardiac dysfunction, suggesting that myocardial contractility may be impaired to a certain degree even in presence of normal ejection fraction and cardiac chamber volumes [79].

Concerning this section of the thesis, our first work aimed to assess the role of left ventricular strain as a potential diagnostic biomarker in patients with mild acute myocarditis, where CMR in already included in the routine clinical workflow. The second study aimed to appraise changes and trends in right ventricular strain in patients with ToF, as strain may help identify those at higher risk of adverse events or higher need for a stricter follow-up.

Diagnostic value of global cardiac strain in patients with myocarditis

(from Secchi F, Monti CB, Alì M, Carbone FS, Cannaò PM, Sardanelli F. Diagnostic value of global cardiac strain in patients with myocarditis - *J Comput Assist Tomogr* 2020)

Background

Myocarditis is a disease characterized by inflammation of the myocardium, possible necrosis, or myocyte degeneration [80]. It may range from subclinical to severe [81,82]. Myocarditis provokes at least 9% of dilated cardiomyopathies and may cause from 6 to 10% of sudden cardiac deaths in young people, being their leading cause [83–86].

The reference standard for diagnosing myocarditis is endomyocardial biopsy, following established histological and immunohistochemical criteria, but it is an invasive investigation which may cause adverse clinical events [87–90]. Different diagnostic techniques have been proposed, to avoid unnecessary endomyocardial biopsies in patients with low risk myocarditis. CMR is considered optimal, thanks to its tissue characterization [91]. The current standard for CMR diagnosis of myocarditis are the Lake Louise criteria, which include evaluation of edema, hyperemia and capillary leakage, represented by early myocardial enhancement after Gd-based contrast agent administration, and necrosis and fibrosis, represented by late myocardial enhancement after Gd-based contrast agent administration. Edema and late enhancement, commonly observed on unenhanced T2-weigheted inversion-recovery magnitude images and on T2-magnetization prepared contrast-enhanced images, constitute the most common parameter combination, with a sensitivity of 67% and a specificity of 91% [92–94]. Therefore, CMR protocols for myocarditis investigation usually include T2-weigheted inversion-recovery, T2-magnetization prepared contrast-enhanced, and cine sequences, the last ones serving as a tool to visualize the heart throughout its entire functional cycle [95]. A reliable CMR diagnosis is particularly useful in patients who have myocarditis

with a preserved left ventricle ejection fraction, where endomyocardial biopsy would bring more risk than benefit [96].

Myocardial strain relates to left ventricle function, by measuring percental deformation of the myocardial wall dividing its spatial shift by its initial position [97]. In the left ventricle, longitudinal, circumferential, or radial strain can be used for functional assessment, and may detect subclinical contractile dysfunction [98]. Abnormal strain absolute values are predictable when cardiac contractility is impaired [99,100]. Strain may be calculated through feature tracking CMR, a post-processing technique, both reliable and reproducible, which only requires cine CMR sequences [101,102].

It may therefore be hypothesized that strain values might be lower in myocarditis patients, whose cardiac function is impaired, even when their ejection fraction is preserved, and that such values could at least partially revert towards normality after resolution.

Since endomyocardial biopsy is not recommended in patients with myocarditis with preserved ejection fraction, the aim of our study was to investigate the diagnostic value of strain obtained using feature tracking CMR in patients with preserved ejection fraction, where CMR is the key of the diagnostic workflow.

Methods

Study design and population

The local Ethics Committee approved this study. There was no overlap with subjects from previous research performed at our Institution. This research received no specific grant from any funding agency in the public, commercial or not-for-profit sectors. Due to the retrospective nature of this study, no specific informed consent was necessary.

Our retrospective case-control study reviewed a total of 138 CMR examinations, performed at our Institution between April 2008 and September 2017. These exams belonged to 46 consecutive patients who had a diagnosis of myocarditis through analysis of clinical data and CMR examinations,

and had undergone two CMR examinations, one during the acute phase with preserved ejection fraction and one at follow-up. Follow-up was defined as at least 3 months after acute myocarditis, since edema, representative of acute inflammation, should subside in under 3 months, leaving only residual scarring to be visualized. Only one patient having two different CMR examinations at a proper time interval had been excluded, due to the presence of extensive artefacts. All acute phase myocarditis patients were positive for edema and late gadolinium enhancement. A control group of 46 age- and gender-matched, otherwise randomized, controls was chosen according to the following criteria: they were to have one negative CMR examination, comprising the same sequences used for the assessment of myocarditis, namely cine, inversion-recovery and sequences for late enhancement. All controls were referred for CMR due to arrhythmias. No controls were excluded after being included for evaluation. Each group was composed by 36 males and 10 females.

Image acquisition

All CMR examinations were performed using a 1.5-T unit, Magnetom Sonata (Siemens Medical Solutions, Erlangen, Germany), with 40-mT/m gradient power, up until September 2014 or a 1.5-T unit, Magnetom Aera (Siemens Medical Solutions, Erlangen, Germany), with 45-mT/m gradient power, after September 2014, using a four-channel surface phased-array coil for the Sonata unit or an eighteen-channel surface phased-array coil for the Aera unit, both of them placed over the thorax of the patient in supine position. Image acquisition was gated to electrocardiographic signal for both MR units.

Fluid-weighted short-axis inversion-recovery sequences, with patient-dependent time of repetition and time of echo, an inversion time of 150 ms, a flip angle of 180°, a slice thickness of 8 mm, and a pixel size of 3.6 mm^2 were used to evaluate myocardial edema. Such sequences analyzed the whole left ventricle. Sequences for late enhancement were acquired 5 to 15 minutes after injection of 0.1 – 0.15 mmol/kg of gadobutrol (Gadovist, Bayer Healthcare, Leverkusen, Germany). The time of echo was 3.33 ms, while the time of repetition was adapted to patients' heart rates and

inversion time was progressively modified from 260 to 330 ms, to blacken cardiac muscle; the flip angle was 25°, slice thickness of 8 mm, and pixel size of 3.6 mm^2. Short-axis and long-axis cine images were acquired with electrocardiographically gated bright-blood steady-state free precession sequences, during expiratory breath holds. Cine sequences had a time of echo of 1.40 ms, a time of repetition of 48.30 ms, a flip angle of 60°, and a slice thickness of 8 mm.

Image analysis

Image analysis was performed, using QMass and QStrain from Medis Suite MR Software (Medis Medical Imaging Systems B.V., Leiden, The Netherlands). The QMass tool was used to evaluate and quantify left ventricle volumes, ejection fraction, edema, and late enhancement, as shown in **Figure 9** and **Figure 10**. Therefore, the left ventricle was manually contoured on short-axis cine, late enhancement, and fluid-weighted sequences, at end-systole and end-diastole in cine sequences, and at end-diastole in late enhancement and fluid-weighted sequences. The software then calculated late enhancement and edema mass and percentage over the myocardium. For edema, a 2-standard deviation (SD) threshold was used, for late enhancement a 6-SD threshold was used.

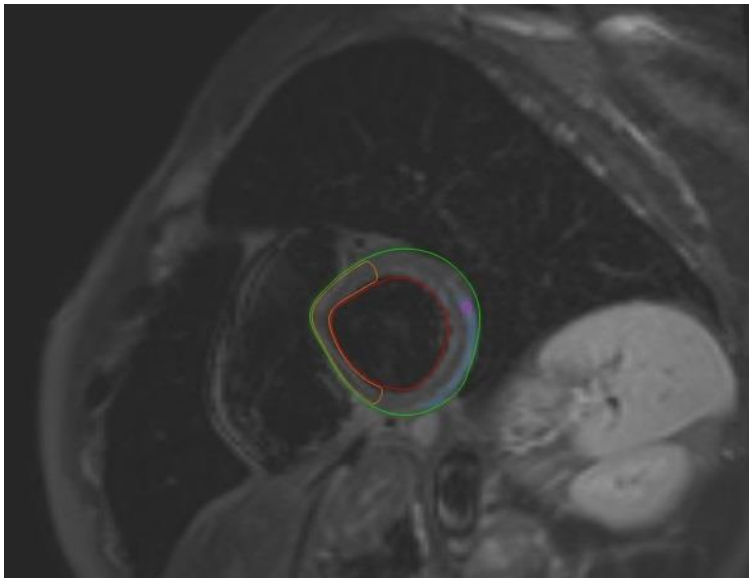

Figure 9 *Edema quantification with QMass in a 16-year-old female myocarditis patient in a short-axis section of the left ventricle*

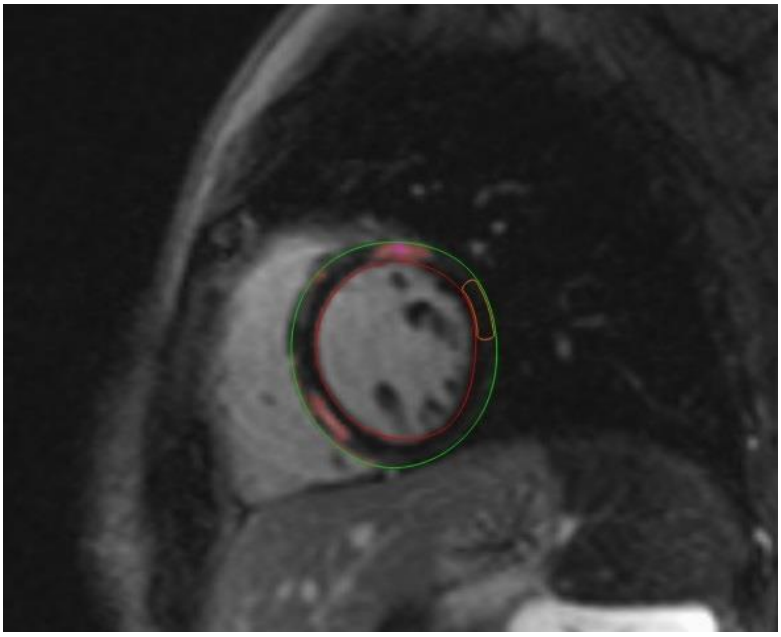

Figure 10 *Late gadolinium enhancement quantification with QMass in a 16-year-old female myocarditis patient in a short-axis section of the left ventricle*

The QStrain tool allowed for the calculation of myocardial global radial and circumferential strain, using the previously drawn contours on short-axis cine sequences, and applying subsequent feature tracking calculations (**Figure 11**). When necessary, manual corrections due to failures in feature tracking were performed.

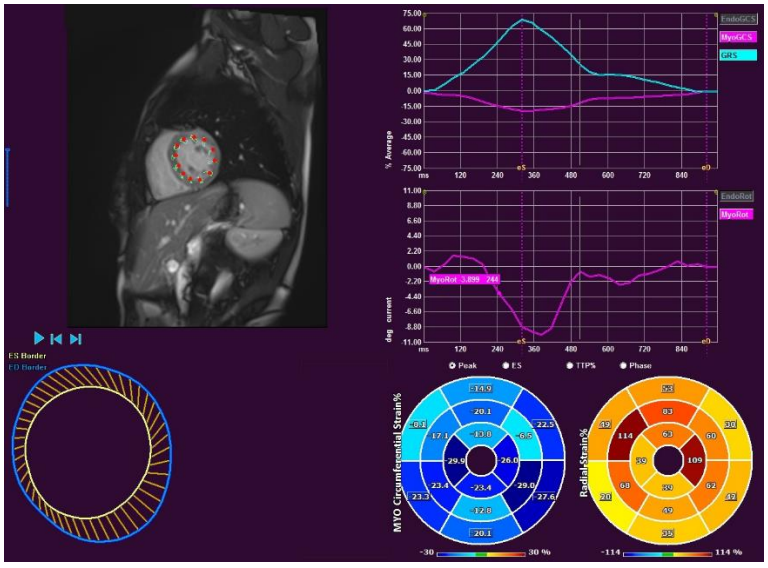

Figure 11 *Screen from QStrain, showing strain in a short-axis projection of the left ventricle in a 16-year-old female myocarditis patient, along with data output from the software*

Two independent readers (R1 and R2), with two and six years of experience in CMR respectively, performed measurements on all examinations, the former twice and the latter once, with at least a 15-day interval between measurement sessions, for a total of three sessions. Such readers had different backgrounds and different levels of training in CMR segmentation.

Statistical analysis

Data were reported as mean and SD or as median and interquartile range (IQR) according to their normal or non-normal distribution. Correlations between different distributions were assessed using Spearman's ρ. Multivariate analyses were conducted, to find data which bore significant differences among the three groups. Significant differences among normal data were assessed using Wilcoxon test when variables were paired, such as between acute and follow-up, or Mann-Whitney U test when non-paired, namely the myocarditis group versus controls. To establish strain thresholds for diagnosing myocarditis with the highest possible combination of sensitivity and specificity, receiver operating characteristics curves were obtained. Reproducibility was appraised with Bland-Altman analyses, and calculated as complement to one of the ratio between coefficient of reproducibility (CoR) and mean measure. Data were reported as reproducibility, CoR and bias.

Statistical analysis was performed using SPSS v.22.0 (IBM SPSS Inc., Chicago, IL, USA), and p-values <.05 were considered statistically significant.

Results

A total of 138 CMR examinations performed in 92 subjects were analyzed: 46 of which 36 males and 10 female patients in the acute phase; 46 in the same patients at follow-up; and 46 of which 36 males and 10 female controls. The average time between acute phase and control scans was 5 months (3–8 months). Demographics of patients and controls are reported in Table 1. Median age was 31 years (IQR 20 – 39 years) in myocarditis patients, and 30 years (IQR 20 – 39 years) in controls, with a non-significant difference (p=0.860). Male myocarditis patients had a median age of 29 years (IQR 19 – 38 years), and female myocarditis patients had a median age of 40 years (IQR 26 – 53 years), with a

non-significant difference (p=0.064). Male controls had a median age of 29 years (IQR 19 – 37 years), while female controls had a median age of 39 years (IQR 26 – 54 years), with a non-significant difference (p=0.076).

Manual corrections of the automated software evaluations were necessary in less than 20% of examinations.

Left ventricular ejection fraction was 67% (IQR 61 – 69%) in acute phase patients, 66% (IQR 63 – 70%) at follow-up, and 67% (IQR 60 – 70%) in controls. No significant differences in ejection fraction were found among groups (p=0.689).

Left ventricle edema percentage was 12.8% (IQR 9.6 – 18.4%) in acute phase patients, 6.7% (IQR 5.4 – 8.6%) in the same patients at follow-up, and 6.4% (IQR 5.3 – 7.7%) in controls. Significant differences were found between acute phase and follow-up (p<0.001) and between acute phase and controls (p<0.001). Left ventricular late enhancement percentage was 6.2% (IQR 4.8 – 9.1%) in acute phase patients, being 4.3% (IQR 3.2 – 6.9%) in the same patients at follow-up, and 4.3% (IQR 3.0 – 5.1%) in controls. Significant differences were found between acute phase and follow-up (p<0.001) and between acute phase and controls (p<0.001). Edema and late enhancement data are reported in **Table 7**.

Global circumferential strain was -18.4% (IQR -21.0 – -16.1%) in acute phase patients and -19.2% (IQR -21.5 – -16.1%) in the same patients at follow-up, while it was -20.4% (IQR -23.4 – -18.6%) in the control group. Global radial strain was 65.8% (IQR 52.9 – 79.5%) in acute phase patients, 73.1% (IQR 58.7 – 86.5%) in the same patients at follow-up, and 82.4% (IQR 62.8 – 104.9%) in controls. Significant differences in global circumferential strain were found between acute phase and controls (p=0.001) and between follow-up and controls (p=0.020) as well as in global radial strain between acute phase and controls (p=0.001) (**Table 7**). There were no significant differences in global circumferential strain between acute phase and follow-up (p=0.205), and in global radial

strain between controls and follow-up (p=0.066). Box-whiskers plots for global circumferential and radial strains are shown in **Figure 12** and **Figure 13**.

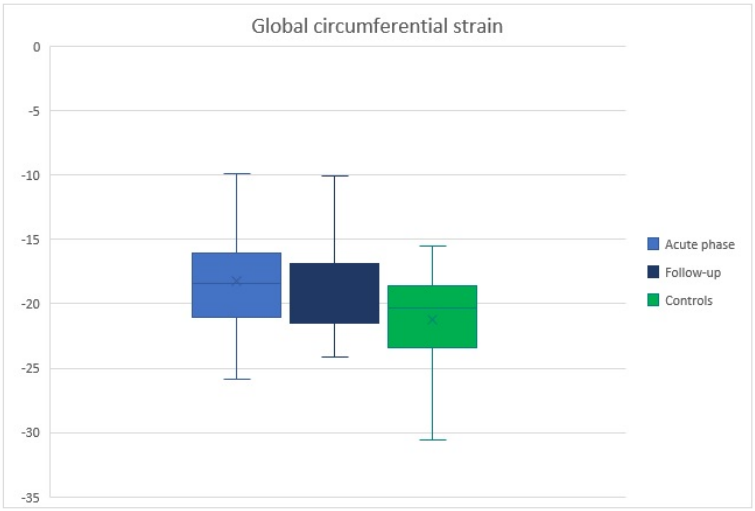

Figure 12 *Box-whiskers plot showing global circumferential strain at acute phase, at follow-up and in controls. A significant difference may be observed between acute phase and controls (p=0.001), and between follow-up and controls (p=0.020)*

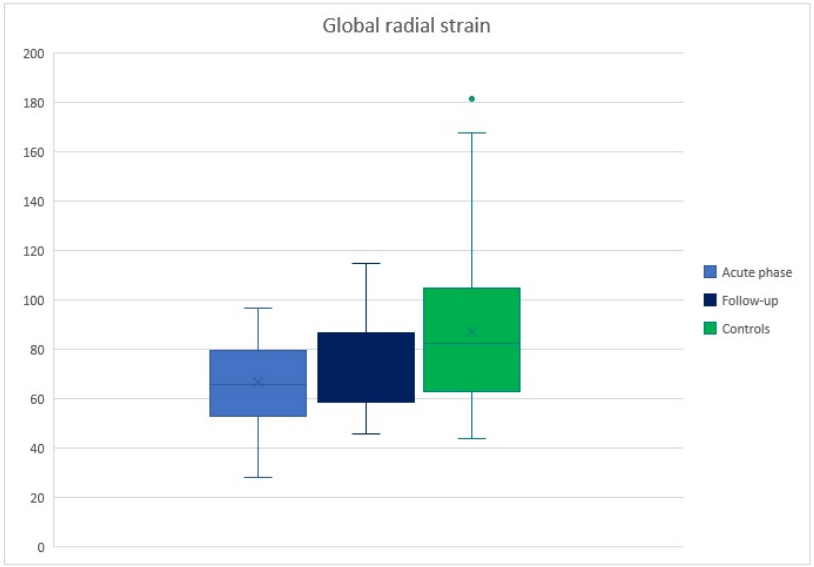

Figure 13 *Box-whiskers plot showing global radial strain at acute phase, at follow-up and in controls. A significant difference may be observed between acute phase and controls (p=0.001)*

	Acute phase	Follow-up	Controls	Overall p-value	Acute vs follow-up	Control vs follow-up	Acute vs control
Age (yo)	31 (20–39)	31 (20–39)	30 (20–39)	.860	-	-	-
Male (%)	78	78	78	-	-	-	-
EF (%)	67 (61–69)	66 (63–70)	67 (60–70)	.689	-	-	-
Edema (%)	12.84 (9.55–18.43)	6.69 (5.41–8.55)	6.41 (5.27–7.67)	<.001*	<.001*	.748	<.001*
LGE (%)	6.16 (4.79–9.11)	4.29 (3.22–6.88)	4.27 (3.00–5.09)	<.001*	<.001*	.223	<.001*
GCS (%)	-18.38 (-21.04– -16.07)	-19.21 (-21.47– -16.90)	-20.37 (-23.42– -18.64)	.002*	.205	.020*	.001*
GRS (%)	65.77 (52.88–79.51)	73.06 (58.73–86.45)	82.39 (62.75–104.92)	.004*	.052	.066	.001*

Table 7 *Study population characteristics*

Significant correlations were found between global circumferential strain and global radial strain in all three study groups, namely at acute phase (ρ=-0.580 p<0.001), follow-up (ρ=-0.382 p=0.009) and throughout controls (ρ=-0.508 p<0.001). Significant correlations were also found between global circumferential strain and delayed enhancement in myocarditis patients, at acute phase (ρ=0.365 p=0.014) and at follow-up (ρ=0.307 p=0.038), and between global circumferential strain and edema at acute phase (ρ=0.459 p=0.006). All correlations are shown in **Table 8**.

	Controls				Acute phase				Follow-up			
	Edema (%)	**LGE (%)**	**GCS (%)**	**GRS (%)**	**Edema (%)**	**LGE (%)**	**GCS (%)**	**GRS (%)**	**Edema (%)**	**LGE (%)**	**GCS (%)**	**GRS (%)**
Edema (%)	-	ρ=0.627 p=0.039*	ρ=-0.236 p=0.484	ρ=0.291 p=0.385	-	ρ=0.220 p=0.211	ρ =.459 p=0.006*	ρ=-0.250 p=0.154	-	ρ=-0.041 p=0.822	ρ=-0.049 p=0.787	ρ=-0.243 p=0.174
LGE (%)		-	ρ=0.046 p=0.763	ρ=-0.345 p=0.019*		-	ρ=0.365 p=0.014*	ρ=-0.332 p=0.026*		-	ρ=0.307 p=0.038*	ρ=0.061 p=0.687
GCS (%)			-	ρ=-0.508 p<0.001*			-	ρ=-0.580 p<0.001*			-	ρ=-0.382 p=0.009*
GRS (%)				-				-				-

Table 8 *Correlations throughout groups*

For global circumferential strain at acute phase, intra-reader reproducibility was 74% with a bias of 0.43% and a CoR of 5.48%, while inter-reader reproducibility was 68% with a bias of 3.57% and a CoR of 6.26%. For global circumferential strain at follow-up, intra-reader reproducibility was 79% with a bias of 0.29% and a CoR of 4.35%, while inter-reader reproducibility was 72% with a bias of 2.44% and a CoR of 5.43%. For global circumferential strain in controls, intra-reader reproducibility was 90% with a bias of -0.45% and a CoR of 2.06%, while inter-reader reproducibility was 83% with a bias of 0.75% and a CoR of 3.64%. For global radial strain at acute phase, intra-reader reproducibility was 45% with a bias of 1.39% and a CoR of 39.67%, and inter-reader reproducibility was 52% with a bias of -9.52% and a CoR of 32.88%. For global radial strain at follow-up, intra-reader reproducibility was 51% with a bias of 0.85% and a CoR of 43.46%, while inter-reader reproducibility was 52% with a bias of -14.47% and a CoR of 39.48%. For global radial strain in controls, intra-reader reproducibility was 59% with a bias of 2.26% and a CoR of 33.99%, while inter-reader reproducibility was 15% with a bias of -2.48% and a CoR of 69.89%.

For global circumferential strain, optimal thresholds resulting from receiver operating characteristics curves obtained comparing the acute phase group to controls resulted to be -17.3%, with 44% sensitivity (20/46), 95% specificity (44/46) and an area under the curve of 0.71, the same data for global radial strain being 93%, 96% (44/46), 37% (17/46), and 0.70 (**Figure 14**). Using these thresholds for the diagnosis of myocarditis, the global circumferential strain obtained a positive likelihood ratio of 8.8 and a negative likelihood ratio of 0.59, the same data for global radial strain being 1.52 and 0.11, respectively.

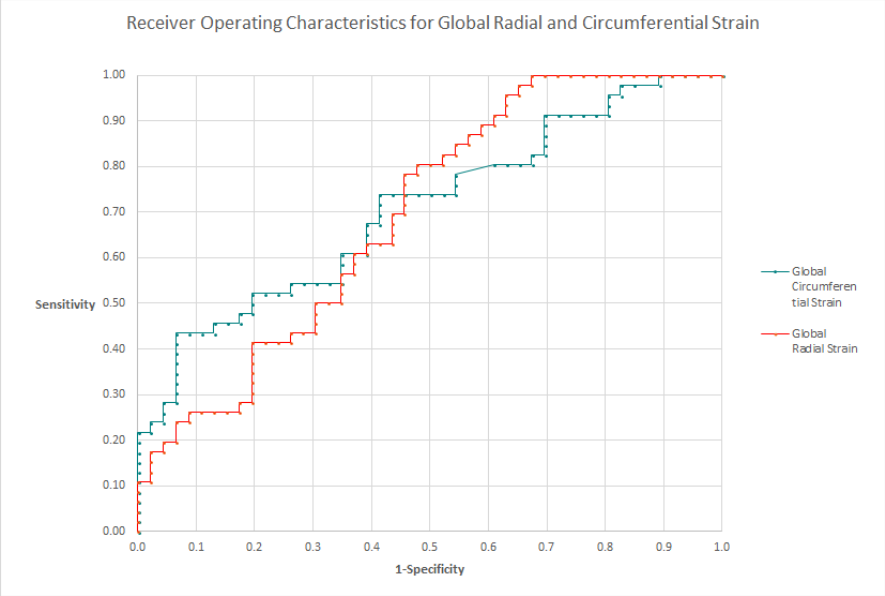

Figure 14 *Receiver operating characteristics for global circumferential and radial strain. The thresholds which best maximized sensitivity and specificity were global circumferential strain -17.28%, with 44% sensitivity, 95% specificity*

Discussion

The main findings of our study involve global radial and circumferential strain, whose absolute values were significantly lower in acute phase myocarditis patients in comparison to controls, along with the absence of significant differences when comparing global circumferential strain between follow-up patients and controls.

During image analysis, manual correction was seldom necessary, most often when calculating myocardial percentages of edema and delayed enhancement, due to signal inhomogeneities which produced errors on the evaluation of standard deviations by the automated software.

Our study population was slightly younger than those most commonly described as affected by myocarditis, likely due to the selection of patients with preserved ejection fraction, which excluded those with other underlying cardiac pathologies, which may be more common as age increases. Our male to female ratio of 3.6 mirrored the one of myocarditis incidence [103,104].

The absence of significant differences in ejection fraction between myocarditis patients and controls may confirm that the analyzed group of patients was composed of individuals with

myocarditis with preserved ejection fraction, for whom CMR is the first proposed imaging technique [105]. Left ventricle late enhancement percentages were well aligned to literature [106].

The fact that global circumferential and radial strain were significantly lower in acute phase myocarditis patients in comparison to controls may indicate that myocardial strain as evaluated by CMR is a good functional index, its absolute value decreasing when contractility is impaired, such as in myocarditis. Literature data support this finding in myocarditis and other cardiac pathologies [107,108]. The absence of significance of differences between acute phase and follow-up could depend on the fact that not all myocarditis patients revert to pre-illness cardiac contractility, some of them retaining residual scarring. The persistence of significant differences between follow-up and controls in global circumferential strain, on the other hand, indicate that not only cardiac function does not improve significantly months after myocarditis, but it also differs from normal values of healthy controls.

The comparison of strain values showed that global circumferential strain is well aligned to literature data [78,109–113] as far as healthy controls are concerned, whereas myocarditis patients [112,113] were reported to have lower global circumferential strain values, likely due to our narrowing to patients with a preserved ejection fraction, while others also comprised patients with a more compromised heart function. Conversely, literature [78,109–113] global radial strain values are noticeably different throughout all groups. Since global radial strain shows significant correlations to global circumferential strain throughout all groups, this is most likely due to the use of a different software for strain calculation.

The significant correlation between global circumferential strain and edema during acute phase can relate the current standard for the CMR diagnosis of myocarditis, namely Lake Louise Criteria [90,91] to global circumferential strain as a new potential diagnostic value. The same is true for correlations between global circumferential strain and late enhancement at both acute phase and follow-up. No correlations could be found between global circumferential strain and edema at follow-

up, since the follow-up interval was set to be longer than three months, and edema, being an indicator of acute inflammation, should have resolved by that time. The significant correlation found between global radial and circumferential strain validates global radial strain as a fellow potential diagnostic value, indirectly related to the current reference standard [91].

The diagnostic performance of global circumferential and radial strain, evaluated through receiver operating characteristics analysis, showed that global circumferential strain may be a good parameter to rule in myocarditis with the best combination of sensitivity and specificity, while global radial strain performs better for ruling out the disease. Global circumferential strain could be used to select negative-testing subjects, in whom sequences other than cine, namely those for late enhancement and for edema, should be performed. Instead, a myocarditis diagnosis can be finalized on these patients who test positive. Conversely, global radial strain may help rule out disease in negative-testing subjects, therefore only performing sequences other than cine on patients testing positive. These biomarkers could help reduce the need of late enhancement and fluid-sensitive sequences, therefore reducing risk of gadolinium retention, patients' discomfort by reducing examination time, and cutting CMR costs in this setting.

While reproducibility was generally good for global circumferential strain, though lower in myocarditis patients, especially at acute phase, the same was not true for global radial strain. Since the contours for strain calculation were the same for both global strain, the lesser reproducibility of global radial strain could probably be explained by its higher absolute values, which may result in higher differences between mean and measurements, and its being more sensitive to accurate contouring than global circumferential strain. In this regard, our data are not aligned with those of Lee et al [113], who report that all strains had an interclass correlation coefficient of 0.87 to 0.98. However, our data is closed by that of Schuster et al [102], who report radial strain to be the least reproducible one, with an interclass correlation coefficient of 0.44, and circumferential strain to have an interclass correlation coefficient of 0.70. The low reproducibility of global radial strain poses

questions with regards to its potential clinical application, while global circumferential strain would seem more reliable in this setting.

Our research has some limitations. It is a single-center, retrospectively designed study, therefore results are related to the specific 1.5-T units used for imaging patients and to the sequences and technical parameters used. However, since 1.5-T units and predefined protocols are commonly used in clinical practice for cardiac imaging, results may be generally accepted. Longitudinal strain could not be assessed, due to three-chamber long-axis sequences missing in a number of patients, thus a precise estimate was not feasible. Moreover, the low reproducibility of global radial strain limits its reliability in diagnosing myocarditis, therefore only global cardiac strain provides a satisfactory performance.

In conclusion, given the diagnostic performance of the two short-axis strain indices, global circumferential strain and global radial strain, CMR-derived strain could potentially have a role in reducing the need of sequences in addition to cine in low-risk myocarditis patients where CMR is the main diagnosing technique. Further studies should be conducted, especially looking at confirmation by using segmental strain. A perspective for properly tailored clinical practice guidelines for cardiac magnetic resonance diagnosis of myocarditis, thus allowing the omission of additional sequences when cine provide enough information, may be open.

Right ventricular strain in repaired Tetralogy of Fallot with regards to pulmonary valve replacement

(from Monti CB, Secchi F, Capra D, Guarnieri G, Lastella G, Barbaro U, Carminati M, Sardanelli F - *European Journal of Radiology* 2020)

Background

Tetralogy of Fallot (ToF) is the most common cyanotic congenital heart defect, with an incidence estimated to be around 5 every 10,000 live births [46]. It is characterized by four main anatomical defects, namely interventricular communication, obstruction of the right ventricular (RV) outflow tract, override of the ventricular septum by the aortic root, and consequent RV hypertrophy [114].

Children with ToF undergo early surgical correction, and their prognosis has considerably improved during latest years, with a 30-year survival rate greater than 90% [115]. Nevertheless, ToF patients require lifelong follow-up to prevent the onset of severe complications. Notably, CMR bears a class I-B recommendation for monitoring RV size and function, pulmonary valve function, pulmonary artery anatomy and left ventricular (LV) abnormalities in repaired ToF [52]. In fact, CMR is the preferred method for non-invasive assessment of ToF patients, as it has proven useful in helping set appropriate timings for further interventions, in particular pulmonary valve replacement (PVR) [116], and in preventing adverse events [117].

Myocardial strain represents the deformation of cardiac fibres through the contractile cycle, and it was first calculated from echocardiography [118]. However, echocardiography bears important intrinsic limitations due to its high operator-dependency and potential technical difficulties [119]. More recently, feature-tracking (FT) strain analysis has been included among the potential post-processing applications of CMR, allowing for a reproducible, quantitative analysis of cardiac contractility with no need for additional sequence acquisition [120]. Strain analysis has been shown

to offer additional information concerning systolic and diastolic dysfunction, beyond that provided by ejection fraction [121], and strain impairment to relate to poor patients' prognosis [122].

Cardiac strain assessed through echocardiography has proven a reliable indicator of ventricular function in adult repaired ToF patients. A previous work by Menting *et al*. [123] highlighted a decrease in RV strain and strain rate, in the presence of impairment of LV septal contractility, indicating how RV dysfunction affects the LV. Given the limitations of echocardiography, strain analysis through FT may represent a simple and non-invasive method to appraise the contractile function of repaired ToF patients who undergo CMR, possibly providing additional data that may aid a more patient-tailored management. While previous studies mostly focused on LV FT-CMR strain [124], RV strain may prove especially interesting considering that the RV is subject to complications from pulmonary valve disease before the LV [125]. More so, previous studies, such as the work by Hamada-Harimura *et al*. [126], observed that RV strain may be a predictor of clinical adverse events.

Thus, the aim of our study was to longitudinally assess RV myocardial strain both globally and segmentally through FT-CMR in ToF patients, with regards to PVR, to appraise its potential value in identifying subclinical impairments of cardiac contractility in such population.

Methods

Study population

This study was approved by the local Ethics Committee (Ethics Committee of BLINDED; protocol code BLINDED; approved on September 14th, 2017 and amended July 18th, 2019). Specific informed consent was waived due to the retrospective nature of this study.

From a total of 246 ToF patients who underwent CMR at our institution between March 2014 and May 2019, 198 were excluded as they did not have a follow-up CMR examination, while 2 were excluded due to the presence of a situs inversus anomaly along with ToF. Thus, we retrospectively included 92 CMR examinations from 46 consecutive patients with a diagnosis of ToF who had undergone two CMR examinations at our institution from March 2014 to June 2019. The population

so obtained was subsequently divided into two groups: those who did not undergo PVR between the two CMR examinations (Group 0), and those who did (Group 1). For each patient, we registered follow-up time between the two CMRs.

Image acquisition

Patients were examined using a 1.5-T unit (Magnetom Aera, Siemens Healthineers, Erlangen, Germany) with 45-mT/m gradient power. According to clinical practice, examinations were performed using a 48-channel surface phased-array coil, placed over the thorax of the patient in supine position. Each exam included a full set of cine images acquired in short-axis and long-axis in 2-, 3-, and 4-chamber view during the whole cardiac cycle, using an electrocardiographic-triggered steady-state free precession pulse sequence, acquired with the following technical parameters: time of repetition 4.0 ms; time of echo 1.5 ms; flip angle 80 degrees; slice thickness 8 mm; time resolution 45 ms. Image acquisition of short- and long-axis views altogether was performed during 10 to 15 breath holds of roughly 20 seconds each, depending on individual patients, for a total acquisition time of about 4-5 minutes.

Image analysis

For each examination, a radiology resident with a 6-year experience in CMR performed segmentation and volumetric analysis. Image analysis was performed using Medis Suite MR Software (Medis Medical Imaging System bv., Leiden, The Netherlands). The QMass tool of the suite was used for evaluation and quantification of ventricular volumes and ejection fraction (EF). The LV and RV endo- and epicardium were manually segmented in cine long and short axis on end-diastolic and end-systolic images. For the purpose of this research, the following data was extrapolated from both CMR exams: LV and RV end-diastolic and end-systolic volumes indexed to body surface area (EDVi and ESVi, respectively), stroke volume (SV), and EF. The RV endo- and epicardium were manually segmented in cine long axis on end-diastolic and end-systolic images.

The QStrain tool of the same suite allowed for calculation of strain and strain rate values, tracing RV endo- and epicardial contours at the end-diastolic and end-systolic phase, and then applying FT calculations. A reader with 3 years of experience in cardiac imaging performed this segmentation. The following strain parameters were extrapolated from both CMR exams: RV global longitudinal strain (G-LS) and global radial strain (G-RS) segmental strains of the RV at the free wall (F-LS and F-RS) and septum (S-LS and S-RS). A depiction of RV segmentation used for strain calculation may be seen in **Figure 15**.

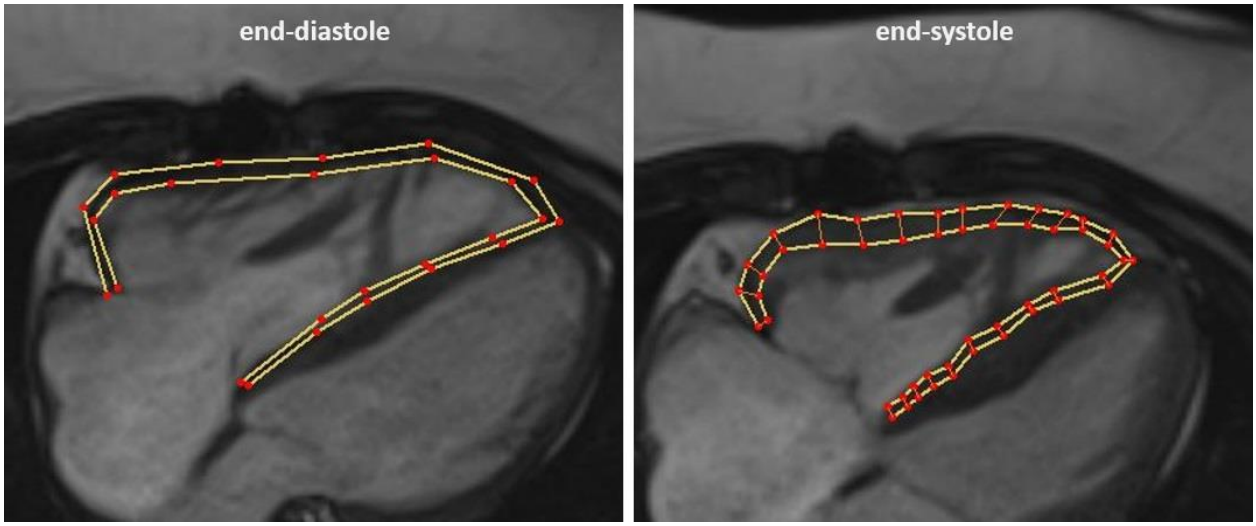

Figure 15 *Example of right ventricular segmentation for strain calculation on a cardiac magnetic resonance during end-diastole and end-systole on a cine 4-chamber acquisition of a 26-year old female tetralogy of Fallot patient.*

Statistical analysis

Shapiro-Wilk tests were conducted to assess data distribution. Normally distributed data were reported as mean ± standard deviation. Non-normally distributed data were reported as median and interquartile range (IQR). To account for potential differences in follow-up duration, volumetric, functional and strain parameters variations between the first and second CMR were computed and then divided by each patient's individual years of follow-up, to obtain a variation rate per year.

Measurements were compared using Student *t* test for normal distributions, Mann-Whitney *U* test for non-normal distributions. Statistical analysis was performed with Python v3.7.6. We considered p-values < 0.05 as significant [127].

Results

Out of the 92 included patients, 30 had not undergone PVR between the two CMRs and belonged to Group 0, while 16 had and hence belonged to Group 1.

Median age was 22 years (IQR 17-29 years) in Group-0, and 21 years (IQR 16-29 years) in Group-1. Demographics for all patients are reported in **Table 9**. The median time between the two CMRs was 2.3 years (IQR 1.9–3.0 years) in Group 0, significantly longer (p = 0.001) than the 1.4 years (IQR 1.0–2.1 years) in Group 1.

	Group 0 (n=30)	**Group 1** (n=16)	***p***
Age (years)	22 (17–29)	21 (16–29)	0.846
Males (n, %)	10 (63)	12 (40)	0.217
Time between CMR 1 and CMR 2 (years)	2.3 (1.9–3.0)	1.4 (1.0–2.1)	**0.001***

Table 9 *Demographical data for the study population. CMR 1, first cardiac magnetic resonance examination; CMR 2, second examination. Data are presented as median and interquartile range.*

Ventricular functional data

Functional data of the LV and RV in our study population are reported in **Table 2**. In particular, at CMR1 RV EDVi was 88 mL/m^2 (IQR 74–111 mL/m^2) in Group 0, significantly lower (p = 0.011) than the 120 mL/m^2 (IQR 104–128 mL/m^2) in Group 1. Similarly, RV ESVi was 40 mL/m^2 (IQR 31–46 mL/m^2) in Group 0, significantly lower (p = 0.015) than the 53 mL/m^2 (IQR 43–59 mL/m^2) in Group 1. Moreover, RV SV appeared borderline significantly lower (p = 0.055) in Group 0 (87 mL, IQR 67–109 mL) than in Group 1 (103 mL, IQR 83–130 mL). No other differences in functional parameters were observed between the two groups at either CMR examination ($p \geq 0.133$).

Right ventricular strain

The RV strain parameters are reported in **Table 10**. No significant differences were observed in RV strain between Group 0 and Group 1 ($p \geq 0.254$) except for RV S-RS, which, at CMR 2, was significantly higher in Group 0 (24.2%, IQR 10.1–52.4%) than in Group 1 (6.0%, IQR -3.3–23.3%) (p = 0.010).

	CMR 1			CMR 2		
	Group 0	**Group 1**	***p***	**Group 0**	**Group 1**	***p***
LV EDVi (mL/m²)	71 (63–82)	70 (62–71)	0.326	78 (67–93)	81 (69–90)	0.999
LV ESVi (mL/m²)	26 (22–32)	24 (21–28)	0.488	33 (26–37)	32 (25–34)	0.460
LV SV (mL)	78 (59–91)	68 (63–81)	0.426	86 (71–101)	83 (64–94)	0.481
LV EF (%)	63 (59–65)	63 (59–67)	0.853	59 (55–63)	63 (59–64)	0.133
RV EDVi (mL/m²)	88 (74–111)	120 (104–128)	**0.011***	96 (80–119)	94 (78–101)	0.289
RV ESVi (mL/m²)	40 (31–46)	53 (43–59)	**0.015***	43 (37–52)	41 (33–48)	0.496
RV SV (mL)	87 (67–109)	103 (83–130)	0.055	85 (65–120)	90 (73–96)	0.556
RV EF (%)	57 (48–65)	54 (51–58)	0.595	55 (49–62)	53 (50–60)	0.661
RV G-LS (%)	-23.0 (-26.9—21.9)	-22.6 (-24.8—19.6)	0.254	-20.5 (-25.3—16.7)	-19.6 (-22.6—17.0)	0.673
RV G-RS (%)	36.0 (16.6–99.8)	41.2 (27.2–70.7)	0.918	40.4 (25.6–68.5)	26.2 (14.4–44.0)	0.310
RV F-LS (%)	-23.1 (-28.1—11.3)	-26.0 (-28.4—21.7)	0.298	-19.9 (-25.7—13.0)	-18.9 (-23.9—8.6)	0.515
RV F-RS (%)	29.6 (10.1–71.6)	41.5 (11.8–67.0)	0.991	33.6 (13.3–56.8)	25.2 (16.0–50.1)	0.758
RV S-LS (%)	-15.6 (-18.9—11.9)	-14.2 (-17.5—10.7)	0.404	-15.0 (-18.8—11.6)	-14.1 (-19.4—8.4)	0.545
RV S-RS (%)	18.8 (2.9–50.5)	21.1 (7.1–50.0)	0.882	24.2 (10.1–52.4)	6.0 (-3.3–23.3)	**0.010***

Table 10 *Functional data for the left (LV) and right (RV) ventricle and RV strain parameters at the first (CMR 1) and second (CMR 2) cardiac magnetic resonance, in patients who did not (Group 0) or did (Group 1) undergo pulmonary valve replacement between CMR 1 and CMR 2. EDVi, end-diastolic volume index; ESVi, end-systolic volume index; SV, stroke volume; EF, ejection fraction; LS, longitudinal strain; RS, radial strain; G, global; F, free wall; S, septal. Data are presented as median and interquartile range.*

Variations between CMR 1 and CMR 2

Variation rates for each of the assessed parameters are reported in **Table 11**.

Concerning functional parameters, LV EDVi displayed a significantly lower (p = 0.023) yearly increase of 2 mL/m² ·year (IQR 0–4 mL/m² ·year) in Group 0 than that in Group 1 of 7 mL/m² per year (IQR 5–10 mL/m2 per year). The same was observed for LV SV, which showed a significantly lower (p = 0.018) yearly increase in Group 0 (2 ml/year, IQR -1–5 mL/year) than in Group 1 (9 mL/year, IQR 2–15 mL/year). There were no significant differences between Group 0 and Group 1 concerning LV ESVi (p = 0.200) and LV EF (p = 0.213). Conversely, RV EDVi showed a significantly higher (p < 0.001) increase in Group 0 (3 mL/m² ·year, IQR -1–5 mL/m² ·year) compared to the decrease in Group 1 (-19 mL/m² per year, IQR -26–-7 mL/m² per year). The same trend was observed for RV ESVi, which showed a variation rate of 2 mL/m² ·year (IQR -2–5 mL/m² ·year) for Group 0, and -9 ml/m2·year (IQR -12–-1 mL/m² per year) for Group 1 (p < 0.001), and RV SV, which had a variation rate of 2 ml/year (IQR -4–8 mL/year) in Group 0, and -19 ml/year (IQR -26–-3 ml/year) in

Group 1 ($p < 0.001$). There were no significant differences in the variation rate of RV EF, which was -1%/year (IQR -4–1%/year) in Group 0, and 0%/year (IQR -2–2%/year) in Group 1 ($p = 0.227$).

RV strain variations over time did not differ significantly between the two groups ($p \geq 0.081$) (**Figure 16**).

	Variation per year		
	Group 0	**Group 1**	***p***
LV EDVi (mL/m²)	2 (0–4)	7 (5–10)	**0.023***
LV ESVi (mL/m²)	2 (0–4)	3 (1–6)	0.200
LV SV (mL)	2 (-1–5)	9 (2–15)	**0.018***
LV EF (%)	-1 (-4–0)	1 (-4–2)	0.213
RV EDVi (mL/m²)	3 (-1–5)	-19 (-26–-7)	**<0.001***
RV ESVi (mL/m²)	2 (-2–5)	-9 (-12–-1)	**<0.001***
RV SV (mL)	2 (-4–8)	-19 (-26–-3)	**<0.001***
RV EF (%)	-1 (-4–1)	0 (-2–2)	0.227
RV G-LS (%)	0.81 (-1.70–2.13)	1.24 (-1.55–3.49)	0.369
RV G-RS (%)	-3.67 (-34.63–19.23)	-10.13 (-34.51–-2.46)	0.187
RV F-LS (%)	2.00 (-0.57–3.57)	1.61 (-4.51–11.12)	0.459
RV F-RS (%)	-4.36 (-11.23–10.05)	-4.32 (-27.44–4.10)	0.271
RV S-LS (%)	0.29 (-2.41–3.09)	0.53 (-2.59–4.40)	0.422
RV S-RS (%)	3.48 (-11.85–48.53)	5.20 (-17.78–0.66)	0.081

Table 11 *Annual variations of left (LV) and right ventricular (RV) functional data and RV strain parameters. EDVi, end-diastolic volume index; ESVi, end-systolic volume index; SV, stroke volume; EF, ejection fraction; LS, longitudinal strain; RS, radial strain; G, global; F, free wall, S, septal. Data are presented as median and interquartile range.*

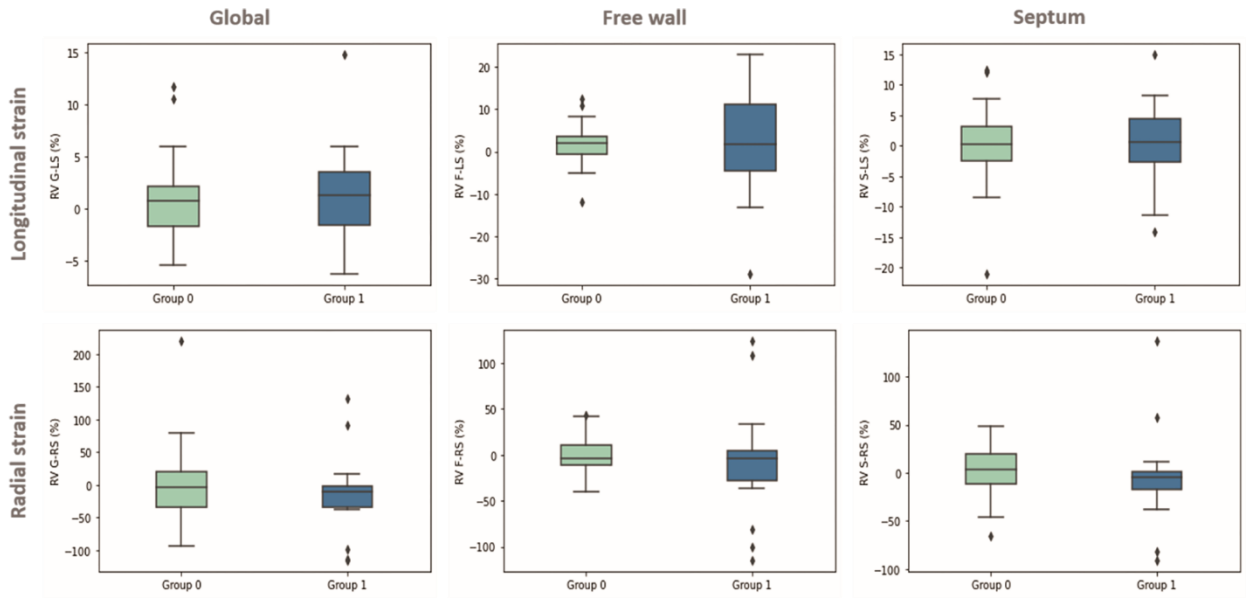

Figure 16 *Boxplots for right ventricular (RV) strain variations per year in the two groups of tetralogy of Fallot patients, who did not undergo (Group 0) or underwent (Group 1) pulmonary valve replacement in the time interval between*

the two cardiac magnetic resonance examinations. No significant differences may be observed between the two groups for any RV strain parameter.

Discussion

While the lifespan of ToF patients is increasing, novel biomarkers which may aid patient monitoring, along with the prediction and prevention of potential adverse events are all the time more sought for. From its recent introduction, myocardial strain assessed through FT-CMR has shown good reproducibility [128] and a potential for a subclinical assessment of cardiac contractility. Thus, in this study, we aimed to assess RV strain and its modifications in a cohort of ToF individuals with regards to PVR intervention.

Our study population appeared well-representative of a cohort of young adult ToF patients, with median ages at the first CMR of 22 and 21 years in patients who did not (Group 0) or did (Group 1) undergo PVR between the two analysed CMR exams, respectively. One study by Harrild *et al*. [129] reported a median age of ToF patients undergoing PVR to be around 21 years, thus our population fits into their estimate, given that a number of our patients underwent PVR soon after. The different timing between the two CMR examinations is probably due to the fact that patients who underwent PVR were in need of a closer imaging follow-up, while the others performed a subsequent CMR examination after about 2 years [130].

The significantly higher RV EDVi, ESVi and SV observed in Group 1 seems indicative of the fact that such individuals were soon referred for PVR due to worse pulmonary valve functionality and RV deterioration. In fact, indications for PVR include the evaluation of RV indexed volumes [51].

Concerning annual variations of functional parameters, the higher increase in LV EDVi and SV and the higher decrease in RV EDVi, ESVi and SV in Group 1 appear likely owing to the concomitant PVR intervention in such population. Appropriate indications for PVR allow for potential RV volume reduction once the regurgitant burden on the RV is lessened [131]. In particular, Oosterhof *et al*. [132] indicate thresholds for RV EDVi and ESVi of 160 mL/m^2 and 82 mL/m^2 respectively, over which PVR may no longer be lead to RV remodeling . Thus, the steep early decline in RV EDVi, ESVi, and SV

in Group 1 patients was expected, as a positive turnaround of PVR. The concomitant greater rise in LV EDVi and SV in Group 1 is in line with findings reported by Chalard *et al*. [133], who observe variations in LV volumes and function as an additional benefit of PVR. While those authors also observed an increase in LV EF after PVR, our population exhibited a median yearly increase in LV EF after PVR of 1%, thus not substantially different from the lack of variations in patients who did not undergo PVR.

No differences between RV global or segmental strain variations over time were observed among the two groups, possibly indicating that, while volumes may find benefit from PVR, the underlying decline in cardiac strain does not seem affected by such intervention. Our findings are in partial agreement with those from one study by Balasubramanian *et al*. [134] who calculated FT-CMR strain in 36 ToF patients who underwent PVR suggesting that such intervention could not determine any changes in the RV strain. The lack of difference with those who did not undergo PVR observed in our work suggests that in both groups RV contractility trends toward a decline, albeit likely not significant at less than one year after PVR intervention, which was the follow-up timing of the work by Balasubramanian *et al*. [134] On the same note, one work by DiLorenzo *et al*. [135] observed a continuous decline in strain in ToF patients after surgical repair, attributing it to a subclinical, subtle initial sign of long-term dysfunction. Moreover, a study by Hallbergson *et al*. [136], suggests that by 7 to 10 years after PVR, RV EDVi and ESVi revert to pre-PVR values associated to higher RV volume and pressure load, thus implying the presence of a constant underlining functional deterioration.

RV strain and its clinical implications have been previously investigated by several studies. For instance, RV strain has shown correlations to clinical outcomes in heart failure, pulmonary embolism, and pulmonary hypertension [126,137–139]. Concerning ToF patients, conversely, Jing *et al*. [140] did not observe significant correlations between FT-CMR strain and functional parameters at a subsequent CMR after about 3 years in a population of 153 patients with ToF. However, considering that the volumetric and functional deterioration that happens in ToF patients is somewhat slow and

that functional parameters may indeed find benefit from treatment, such findings may have been influenced by a short follow-up time and different patient management. More so, as volumes and function may macroscopically improve after interventions such as PVR, they may not prove the only predictors of adverse events in ToF patients [141]. In this regard, myocardial tissue characterization may play an interesting role, as recently a growing number of studies has observed that RV focal scar and diffuse fibrosis may help predict the onset of ventricular arrhythmias [142], also in ToF patients [143]. In particular, in this latter population, the decline in RV strain may relate to the subtle functional decline related to myocardial fibrosis [144].

Our study has some important limitations. First, as follow-up times were not standardized, it was not possible to assess and compare overall variations of functional data and RV strain in the two groups, as results might have been biased by such heterogeneity. Nevertheless, the assessment of yearly variations in such parameters may provide some insight in this regard. Secondly given the relatively short follow-up time in our study (shorter than 6 years) we were unable to relate strain variations to adverse events, as such events may need longer follow-up to be observed. Therefore, to find clinical correlations between strain and adverse events, a prospective longitudinal study with appropriate follow-up time would be warranted. Another potential limitation may rise from the different time intervals between CMR examinations, due to the fact that patients who underwent PVR were subject to a stricter follow-up, which led to the impossibility to compare raw volumetric and functional data between groups. To overcome this limitation, we assessed variations over time, normalizing for intercurrent intervals.

As already known from previous studies, performing PVR at the appropriate timing leads to improvements in the myocardial function of ToF patients, in particular relating to the reduction in RV volumes. Nevertheless, regardless of this functional improvement, RV strain continues to deteriorate over time, comparably to what happens in patients who do not undergo PVR. Therefore, considering the proven clinical significance of RV strain in cardiovascular disease, it might be useful

to keep such parameter into consideration while assessing ToF patients as a potential predictor of adverse events. Further prospective longitudinal studies are warranted to confirm this hypothesis.

EXTRACELLULAR VOLUME FRACTION

Myocardial ECV represents the fraction of the heart that is composed by extracellular matrix as opposed to cardiomyocytes [2]. A first non-invasive method to appraise myocardial ECV was introduced via CMR, combining the analysis of pre- and post-GBCA contrast injection T1 time maps with individual hematocrit values, according to the following formula [145]:

$$ECV = (1 - haematocrit)\frac{\frac{1}{post\ contrast\ T1\ myo} - \frac{1}{native\ T1\ myo}}{\frac{1}{post\ contrast\ T1\ blood} - \frac{1}{native\ T1\ blood}}$$

This formula helps assess the difference in GBCA concentration variations between the myocardium and blood pool, which are highly dependent on tissue wash-out patterns, that in turn derive from tissue composition [146]. In particular, a higher prevalence of extracellular matrix leads to longer wash-out times. Thus, post-contrast T1 maps need to be acquired at equilibrium times, around 10 minutes after GBCA injection [147].

Healthy subjects have been described to have a median ECV of about 25% [148]. Patients with pathologies which lead to an increase of the fatty content of the myocardium and thus a decrease of the extracellular matrix, such as lipomatous metaplasia or Fabry disease, report a decrease in ECV values. Conversely, patients who present with myocardial fibrosis, inflammation or increased deposition of extracellular matrix, such as in amyloidosis, report higher ECV values [149].

While CMR-derived ECV has shown strong correlations with histology, proving a reliable indicator of myocardial fibrosis or extracellular compartment increase, its evaluation requires both additional sequences which are not routinely performed, and the availability of hematocrit values close to the date when CMR is performed [150]. Therefore, given the analogous extracellular nature of GBCAs used for CMR and iodine-based contrast agents used for CT, some authors proposed a novel method for evaluating ECV from contrast-enhanced CT examinations, using both a baseline acquisition, and a delayed, post-contrast equilibrium scan.

The assessment of ECV in cardiac pathology has provided interesting insight, with its gaining prominence as a biomarker of both cardiac involvement and prognosis [151]. Nevertheless, while cardiovascular diseases are still the main cause of global morbidity and mortality, the incidence of malignant tumors is rapidly increasing, and the two entities cannot be considered entirely separate due to both having common risk factors, and to the potential cardiac toxicity of numerous cancer treatments [152]. Therefore, the aim of this section of the work was to evaluate the role of ECV as a biomarker of cardiotoxicity in patients undergoing cancer treatment, to ascertain whether its assessment could help identify patients more likely to encounter adverse effects, and tailor their treatment accordingly.

Native T1 mapping and extracellular volume fraction as CMR biomarkers of cancer treatment cardiotoxicity: a systematic review

(under review)

Background

Mortality from most types of cancer has greatly decreased in the last years, due to the improvement in screening programs and, more importantly, in treatment efficacy [153]. However, cancer treatments yield a significant burden of side effects, among which cardiovascular complications arising from non-reversible cardiotoxicity are a major concern [154]. The main treatments associated with cardiotoxicity are chemotherapy with anthracyclines, radiation therapy, and targeted therapies such as monoclonal antibodies [155].

Cardiotoxicity from cancer treatment is defined as a decline of 10% or more in left ventricular ejection fraction (LVEF) during or after treatment. Nevertheless the heart presents a significant functional reserve, thus substantial damage may occur before an overt LVEF reduction [156]. The American Heart Association/American College of Cardiology guidelines [157,158] for anthracycline-induced cardiotoxicity monitoring recommend the use of radionuclide imaging, including multi-gated acquisition scans, and echocardiography for LVEF monitoring. Over the years, different potential biomarkers have been proposed, however none so far has yielded high accuracy in detecting subtle myocardial changes before overt heart failure in clinical practice [159].

In recent years, parametric mapping techniques from CMR emerged as tools to assess myocardial tissue composition. In particular, native T1 (nT1) mapping techniques provide non-contrast T1 relaxation times for the whole myocardium on a voxel-by-voxel basis [2]. Increases in nT1 may be expected in case of oedema or fibrosis, which are the macroscopic signs of cellular death

by apoptosis and necrosis. Extracellular volume fraction (ECV) reflects the percentage of the heart that is not composed by cells, and thus ECV too increases in presence of oedema or extracellular deposition, such as in fibrosis or amyloidosis [160]. Myocardial nT1 mapping and ECV present as two emerging biomarkers that allow cardiac tissue characterization, their values rising with interstitial expansion in conditions such as myocardial inflammation or fibrosis [145]. Both nT1 mapping and ECV showed a good correlation with histological findings [161]. As cardiotoxicity from cancer treatment is represented by cardiomyocyte death which eventually leads to fibrosis, such techniques may allow an early and accurate detection of subtle changes in the myocardial tissue.

Therefore, the aim of this systematic review was to investigate the studies exploring the role of native T1 mapping and ECV as biomarkers of cardiotoxicity to better understand their clinical role in this setting.

Methods

Search strategy and eligibility criteria

Ethics committee approval was not required for this systematic review. The systematic review was reported according to the Preferred Reporting Items for Systematic reviews and Meta-Analyses (PRISMA) statement [162] and the study was registered on ResearchGate.

In October 2019, a systematic search on EMBASE (Excerpta Medica dataBASE, embase.com) and PubMed (U.S. National Library of Medicine, pubmed.ncbi.nlm.nih.gov) for articles on the use of CMR-derived T1 mapping and ECV as a cardiotoxicity biomarker.

The search string adopted included MeSH terms and candidates such as ‘neoplasms’, 'chemotherapy', 'radiotherapy', 'nuclear magnetic resonance imaging', and 'extracellular volume fraction'. The search was limited to unique articles describing original studies performed on human subjects with available abstract and written in the English language. No limits were applied to publication date.

Data extraction

Two readers (with 3 and 2 years of experience in CMR), in consensus, performed a first selection based on title and abstract only. All selected articles, including those with abstracts lacking complete information to determine exclusion/inclusion, were then downloaded, and, after full-text screening, only those reporting CMR nT1 mapping or ECV values after or during cancer treatment were included. Lastly, references from the included articles that could potentially meet the inclusion criteria were subsequently manually screened.

The same researchers who performed the literature search independently extracted all data and disagreements were resolved by consensus. For each included article, when available, the following data were extracted: year of publication and country of origin, study design (prospective or retrospective), population demographics and clinical data (e.g. gender and LVEF), type of malignancy and treatment, CMR protocol, values of myocardial nT1 mapping, and ECV.

Results

Study selection

From 271 initially retrieved articles, 28 were included after the first selection based on article title and abstract. Out of the excluded articles, 111 referred to a non-cardiac extracellular volume (i.e. hepatic), 79 were case reports, 29 were reviews, and 24 did not report results from CMR. Out of the 28 articles included at the first selection, 17 did not report ECV or T1 values in the full text, leading to a final number of 11 included papers.

Included works [163–173] were published between 2013 and 2019, and all but one [165] had a prospective design. Three studies included only patients with breast cancer [167,168,170], one studied patients with oesophageal cancer [172], while the others included patients with mixed types of neoplasm, most commonly breast, hematologic malignancies and sarcomas. Concerning cancer treatment, 8 articles analysed the cardiotoxic effects of anthracyclines [163–168,170,171], 1 focused on radiation therapy [172], 1 on bortezomib-based regimens [169], and 1 on different treatment combinations [173].

Scans were performed in 1.5-T (n = 4) and 3-T systems (n = 5); two studies did not report this data. Clinical and MRI data for each study are reported in **Table 12** and **Table 13**, respectively.

Native T1 quantification

We analyzed 8 studies reporting myocardial nT1 values [164–167,170–173], with findings summarized in **Figure 17**.

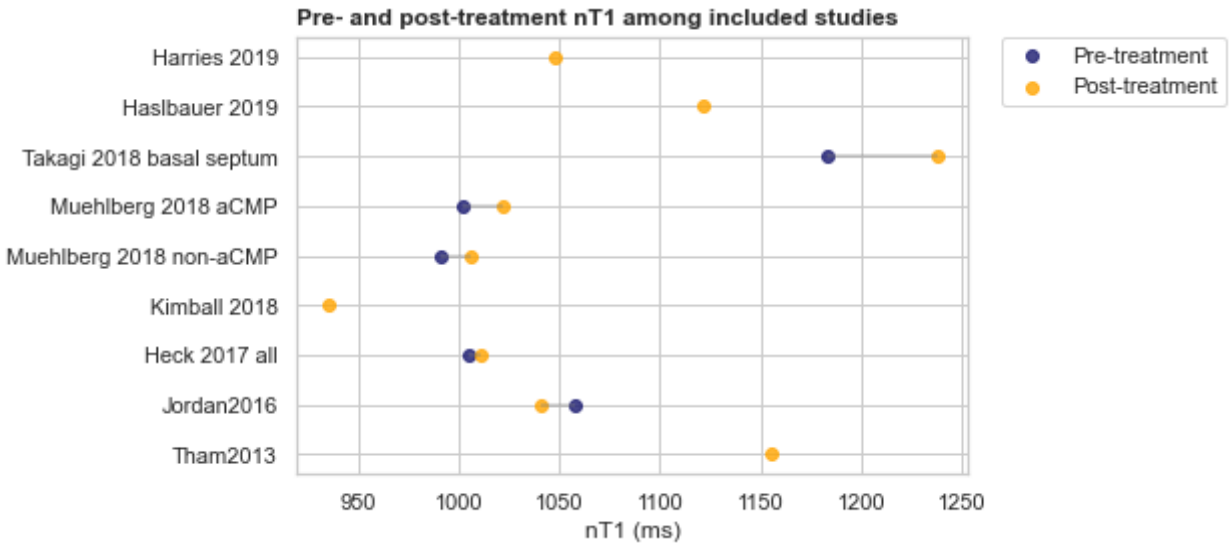

Figure 17 *Values of myocardial nT1 reported among the included studies*

Most of the included works observed a trend towards the increase of nT1 values with cancer treatment. Jordan et al. [166] found elevated nT1 in cancer patients before and after treatment with anthracyclines, compared to healthy controls (1058 ± 7 ms and 1041 ± 7 ms, respectively vs 965 ± 3 ms, $p < 0.01$). Tham et al. [164] observed an elevated post-treatment nT1 (1155.3 ± 56.5 ms) in 30 patients treated with anthracyclines. Harries et al. [165] found an elevated nT1 in 13 patients treated with anthracyclines (1023 ± 28 ms vs 1092 ± 20 ms), with a concomitant rise in LVEF. Takagi et al. [172] observed a significant rise in nT1 in patients with esophageal cancer treated with radiation therapy, in particular, concerning the basal septum, which was included in the radiation field: nT1 was 1183 ± 46 ms at baseline, 1257 ± 35 ms six months after treatment and 1238 ± 56 ms eighteen months after treatment. Haslbauer et al. [173] found a nT1 of 1137 ± 61 ms in patients treated with

anthracyclines for breast cancer within the previous 3 months, and of 1121 ± 46 ms in those treated more than 1 year before.

Conversely, other works found no differences in nT1 values after cancer treatment. For instance, Kimball et al. [170] reported a nT1 of 935 ± 48 ms, well within normal limits, 5 years after the end of treatment with anthracyclines and trastuzumab. On a similar note, Heck et al. [167] observed normal nT1 values before (from 1004 ± 33 ms and 1006 ± 31 ms) and after treatment with low and high anthracycline doses (1012 ± 34 ms and 1006 ± 31 ms, respectively), without significant differences.

Additional evidence revealed a decrease in nT1 soon after treatment with anthracyclines. One retrospective study by Muehlberg et al. [171] observed significantly decreased nT1 values were (956.5 ± 29.2 ms, $p < 0.01$ vs pre-treatment) in a subgroup showing cardiotoxicity, but not in the other subgroup not showing cardiotoxicity (978.4 ± 57.4 ms; $p = 0.08$ vs pre-treatment).

Extracellular volume

We reviewed eight studies analyzing the role of ECV as a cardiotoxicity biomarker [163,164,166–169,171,172]. Findings from such works are reported in **Figure 18**.

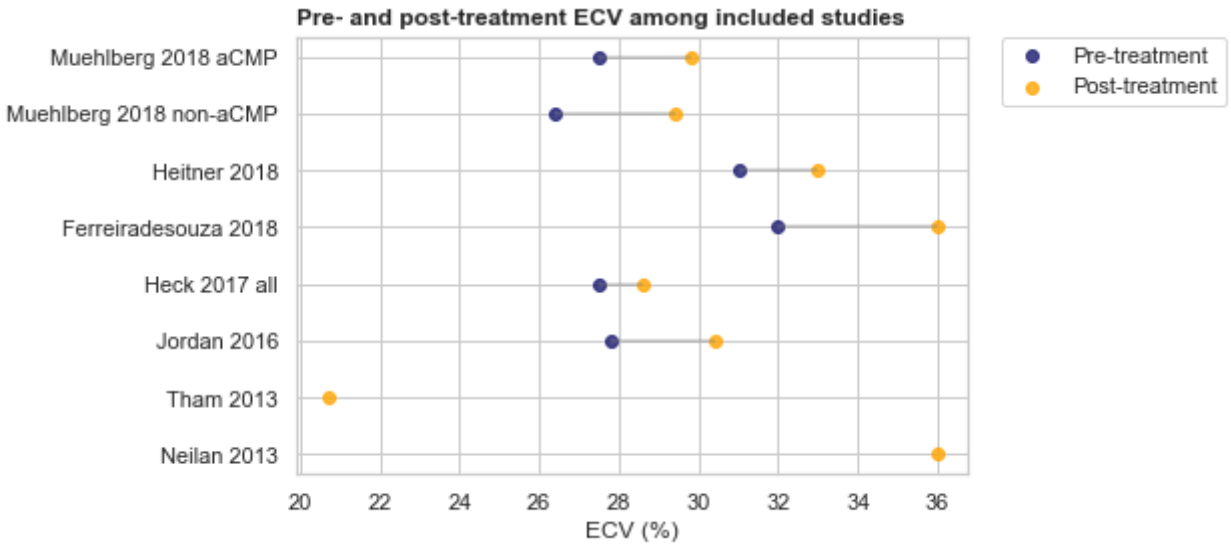

Figure 18 *Values of extracellular volume (ECV) reported among the included studies. Of note, the work by Tham et al. includes a pediatric population, where ECV is generally lower than adults*

Most studies found evidence that ECV may be a viable early biomarker of cardiotoxicity, with increased values after chemotherapy compared to healthy controls or patients' previous own values. In the work by Neilan et al. [163] the average myocardial ECV was higher in patients treated with anthracyclines with preserved LVEF compared to 15 age- and sex-matched healthy controls (36 ± 2% vs 28 ± 2%, $p < 0.001$). Similarly, Muehlberg et al. [171] found that ECV in patients with cardiotoxicity rose significantly from 27.5 ± 2.7% at baseline to 29.8 ± 1.7% at treatment completion. Furthermore, Heck et al. [167] described that ECV rose from 27.5 ± 2.7% to 28.6 ± 2.9 % in patients treated with epirubicin for breast cancer, and from 27.3 ± 3.1% to 30.6 ± 3.7% in patients treated with higher epirubicin doses. Jordan et al. [166] found ECV to be borderline significantly higher in patients treated with anthracyclines (30.4 ± 0.7%) than non-anthracycline patients (29.5 ± 1%, $p = 0.11$). Moreover, ECV in anthracyclines patients was significantly higher than in cancer patients before treatment (27.08 ± 0.70%, $p < 0.01$) and healthy controls (26.9 ± 0.2%, $p < 0.001$). Ferreira de Souza et al. [168] performed CMRI on women with breast cancer treated with anthracyclines registering a baseline LVEF of 69.4 ± 3.6% and ECV of 32 ± 3.8%. ECV increased at all follow up times, peaking at a value of 36 ± 4% 351 to 700 days after the end of treatment ($p = 0.0035$) and was associated with a reduction in LVEF of more than 10%. ECV as an early biomarker of cardiotoxicity was also investigated for radiation therapy: Takagi et al. [172] studied 24 esophageal cancer patients who underwent chemoradiotherapy. In the basal septum, ECV rose significantly to 33 ± 3% on 21 patients at 6 months, whereas at 1.5 years on 14 patients it was not elevated compared to baseline.

Other studies did not observe differences in ECV related to cancer treatment. One study by Tham et al. [164] did not find an impaired ECV in 30 cancer survivors aged 15.2 ± 2.7 years who had been treated with anthracyclines, in remission for at least two years. Nevertheless, ECV value correlated with anthracycline doses ($r = 0.40$, $p = 0.036$). ECV was also appraised in one study investigating the potential cardiotoxicity of bortezomib, a proteasome inhibitor, which saw no difference in ECV values between baseline and end of treatment [169].

Discussion

Cardio-oncology is an emergent cross-disciplinary field [174]. Even though comorbidity of cancer in patients with cardiovascular disease and *vice versa* is a very large topic fueled by increasing longevity worldwide, cardio-oncology is mainly considered a kind of "collaborative subspecialty focused on the prevention, management and mitigation of cardiovascular disease in cancer patients in order to achieve optimal patient outcomes" [175]. In this framed field, cardiotoxicity from anti-cancer treatment occupies a central position.

Currently, cardiotoxicity is monitored through recurrent echocardiographic examinations, and detected by a decline in LVEF [176]. Nevertheless, LVEF decreases only when the systolic function is considerably damaged, thus such monitoring only detects overt cardiotoxicity, and does not allow early identification of high-risk patients.

For this purpose, different biomarkers have been proposed. For instance, different studies assessed the role of troponin I as indicating cardiac damage, albeit with inconsistent results among different neoplasms and treatment, likely due to the fact that troponin I responds to early cardiac damage rather than fibrosis [177,178]. Similarly, natriuretic peptides have been studied in patients treated with trastuzumab, anthracyclines or radiation therapy, again with varying results [179,180].

Other imaging techniques, such as nuclear medicine, have been proposed for the early detection of cardiotoxicity. For instance, multiple gated acquisition scintigraphy, which allows LVEF estimation, has been utilized as a surrogate of echocardiography [181]. Nevertheless, such techniques imply a substantial radiation exposure, and bears the same limitations of echocardiography, identifying cardiotoxicity only when it has already caused overt functional damage.

More recently, MR myocardial tissue characterization techniques such as nT1 and ECV have been proposed as early biomarker of cardiotoxicity [2]. A rise in nT1 is expected in the presence of edema or protein deposition as in fibrosis, while a fall in nT1 in the case of iron or fat accumulation [182]. A

rise in ECV reflects myocardial interstitial expansion as in myocardial fibrosis or amyloidosis [149], whereas a decrease is associated with thrombus or lipomatous metaplasia [145]. Normal myocardial nT1 values in healthy subjects have been estimated to be 976 ms (95% confidence interval [CI] 969–983 ms) in a meta-analysis by Gottbrecht et al. [183]. With regards to ECV, the reference normality interval obtained from a recent meta-analysis [148] ranges from 19.6 to 31.6%, with a point estimate of 25.6%.

Concerning the role of nT1 as a biomarker of cardiotoxicity, there seems to be a rise of nT1 in association to cancer treatments that yield known cardiovascular adverse effects, such as anthracyclines and radiation therapy [164–166,172,173]. This rise in nT1 is expected, as cardiotoxicity from such treatment options ultimately leads to cell death by apoptosis or necrosis, and thus myocardial edema and fibrosis, the latter of which is irreversible [184]. In fact, the persistence of the rise of nT1 of the irradiated portion of the heart at follow-up observed by Takagi et al. [172] for esophageal cancer patients undergoing radiation therapy confirms this hypothesis. In most of the studies reporting increases in nT1, the fact that LVEF was well within normal range suggests that the variation of nT1 may be an early biomarker, capable of detecting changes related to cardiotoxicity such as edema or fibrosis before cardiac function is impaired. However, not all evidence is in agreement in detecting a rise in nT1 after treatment [167,170]. This may be explained by the fact that relative changes in nT1 consequent to cardiotoxicity were (relatively) small compared to its absolute value. Moreover, nT1 mapping is unable to identify extracellular space, thus it may be of limited utility in an early inflammatory phase [185].

Regarding the potential role of ECV as a biomarker of cardiotoxicity, an increase in ECV was consistently found across all the analysed studies [163,166–168,171] assessing anthracycline-based chemotherapy, and its increased value was found to be consequently related to anthracycline doses [164,167]. Such a rise was expected, as the key mechanism of anthracycline cardiotoxicity is myocyte death via necrosis or apoptosis [181], resulting in myocardial fibrosis. Moreover, after

chemotherapy, ECV was found to be elevated both in patients with normal LVEF [163,166,167] and in those with impaired LVEF [163,168,171], with a greater rise in patients who developed cardiotoxicity. This suggests the ability of ECV to detect not only overt, but also subtle changes in myocardial composition that might be compensated from a functional viewpoint.

Thus, considering both biomarkers, it may seem that ECV might have an edge over nT1, because even though the latter does not require contrast agent administration, the former has shown to associate to patient prognosis [186], and may therefore provide additional clinical information. Additionally, ECV does not depend on magnetic field strength, whereas nT1 does, leading to difficulties in establishing global reference ranges [145]. Moreover, while the evaluation of nT1 pertains only to MRI, the evaluation of ECV can also be performed at computed tomography (CT) [160], which may prove to be advantageous as chest CT is already included in the workflow for diagnosis and follow-up of a number of different neoplasms [187]. CT-derived ECV has shown strong correlations to MRI-derived ECV [150], thus findings related to the role of ECV in monitoring cardiac toxicity from cancer treatment may potentially translate from MRI to CT, and the two modalities could also be used interchangeably for monitoring cardiotoxicity according to clinical needs. Patients with certain cardiac pathologies or an increased myocardial fibrosis, who are at higher risk of treatment-related cardiotoxicity, may present with a higher ECV, so screening patients for ECV before cancer treatment may potentially identify high-risk subjects, in need of stricter monitoring. More so, ECV could be monitored in patients undergoing cancer treatment, so that any subclinical dysfunction represented by ECV raises may be promptly detected, and appropriate actions could be undertaken.

The studies included in our review displayed high heterogeneity concerning both clinical and technical aspects of nT1 and ECV analysis. In fact, despite anthracyclines being the most commonly treatment regimen studied in association to cardiotoxicity, the study groups included in the review had different types of cancer and underwent different treatment regimens. Moreover, nT1 and ECV were assessed with different MRI units with different magnetic field strengths and different pulse

sequences and contrast agents. Follow-up timings were not uniform and the relationship with LVEF was not analysed within the same framework. This led to the difficulties in conducting a reliable meta-analysis on both nT1 or ECV values, and thus the lack of reference values indicating early cardiac damage, allowing to only draw conclusions concerning potential trends.

Future prospective studies may be conducted to determine whether and to what extent monitoring ECV may help prevent or treat cardiotoxicity stemming from cancer therapy. In particular, imaging studies might be performed before starting cancer treatment to obtain baseline reference values for each patient, and then at predetermined intervals during treatment, after treatment and at follow-up. More so, clinical events should be registered, so to potentially find a minimum ECV variation related to clinical adverse outcomes.

In conclusion, data from literature suggest that nT1 and ECV well reflect early subclinical changes in the myocardial structure associated to cancer treatment cardiotoxicity. Further studies on large samples with more standardised clinical and technical parameters and follow-up timings are warranted to identify reference values that indicate the occurrence of cardiac changes related to cardiotoxicity. This may allow a timely detection of patients at risk, thus permitting the implementation of measures to prevent overt treatment-related cardiac pathology.

Name	Study design	Study group	Country	Cancer location or type	N.	N. females	Age
Neilan 2013	Prospective	All patients	US	lymphoma, leukemia, breast, bone	42	21	55
		Subgroup: preserved LVEF			28	15	56
		Subgroup: reduced LVEF			14	6	56
Tham 2013	Prospective	Healthy controls	Canada	lymphoma, leukemia, bone, kidney	15	8	56
		Children			30	15	15
Jordan 2016	Prospective	Healthy controls	US	breast, hematologic, sarcoma	236	140	
		Subgroup: newly diagnosed			37	25	
		Subgroup: AC cancer survivors			37	29	
		Subgroup: non-AC survivors			17	17	
Heck 2017	Prospective	Subgroup: Candesartan	Norway	breast	38	38	
		Placebo			31	31	
		All patients			69	69	
		AC Low dose			58	58	
		AC High dose			11	11	
Ferreira de Souza 2018	Prospective	All patients	US	breast	27	27	
Heitner 2018	Prospective	All patients	US	multiple myeloma	11	4	55
Kimball 2018	Prospective	All patients	Australia	breast	26	26	53
Muehlberg 2018	Prospective	non-aCMP	Germany	sarcoma	14		
		aCMP			9		
Takagi 2018	Prospective	basal septum	Japan	esophagus	24	10	63
		basal septum, 0.5y			21		
		basal septum, 1.5y			14		
		apical lateral wall			24	10	63
		apical lateral wall, 0.5y			21		
		apical lateral wall, 1.5y			14		
Haslbauer 2019	Prospective	All patients	Germany	any	115	60	59
		early (within 3 months)			52		
		late (>12 months)			63		
		Controls			57	31	54
Harries 2019	Retrospective	Longitudinal group	UK	any	25		
		normal T1			23		
		increased T1			13		

Table 12 *Study characteristics for the works included in the review. LVEF: left ventricular ejection fraction; AC: anthracyclines*

Name	Study group	MR unit	MFS (T)	Contrast agent	Dose (mmol/kg)	MR-I
Neilan 2013	All patients Subgroup: preserved EV Subgroup: reduced EF	Tim Trio (Siemens)	3	gadopentetate dimeglumine	0.15	
Tham 2013	Healthy controls Children	Sonata (Siemens)	1.5	gadopentetate dimeglumine	0.125	
Jordan 2016	Healthy controls Subgroup: newly diagnosed Subgroup: AC cancer survivors Subgroup: non-AC survivors	Magnetom Avanto (Siemens)	1.5	gadopentetate dimeglumine/gadoteridol	0.15 / 0.2	((
Heck 2017	Subgroup: Candesartan Placebo All patients AC Low dose AC High dose	Achieva (Philips)	1.5	gadolinium-DOTA	0.2	62. 63. 62. 62. 63.
Ferreira de Souza 2018	All patients	Achieva (Philips)	3	gadoterate dimeglumine	0.2	69.
Heitner 2018	All patients	Tim Trio (Siemens)	3	macrocyclic gadolinium chelate	0.15	62.6
Kimball 2018	All patients					72.
Muehlberg 2018	non-aCMP aCMP	Avanto Fit (Siemens)	1.5	gadoteridol	0.2	59. 63.
Takagi 2018	basal septum basal septum, 0.5y basal septum, 1.5y apical lateral wall apical lateral wall, 0.5y apical lateral wall, 1.5y	Tim Trio (Siemens)	3	gadopentetate dimeglumine	0.15	6 6
Haslbauer 2019	All patients early (within 3 months) late (>12 months) Controls	Achieva (Phillips) / Skyra (Siemens)	3	N.A.		6
Harries 2019	Longitudinal group normal T1 increased T1	Avanto (Siemens)	1.5	N.A.		

Table 13 *Cardiac magnetic resonance (MR) data for studies include in the review. MFS: Magnetic field strength; LVEF: left ventricular ejection fraction; ECV: extracellular volume fraction; nT1: native T1*

Assessment of myocardial extracellular volume on body computed tomography in breast cancer patients treated with anthracyclines

(from Monti CB, Zanardo M, Bosetti T, Alì M, De Benedictis E, Luporini A, Secchi F, Sardanelli F - *Quantitative Imaging in Medicine and Surgery* 2020)

Background

Breast cancer (BC) is the most common cancer in women, with 523,000 new cases and 138,000 deaths in Europe in 2018 [188]. The average woman has a 1 in 8 chance of developing BC in their lifetime [189].

Among BC patients, anthracyclines represent a treatment mainstay, used to manage both early state and metastatic disease [187,190]. However, anthracyclines may cause cardiotoxicity ultimately leading to myocardial fibrosis, with cumulative effect (thought to be irreversible), and no options for a safe dosage [191]. Fibrosis may lead to asymptomatic left ventricular ejection fraction (LVEF) drops, hypertension, arrhythmias, QTc-interval prolongation, overt heart failure or myocardial ischemia [192,193].

Even though different potential biomarkers for chemotherapy cardiotoxicity have been proposed, none has so far been proved to be able to timely detect subclinical myocardial changes [176]. Therefore, there is a need for reliable and sensitive biomarkers, which could allow an early detection of myocardial changes, to guide physicians to act for the prevention of cardiac dysfunction in women at risk [194]. Detecting cardiotoxicity in a timely manner would in fact allow physicians to undertake preventive measures such as the administration of Dexrazoxane [195].

Extracellular volume (ECV) is an imaging biomarker which reflects the percentage of myocardium not constituted by cells and can increase in presence of fibrosis, inflammation or pathological depositions such as those of amyloidosis [2,145]. When assessed CMR through dedicated pulse sequences, ECV has been shown to correlate well with histological collagen volume

fraction, and an increase of ECV represents a risk factor for heart failure or cardiac-related death [196,197]. Normal value ranges have been proposed as a reference for CMR-derived ECV [148,183].

Over the last few years, ECV calculation by computed tomography (CT) has also been proposed [150]. So far, CT-derived ECV has only been assessed through dedicated cardiac CT examinations [150]. Bandula et al. [160] have shown that CT-derived ECV displays a robust correlation with both CMR-derived ECV and histological findings.

In the guidelines for clinical management of BC, contrast-enhanced chest CT is recommended for staging or restaging at all clinical stages if pulmonary involvement is suspected, and it is always recommended for clinical stage III patients, albeit not being recommended for screening of disease recurrence in asymptomatic patients [187]. Oncologic CT protocols may include a non-contrast scan, an arterial phase scan, a portal-venous phase scan at 1 min after contrast administration and delayed-phase scans from 3 min after contrast administration [198], either on both chest and abdomen or on the abdomen only. Notably, a standard contrast-enhanced chest CT allows for the visualization of the heart. The left ventricle is usually at least partially visible even in abdominal scans.

A key topic in this context is major relevance of cardiac disease in BC survivorship. Older women diagnosed with BC are almost equally likely to die because of cardiovascular disease as they are to die because of BC [199].

Thus, the aims of our study were: 1) to assess whether BC treatment with anthracyclines was associated to an increase in ECV even without clinical, echocardiographic, or electrocardiographic signs of cardiac damage; and 2) to appraise whether any increase in myocardial ECV after treatment remained unchanged at follow-up.

Methods

Ethical statement and study design

The local Ethics Committee approved this study (Ethics Committee of San Raffaele Clinical Research Hospital; protocol code "CardioRetro", number 122/int/2017; approved on September 14th, 2017 and amended on May 10th, 2018). This study was partially supported by Ricerca Corrente funding from the Italian Ministry of Health to IRCCS Policlinico San Donato. Due to the retrospective nature of this study, specific informed consent was waived.

Study population

All patients who had undergone chemotherapy including anthracyclines for BC at our institution between May 2012 and May 2018, whose contrast-enhanced CT examinations prior to and no longer than 5 months after the end of anthracycline treatment were available in our database, were included. All patients had been treated according to guidelines [187], and anthracycline treatment had been administered in intravenous bolus for 5 min, once every three weeks. Treatment would have been postponed for one week if neutrophils were under 1500/mm^3, and the dose would have been reduced to 75% in case of febrile neutropenia. As per clinical recommendations, CT examinations were performed for staging and re-staging patients advanced stage disease, or in patients with symptoms of potential pulmonary involvement.

Exclusion criteria were the lack of haematocrit values obtained from 4 weeks before to the date of the pre-treatment CT examination, and further than 4 weeks for subsequent examinations or intercurrent surgeries or blood transfusions in the time between haematocrit measurements and CT scans. Other exclusion criteria were incomplete heart scans or the presence of artefacts in the longitudinal view of the heart in the unenhanced scan or in any of the contrast-enhanced scans. Moreover, patients who had undergone radiation therapy for cancer in the left breast were excluded due to its potential for cardiotoxicity which may lead to potential confounding [200]. Patients also underwent an electrocardiogram and echocardiography, and patients with underlying cardiac pathology were excluded.

For follow-up assessment, we considered all patients who had undergone an additioanl contrast-enhanced CT examination at least 5 months after the end of anthracycline chemotherapy and at least 3 months after the first follow-up CT, so that any leftover oedema from acute toxicity should have resolved [201], At this stage, we excluded those who had undergone radiation therapy in the left breast or other cardiotoxic chemotherapy or targeted therapy (i.e., trastuzumab), and those who either lacked haematocrit values no further than 4 weeks from CT examination, or underwent surgery or blood transfusion in the time between haematocrit measurements and CT scans.

CT acquisition protocol

Patients were studied using one of two CT scanners, one 64-slice unit and one 16-slice unit. For the 64-slice CT unit (Somatom Definition, Siemens), the following technical parameters were used: tube voltage 120 kVp; tube current from 100 to 200 mAs, depending on automatic exposure control system (CARE Dose 4D, Siemens); rotation time 0.5 s; pitch 1; kernel reconstruction technique B30f medium smooth. For the 16-slice CT unit (Emotion 16, Siemens), the following technical parameters were used: tube voltage 130 kVp; tube current from 100 to 200 mAs, depending on automatic exposure control system (CARE Dose 4D, Siemens), rotation time 0.5 s; pitch 1, kernel reconstruction technique B30f medium smooth. All patients underwent total body CT scans including the abdomen, at least part of the chest and the heart, and head. Slice thickness was 5 mm.

An iodinated contrast agent (iopamidol, Iopamiro 370; 370 mg I/mL; Bracco Imaging) was injected intravenously at a dose of 1.2 mL/kg through a 20-gauge needle using an automatic injector (EmpowerCTA Contrast Injection System, Bracco Imaging) at the rate of 3 mL/s, followed by 50 mL of saline solution at the same rate.

Scan delay was determined using an automated triggering hardware and a dedicated software (Bolus Tracking, Siemens). Specifically, low-dose monitor images were obtained in a single axial slice of the aorta after contrast injection. After obtaining a pre-contrast scan, when the descending aorta enhanced more than 100 HU, the first contrast-enhanced series was acquired (arterial phase, about

15–18 s after contrast injection). Afterwards, additional scans were acquired for obtaining portal venous (1 min after contrast injection) and delayed phases at 7 min after contrast injection.

Patients were instructed to hold their breath during acquisition and craniocaudal (top-down) scanning was the preferred direction for all scans. Radiation doses were reported using dose-length product (DLP), expressed in mGy×cm, and the total DLP value per patient were extracted.

Image analysis

All images were reviewed by a reader with 2 years of experience in body CT, and half of them, randomly chosen, were reviewed by another reader with 3 years of experience. First, the observer chose the best slice to visualize a longitudinal view of the cardiac chambers. Then, measurements were obtained by manually placing a round region of interest (ROI) as large as possible in the mid-level ventricular septum and a second ROI in the intraventricular blood pool at the same level, again as large as possible but avoiding papillary muscles (based on contrast-enhanced scans). This was done on scans acquired at 1, and 7 min, as shown in **Figure 19**. Concerning unenhanced scans, ROI placements were copied from the 1 min scan, and placed in the same positions. Then subtle adjustments were performed considering density, as the myocardium is slightly denser than the blood on basal scans, as shown in **Figure 20**. As scans were not synchronized to an electrocardiogram, while placing ROIs, cardiac movement was considered: ROIs were mainly placed in the middle of the septum, excluding the boundaries close to the intraventricular blood pool.

Septal ECV was calculated using the following formula, according to Bandula et al. [14]:

$$ECV = (1 - haematocrit) \cdot [(HU_{myo_{post}} - HU_{myo_{pre}})/(HU_{blood_{post}} - HU_{blood_{pre}})]$$

where: myo = myocardium; pre = pre-contrast; post = post-contrast.

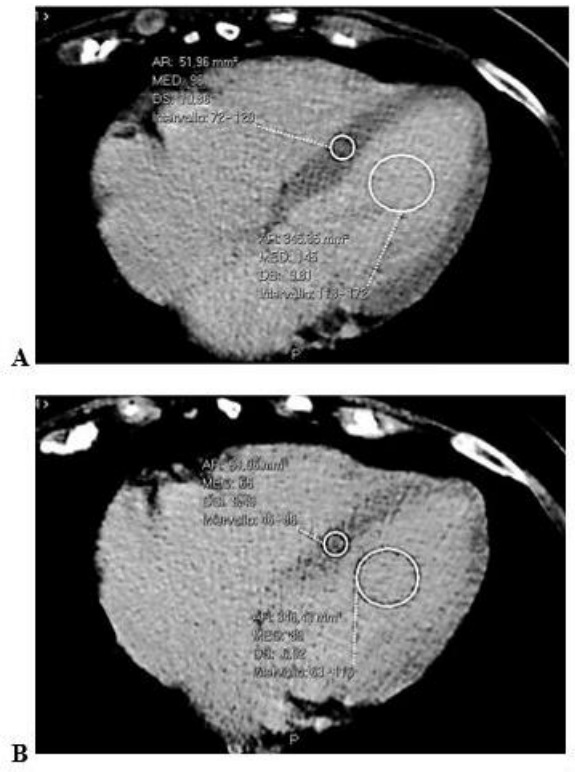

Figure 19 *Examples of regions of interest used for extracellular volume estimation, in computed tomography scans in a 77-year-old woman: A (at 1 min); B (at 7 min).*

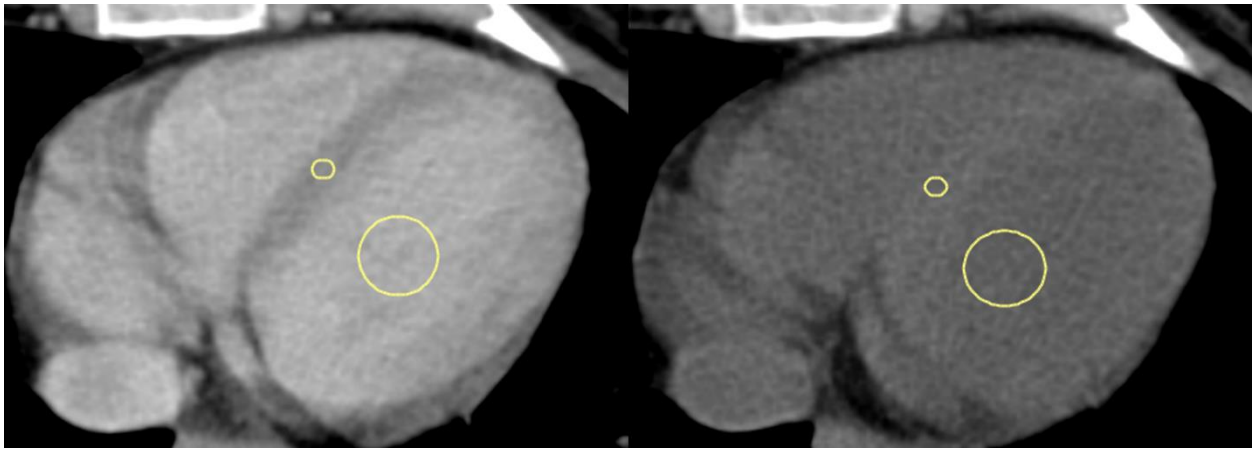

Figure 20 *Depiction of region of interest placement on basal and 1 min post-contrast scan in a 30-year-old female patient. The regions of interest were first placed in the 1 min scan, where the myocardium and blood were more clearly discernible, and then copied in the same positions in the basal scan.*

Moreover, we also recorded standard deviation (SD) for each ROI placed in the myocardium, and SD of background air as a measure of background noise, to appraise a potential contamination of measurements of myocardial HUs by motion artifacts and subsequent presence of blood in the ROI. An example of ROI placement in presence of motion artifacts is shown in **Figure 21**.

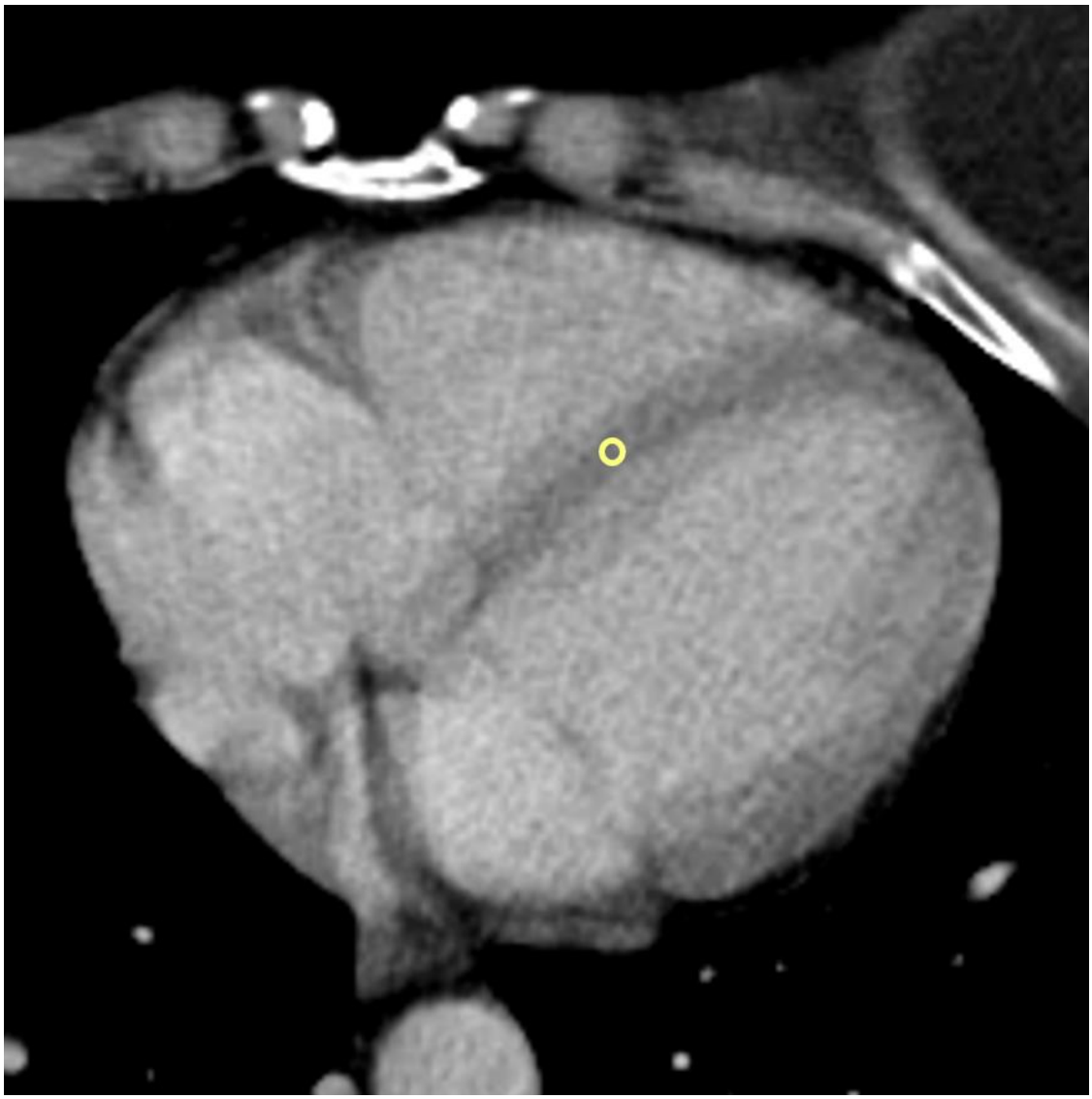

Figure 21 *Region of interest placement in a 62-year-old female patient, presenting motion artifacts involving the heart. The region of interest was placed in the mid-septum, excluding the areas closer to the ventricular cavity, where blood contamination was expected.*

Statistical analysis

Continuous variables were tested for normality with the Shapiro-Wilk test. Parametric data were reported as mean ± standard deviation, while non-parametric data were reported as median and interquartile range (IQR).

Inter-reader reproducibility of CT-derived ECV was assessed in a subset of randomly chosen patients on the pre-treatment scans, with a two-way, mixed-effects interclass correlation coefficient (ICC). ICCs were reported and interpreted according to Koo and Li [202].

Correlations were studied with Pearson r or Spearman ρ with regards to data normality. Correlation coefficients were interpreted according to Evans [203]. When correlations between ECV at different timings were present, Bland-Altman analyses were conducted to evaluate data consistency. Differences were appraised with t-test when variables were normal, or with Wilcoxon test when variables were not normal.

Potential contamination of the HU of the myocardial ROIs was studied comparing the ratio between myocardial HU SD and background noise, represented by the SD of background air, to 1, with a one-sample parametric or non-parametric test, t-test or Mann-Whitney U respectively, with regards to data distribution.

Statistical analysis was performed with SPSS v20 (IBM SPSS Inc.). P-values < 0.05 were considered as significant [127].

Results

Study population

Based on the availability of studies, 42 female patients were originally considered for analysis. After the application of exclusion criteria, our population for ECV assessment before and after treatment was composed by 32 patients. From the initial population, 8 patients were excluded due to haematocrit values being out of the desired time interval, 1 due to incomplete CT scans, and 1 since she underwent left radiation therapy. For ECV follow-up, 13 patients were excluded for the lack of an additional CT examination at appropriate timing and 8 since they underwent left radiation therapy

between the two CT examinations, leading to 32 patients being available for ECV comparison between pre- and post-chemotherapy, and 11 patients available for follow-up analysis (**Figure 22**).

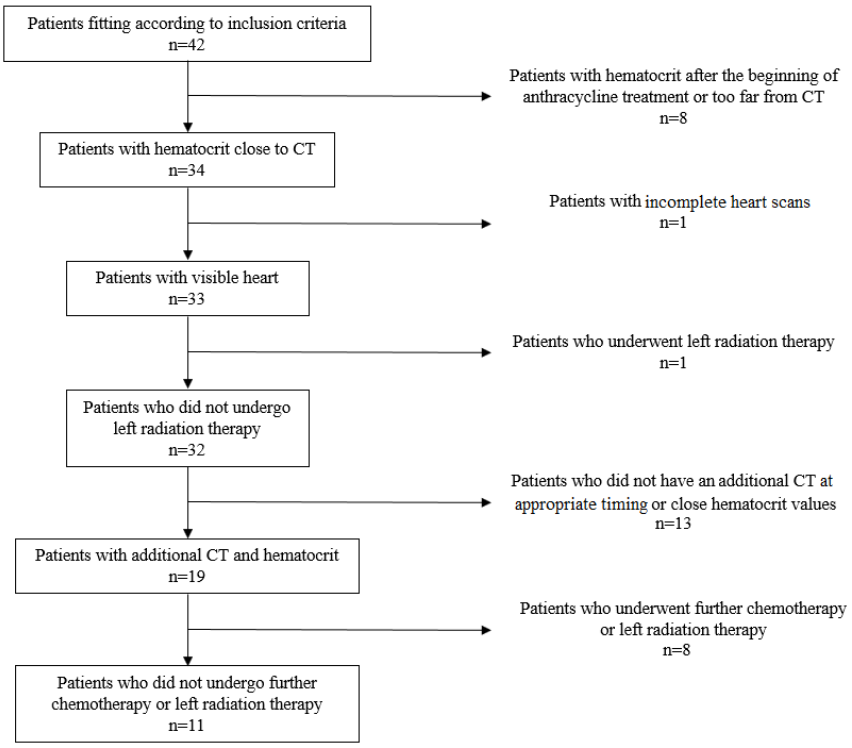

Figure 22 *Flowchart describing patient selection. From the initial population of 42 women complying to inclusion criteria, 10 patients were excluded due to: lack of close haematocrit values (n =8); pre-treatment scan not including any analysable portion of the heart (n=1); intercurrent radiation therapy to the left breast (n=1). After the post-treatment evaluation, 21 additional patients were excluded due to: lack of a further computed tomography examination or close haematocrit (n=13); intercurrent radiation therapy to the left breast (n=8).*

Age at the first CT was 57 years ± 13 years; 29 patients had an infiltrating ductal carcinoma, 2 a poorly differentiated carcinoma, and 1 a neuroendocrine breast carcinoma. All patients had stage II or higher disease. Mean haematocrit before chemotherapy was 38% ± 4%, while electrocardiogram and echocardiography showed no abnormal findings, and LVEF at echocardiography was 64% ± 6%. Baseline characteristics of the study population are presented in **Table 14**. No subject showed cardiotoxicity during or after anthracycline treatment, with cardiotoxicity defined as a decrease in LVEF of more than 10% to below the lower limit of normal [204]. No subject experienced symptoms

of cardiac toxicity either. All patients underwent chemotherapy with dosages adjusted to body weight and body surface area according to clinical guidelines [3]. No patient received reduced doses or less treatment cycles due to toxicity. 26 patients received Epirubicin at 90 mg/m^2 per cycle (total 4 cycles) for a total dose of 360 mg/m^2; 4 patients received mitoxantrone at 10 mg/m^2 per cycle (total 4 cycles) for a total dose of 40 mg/m^2; and 2 received dosages of 60 mg/m^2 of Adriamycin per cycle (total 4 cycles) for a total dose of 240 mg/m^2. Out of 75 total CT examinations (32 pre-treatment, 32 post-treatment and 11 at follow-up), all 75 examinations included the abdomen, part of the chest and the heart, and the head. DLP were highly variable due to the different CT acquisition protocols (chest or abdomen) and total scan volume: mean and standard deviation were 3,847±934 mGy×cm, with a minimum DLP value of 2,093 mGy×cm and a maximum value of 5,680 mGy×cm.

Baseline population characteristics	
N	32
Age (years)	57 ± 13
Type of carcinoma:	
- infiltrating ductal	29
- poorly differentiated	2
- neuroendocrine	1
Disease stage:	
- II	10
- III	13
- IV	9
LVEF (%)	64 ± 6
Hematocrit (%)	38 ± 4

Table 14 *Baseline characteristics of the study population. LVEF: left ventricular ejection fraction.*

Pre-treatment myocardial ECV and reproducibility

Thirty-two patients were analysed for pre-treatment analyses. Pre-treatment ECV was 27.0% ± 2.9% (mean± standard deviation) at 1 min, and 26.4% ± 3.8% at 7 min (**Figure 23**). Inter-reader reproducibility was good at all scanning times: ICC was 0.78 (95% confidence interval [CI] 0.39–0.92) at 1 min, and 0.80 (95% CI 0.42–0.93) at 7 min.

Pre-treatment ECV at 1 min showed a strong significant positive correlation with pre-treatment ECV 7 min (r = 0.743, p < 0.001). Bland-Altman analysis between ECV at 1 and 7 min showed a bias of 0.91% and a coefficient of repeatability of 12%.

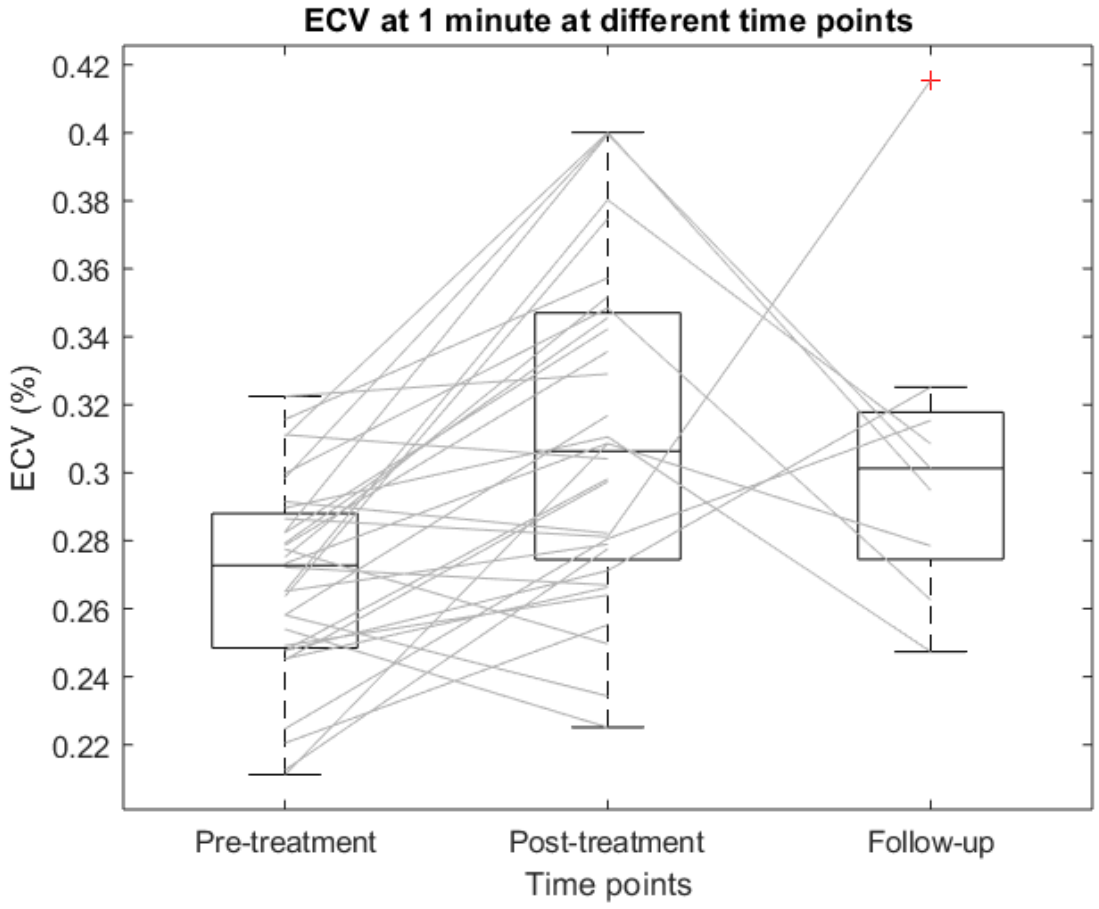

Figure 23 *Boxplot depicting values of myocardial extracellular volume (ECV) at 1 min at different time points, namely before treatment, after treatment and at follow-up. Individual subjects ECV variations are represented by connecting lines.*

Myocardial ECV after therapy

The median interval between the end of chemotherapy and the first CT after treatment was 89 days (IQR 23–127 days); 32 patients were analysed for post-treatment analysis.

Post-treatment haematocrit was 35% ± 3% (mean ± standard deviation), with a significant decrease from pre-treatment values (p = 0.001). Post-treatment ECV was 31.1 ± 4.9% at 1 min, and 30.0% ± 5.1% at 7 min, values significantly higher than those obtained before therapy at all scan

times, with $p < 0.001$ at 1 min, and $p = 0.002$ at 7 min. The average increase in ECV was 4.1% (IQR 1.2–6.5%), and 2.7% (IQR 0.2–5.9%), respectively (see **Figure 23**).

Follow-up

The median interval from post-treatment CT to follow-up CT was 135 days (IQR 116–159 days), the median interval from pre-treatment CT to follow-up CT was 312 days (IQR 242-401 days); 11 patients were analysed for follow-up analyses.

At follow-up, haematocrit was 35% ± 3% (mean ± standard deviation). ECV was 31.0% ± 4.5% at 1 min, and 27.7% ± 3.7% at 7 min. There were no significant differences between follow-up and post-treatment ECV at 1 min ($p = 0.669$), and 7 min ($p = 0.549$). Follow-up ECV was significantly higher than pre-treatment ECV at 1 min ($p = 0.002$), but not at 7 min ($p = 0.288$, see **Figure 23**).

Image quality of the myocardium

The median SD of myocardial ROIs was 7.25 HU (IQR 6.26–8.60 HU) for the basal scan, 8.62 HU (IQR 6.74–9.91 HU) at 1 min, and 8.73 HU (IQR 7.06–10.11 HU) at 7 min. The median SD of the background was 8.45 HU (IQR 5.98–11.75 HU) for the basal scan, 8.98 HU (IQR 6.33–11.63 HU) at 1 min, and 9.21 HU (IQR 6.79–11.76 HU) at 7 min. The median ratios between SD of the myocardium and background were 0.92 (IQR 0.66–1.18) for the basal scan, 0.96 (IQR 0.75–1.23) at 1 min, and 0.96 (IQR 0.75–1.24) at 7 min, and neither ratio was significantly different from 1 ($p = 0.187$, $p = 0.921$, and $p = 0.817$, respectively).

Discussion

In this study we demonstrated the feasibility of using ECV from CT scans as a biomarker of myocardial toxicity in oncologic patients undergoing potentially cardiotoxic chemotherapy.

Our relatively small population can be considered representative of the average advanced BC patients in terms of age (57 ± 13 years). In fact, women are diagnosed with BC at a median age of 61 years, and patients with metastatic disease undergoing chemotherapy tend to be slightly younger [205,206]. Considering that none of our patients was ever reported to have cardiac disease, with

normal electrocardiogram and LVEF at echocardiography, we can assume them to have had a healthy heart prior to chemotherapy.

Our pre-treatment myocardial ECV values are in agreement with those reported by Kurita et al. in 14 healthy women at 7 min post-contrast injection [207], demonstrating that ECV values obtained by body CT are consistent with those obtained by dedicated cardiac CT. Our higher limit for ECV range compared to the study by Kurita et al. may be due to their stricter criteria for cardiac health condition, for instance excluding all subjects with a calcium scoring ≥100. The good inter-reader reproducibility at all scanning times suggests that CT-derived ECV should be not only accurate but also precise. The positive correlations between ECV measured at different times may indicate that all values are related to the extent of ECV.

Patients were treated with anthracyclines according to current guidelines [187]. Although they were treated with different drugs, all anthracycline-based drugs have been proven to be cardiotoxic at such doses [208]. The significant difference in ECV between pre- and post- treatment can be explained by the known mechanisms of anthracycline cardiotoxicity, classified as type I damage according to Ewer et al. [209], leading to cell apoptosis and necrosis, thus to oedema at acute phase, and consequent fibrosis, both determining an increase in ECV [2].

The average increase in ECV we found in this study presented a wide distribution of values. This suggests that patients may respond differently to anthracycline treatment in terms of myocardial oedema and fibrosis, with some experiencing a steep increase most likely due to oedema and fibrosis following necrosis, and others maintaining a constant ECV. In fact, different predictors of response to anthracycline cardiotoxicity have been reported [210], and patients could react differently due to pre-existing conditions such as diabetes, overweight, smoking, or sedentary life [211]. An earlier identification of patients more susceptible to anthracycline cardiotoxicity may help adopting preventive actions, such as the administration of cardioprotectors such as Dexrazoxane [195].

Our follow-up results confirmed that CT-derived ECV reflects anthracycline cardiotoxicity. Of note, type I cardiotoxicity is considered as irreversible [209]. Thus, since our ECV values did not revert to pre-treatment levels months after the end of therapy, we may hypothesize for this ECV increase to be permanent or at least markedly prolonged. This phenomenon resulted to be clear for ECV values obtained at 1 min after contrast injection. For ECV values obtained at 7 min, we observed a highly significant increase from pre-treatment (26.4 ± 3.8%) to post-treatment (30.0 ± 5.1%) and a reduction to 27.7 ± 3.7% at follow-up, the last value being not significant different from that of both pre-treatment and post-treatment. This plays in favour of a partial revert of ECV to pre-treatment values but also opens the issue of which timing after contrast injection is optimal for estimating ECV using CT scans before/after the injection of iodinated contrast material, to be investigated in future researches. Our timing of 7 min is close to the acquisition timing of 5 min post-contrast injection which was found to be ideal for calculating ECV on CT scans by Treibel et al. [212]. Moreover, one study by Hamdy et al. [213] showed that delay times of 3, 5, and 7 min after contrast injection provided compatible ECV values, and our strong correlation and good agreement between values obtained at 1 and 7 min suggests the presence of a common denominator which may be evaluated at both times. The presence of scans acquired at different times stems from the use of a past imaging protocol, including more scans than currently recommended. We thus utilized the available scans at different timings to evaluate the feasibility of calculating ECV from contrast-enhanced CT.

The detection of chemotherapy cardiotoxicity has already been proposed among the possible clinical uses of ECV [214]. In fact, Jordan et al. [166] and Neilan et al. [163], assessed ECV as a biomarker of anthracycline cardiotoxicity using CMR T1-mapping before/after the administration of gadolinium-based contrast agent. Both studies concluded that years after the end of treatment with anthracyclines, ECV was still elevated compared to patients not treated with cardiotoxic drugs. This agrees with our findings at follow-up. However, we should consider that both studies assessed myocardial ECV via CMR, which is a relatively high-cost examination, not included into the

assessment of BC patients undergoing chemotherapy. In addition, CMR is more time-consuming than CT, it has additional contraindications such as obesity or claustrophobia, and concerns about the safety of repeated injections of gadolinium-based contrast agents have been raised [215].

DLP was elevated and highly variable considering that patients underwent different CT protocols on two different CT scanners, one of them being an old 16-row unit, and all patients performed a total body CT scan (head, chest, abdomen and pelvis), reporting in these cases high values of DLP, however still under the DRL reverences values [216]. Nevertheless, an ideal protocol for the analysis of ECV on CT would include a basal acquisition on the heart, and venous phase scan, totalling around 0.3-0.4 mSv and 4-5 mSv respectively [217].

Limitations

This study has some limitations. First, it is retrospective and monocentric, and thus a non-negligible number of subjects were not included due to the lack of contemporary haematocrit values, scans not sufficiently including the heart, or missing CT examinations. These factors reduced the sample size, limiting the statistical power, as discussed for ECV values obtained at 7 min at follow-up. Moreover, haematocrit measurement times were not standardized. However, the intrinsic variability of haematocrit is estimated to be around 10% as observed by Thirup et al. [218], i.e. 0.42 to 0.47, in the absence of significant events as bleeding or treatment suppressing the bone marrow. Patients who experienced such events were excluded from the study as per exclusion criteria, and while their timings of haematocrit measurement remain indeed varied, we may estimate such variation to be small and follow a random pattern, leading to a casual distribution which would not affect the eventual mean over the whole sample. Nevertheless, this initial experience showed the clinical feasibility of myocardial ECV estimate on oncologic CT scans. Moreover, while CT is not recommended as a screening tool for disease recurrence, or as a staging and re-staging imaging technique for asymptomatic, early stage breast cancer, a non-negligible number of patients undergoing heavily cardiotoxic treatments has advanced disease. Thus, CT may indeed be part of

their clinical workflow. Second, we used two different CT units (64- or 16- slice equipment), and our patients had undergone imaging according to a past protocol, including scans that are not currently recommended for disease staging and re-staging. Concerning the CT unit, as densitometry measured on CT scans is always standardized to water density [219], measurements should be considered reliable on both units. Regarding the use of an obsolete protocol, the main aim of our work was to evaluate feasibility of ECV from contrast-enhanced CT, and its results do not imply that a proposed prospective protocol for ECV assessment would need to include all the acquisitions that were performed on our patients. In fact, given the results obtained in the study, ECV could likely be calculated only using the 1 min scan, representing venous phase and thus recommended in staging and re-staging protocols, and one basal slice acquired on the heart to obtain pre-contrast HU values. Third, image time points were not standardized. However, studies on anthracycline cardiotoxicity showed that it is characterized by necrosis and subsequent fibrosis [209] Thus, knowing that the insult on patients' hearts ceased with the end of chemotherapy, we may assume oedema to be resolved by 312 days. Therefore, we may assume that our follow-up data reflects irreversible fibrosis. Fourth, our images were not triggered ad not synchronized to the cardiac cycle. Nevertheless, we performed measurements to mid-septum, thus reducing the impact of this limitation. Moreover, we appraised potential contamination of ROI values by motion artifacts and presence of blood, analysing the ratio between myocardial SD and background noise and tested the hypothesis that such ratio was equal to one. This would signify that the two variables were equal and thus all the variation in myocardial HUs was due to background noise. We found that for every scan timepoint, we could not reject the null hypothesis that variation in myocardial HUs was compatible with background noise ($p=0.187$, 0.921 and 0.817 for basal, 1.5- and 7-min scans respectively). Another limitation is the lack of a control group for ECV comparisons, and of a reference standard for our measurements of ECV via contrast-enhanced CT scans. However, the former issue is due to the fact that it is difficult to include in a retrospective study patients with breast cancer who underwent CT and did not undergo

treatments that may cause cardiotoxicity, as even trastuzumab or radiation therapy may bear cardiac-related adverse effects. Thus, reference values would need to be established via prospective studies before ECV assessment may be included in clinical practice.

In conclusion, we showed that myocardial ECV can be estimated on CT scans in BC patients undergoing anthracycline-based treatment, and that a significant ECV increase can be appreciated after treatment. In a clinical perspective, as survival rates for patients diagnosed with BC constantly increase, detection of toxicities related to treatments become a crucial issue. In this setting, CT-derived ECV could be an imaging biomarker for monitoring therapy-related cardiotoxicity, allowing for potential secondary prevention of cardiac damage, using data derived from an examination that could be part of patients' clinical workflow. Prospective studies are warranted to define the role of CT-derived myocardial ECV in BC patients.

CONCLUSIONS

Quantitative imaging biomarkers may be helpful in a clinical setting both as diagnostic and prognostic indicators, as they may help detect issues which would not be immediately evident at a qualitative general analysis.

Nevertheless, the main issue which could limit the use of quantitative imaging biomarkers is the fact that they often require dedicated image post-processing which may be lengthy, time-consuming, and hard to integrate in an increasingly busy clinical practice [220]. Future developments in this regard may include the use of automated systems based on artificial intelligence (AI) for both the extraction of biomarker data from images, and for a deeper statistical assessment of their clinical significance [221].

REFERENCES

1. Dweck, M.R.; Williams, M.C.; Moss, A.J.; Newby, D.E.; Fayad, Z.A. Computed Tomography and Cardiac Magnetic Resonance in Ischemic Heart Disease. *J. Am. Coll. Cardiol.* **2016**, *68*, 2201–2216, doi:10.1016/j.jacc.2016.08.047.
2. Cannaò, P.M.; Altabella, L.; Petrini, M.; Alì, M.; Secchi, F.; Sardanelli, F. Novel cardiac magnetic resonance biomarkers: native T1 and extracellular volume myocardial mapping. *Eur. Heart J. Suppl.* **2016**, *18*, E64–E71, doi:10.1093/eurheartj/suw022.
3. MRI Safety Home Available online: http://www.mrisafety.com/index.html (accessed on Jan 28, 2019).
4. Wertman, R.; Altun, E.; Martin, D.R.; Mitchell, D.G.; Leyendecker, J.R.; O'Malley, R.B.; Parsons, D.J.; Fuller, E.R.; Semelka, R.C. Risk of Nephrogenic Systemic Fibrosis: Evaluation of Gadolinium Chelate Contrast Agents at Four American Universities. *Radiology* **2008**, *248*, 799–806, doi:10.1148/radiol.2483072093.
5. Kanda, T.; Ishii, K.; Kawaguchi, H.; Kitajima, K.; Takenaka, D. High Signal Intensity in the Dentate Nucleus and Globus Pallidus on Unenhanced T1-weighted MR Images: Relationship with Increasing Cumulative Dose of a Gadolinium-based Contrast Material. *Radiology* **2014**, *270*, 834–841, doi:10.1148/radiol.13131669.
6. Yu, L.; Liu, X.; Leng, S.; Kofler, J.M.; Ramirez-Giraldo, J.C.; Qu, M.; Christner, J.; Fletcher, J.G.; McCollough, C.H. Radiation dose reduction in computed tomography: techniques and future perspective. *Imaging Med.* **2009**, *1*, 65–84, doi:10.2217/iim.09.5.
7. Mostafavi, L.; Marfori, W.; Arellano, C.; Tognolini, A.; Speier, W.; Adibi, A.; Ruehm, S.G. Prevalence of coronary artery disease evaluated by coronary CT angiography in women with mammographically detected breast arterial calcifications. *PLoS One* **2015**, *10*, e0122289, doi:10.1371/journal.pone.0122289.
8. Doltra, A.; Amundsen, B.; Gebker, R.; Fleck, E.; Kelle, S. Emerging Concepts for Myocardial Late

Gadolinium Enhancement MRI. *Curr. Cardiol. Rev.* **2013**, *9*, 185–190, doi:10.2174/1573403X113099990030.

9. Pan, J.A.; Kerwin, M.J.; Salerno, M. Native T1 Mapping, Extracellular Volume Mapping, and Late Gadolinium Enhancement in Cardiac Amyloidosis. *JACC Cardiovasc. Imaging* **2020**, *13*, 1299–1310, doi:10.1016/j.jcmg.2020.03.010.
10. Kim, R.J.; Shah, D.J.; Judd, R.M. How We Perform Delayed Enhancement Imaging. *J. Cardiovasc. Magn. Reson.* **2003**, *5*, 505–514, doi:10.1081/JCMR-120022267.
11. Kellman, P.; Arai, A.E. Cardiac imaging techniques for physicians: late enhancement. *J. Magn. Reson. Imaging* **2012**, *36*, 529–42, doi:10.1002/jmri.23605.
12. Aquaro, G.D.; Positano, V.; Pingitore, A.; Strata, E.; Di Bella, G.; Formisano, F.; Spirito, P.; Lombardi, M. Quantitative analysis of late gadolinium enhancement in hypertrophic cardiomyopathy. *J. Cardiovasc. Magn. Reson.* **2010**, *12*, 21, doi:10.1186/1532-429X-12-21.
13. Ferreira, V.M.; Schulz-Menger, J.; Holmvang, G.; Kramer, C.M.; Carbone, I.; Sechtem, U.; Kindermann, I.; Gutberlet, M.; Cooper, L.T.; Liu, P.; et al. Cardiovascular Magnetic Resonance in Nonischemic Myocardial Inflammation. *J. Am. Coll. Cardiol.* **2018**, *72*, 3158–3176, doi:10.1016/j.jacc.2018.09.072.
14. Iles, L.M.; Ellims, A.H.; Llewellyn, H.; Hare, J.L.; Kaye, D.M.; McLean, C.A.; Taylor, A.J. Histological validation of cardiac magnetic resonance analysis of regional and diffuse interstitial myocardial fibrosis. *Eur. Hear. J. - Cardiovasc. Imaging* **2015**, *16*, 14–22, doi:10.1093/ehjci/jeu182.
15. Weng, Z.; Yao, J.; Chan, R.H.; He, J.; Yang, X.; Zhou, Y.; He, Y. Prognostic Value of LGE-CMR in HCM. *JACC Cardiovasc. Imaging* **2016**, *9*, 1392–1402, doi:10.1016/j.jcmg.2016.02.031.
16. Alba, A.C.; Gaztañaga, J.; Foroutan, F.; Thavendiranathan, P.; Merlo, M.; Alonso-Rodriguez, D.; Vallejo-García, V.; Vidal-Perez, R.; Corros-Vicente, C.; Barreiro-Pérez, M.; et al. Prognostic Value of Late Gadolinium Enhancement for the Prediction of Cardiovascular Outcomes in Dilated

Cardiomyopathy. *Circ. Cardiovasc. Imaging* **2020**, *13*, doi:10.1161/CIRCIMAGING.119.010105.

17. Di Marco, A.; Anguera, I.; Schmitt, M.; Klem, I.; Neilan, T.G.; White, J.A.; Sramko, M.; Masci, P.G.; Barison, A.; Mckenna, P.; et al. Late Gadolinium Enhancement and the Risk for Ventricular Arrhythmias or Sudden Death in Dilated Cardiomyopathy. *JACC Hear. Fail.* **2017**, *5*, 28–38, doi:10.1016/j.jchf.2016.09.017.
18. Townsend, N.; Wilson, L.; Bhatnagar, P.; Wickramasinghe, K.; Rayner, M.; Nichols, M. Cardiovascular disease in Europe: epidemiological update 2016. *Eur. Heart J.* **2016**, *37*, 3232–3245, doi:10.1093/eurheartj/ehw334.
19. Antman, E.; Bassand, J.-P.; Klein, W.; Ohman, M.; Lopez Sendon, J.L.; Rydén, L.; Simoons, M.; Tendera, M. Myocardial infarction redefined—a consensus document of The Joint European Society of Cardiology/American College of Cardiology committee for the redefinition of myocardial infarction. *J. Am. Coll. Cardiol.* **2000**, *36*, 959–969, doi:10.1016/S0735-1097(00)00804-4.
20. Kinno, M.; Nagpal, P.; Horgan, S.; Waller, A.H. Comparison of echocardiography, cardiac magnetic resonance, and computed tomographic imaging for the evaluation of left ventricular myocardial function: Part 1 (global assessment). *Curr. Cardiol. Rep.* **2017**, *19*, 9, doi:10.1007/s11886-017-0815-4.
21. Rajiah, P.; Desai, M.Y.; Kwon, D.; Flamm, S.D. MR Imaging of Myocardial Infarction. *RadioGraphics* **2013**, *33*, 1383–1412, doi:10.1148/rg.335125722.
22. Muscogiuri, G.; Rehwald, W.G.; Schoepf, U.J.; Suranyi, P.; Litwin, S.E.; De Cecco, C.N.; Wichmann, J.L.; Mangold, S.; Caruso, D.; Fuller, S.R.; et al. T(Rho) and magnetization transfer and INvErsion recovery (TRAMINER)-prepared imaging: A novel contrast-enhanced flow-independent dark-blood technique for the evaluation of myocardial late gadolinium enhancement in patients with myocardial infarction. *J. Magn. Reson. Imaging* **2017**, *45*, 1429–1437, doi:10.1002/jmri.25498.

23. Reimer, K.A.; Jennings, R.B. The "wavefront phenomenon" of myocardial ischemic cell death. II. Transmural progression of necrosis within the framework of ischemic bed size (myocardium at risk) and collateral flow. *Lab. Invest.* **1979**, *40*, 633–44.

24. Kaandorp, T.A.M.; Lamb, H.J.; Viergever, E.P.; Poldermans, D.; Boersma, E.; van der Wall, E.E.; de Roos, A.; Bax, J.J. Scar tissue on contrast-enhanced MRI predicts left ventricular remodelling after acute infarction. *Heart* **2007**, *93*, 375–376, doi:10.1136/hrt.2006.097675.

25. Yoneyama, K.; Venkatesh, B.A.; Bluemke, D.A.; McClelland, R.L.; Lima, J.A.C. Cardiovascular magnetic resonance in an adult human population: serial observations from the multi-ethnic study of atherosclerosis. *J. Cardiovasc. Magn. Reson.* **2017**, *19*, 52, doi:10.1186/s12968-017-0367-1.

26. Flett, A.S.; Hayward, M.P.; Ashworth, M.T.; Hansen, M.S.; Taylor, A.M.; Elliott, P.M.; McGregor, C.; Moon, J.C. Equilibrium contrast cardiovascular magnetic resonance for the measurement of diffuse myocardial fibrosis: Preliminary validation in humans. *Circulation* **2010**, *122*, 138–144, doi:10.1161/CIRCULATIONAHA.109.930636.

27. Thomsen, H.S.; Morcos, S.K.; Almén, T.; Bellin, M.F.; Bertolotto, M.; Bongartz, G.; Clement, O.; Leander, P.; Heinz-Peer, G.; Reimer, P.; et al. Nephrogenic systemic fibrosis and gadolinium-based contrast media: Updated ESUR Contrast Medium Safety Committee guidelines. *Eur. Radiol.* **2013**, *23*, 307–318, doi:10.1007/s00330-012-2597-9.

28. Kanda, T.; Fukusato, T.; Matsuda, M.; Toyoda, K.; Oba, H.; Kotoku, J.; Haruyama, T.; Kitajima, K.; Furui, S. Gadolinium-based contrast agent accumulates in the brain even in subjects without severe renal dysfunction: evaluation of autopsy brain specimens with inductively coupled plasma mass spectroscopy. *Radiology* **2015**, *276*, 228–232, doi:10.1148/radiol.2015142690.

29. Rossi Espagnet, M.C.; Bernardi, B.; Pasquini, L.; Figà-Talamanca, L.; Tomà, P.; Napolitano, A. Signal intensity at unenhanced T1-weighted magnetic resonance in the globus pallidus and dentate nucleus after serial administrations of a macrocyclic gadolinium-based contrast agent

in children. *Pediatr. Radiol.* **2017**, *47*, 1345–1352, doi:10.1007/s00247-017-3874-1.

30. Nacif, M.S.; Arai, A.A.; Lima, J.A.; Bluemke, D.A. Gadolinium-enhanced cardiovascular magnetic resonance: administered dose in relationship to united states food and drug administration (FDA) guidelines. *J. Cardiovasc. Magn. Reson.* **2012**, *14*, 18, doi:10.1186/1532-429X-14-18.
31. Ishida, M.; Kato, S.; Sakuma, H. Cardiac MRI in ischemic heart disease. *Circ. J.* **2009**, *73*, 1577–88.
32. Khalid, A.; Lim, E.; Chan, B.T.; Abdul Aziz, Y.F.; Chee, K.H.; Yap, H.J.; Liew, Y.M. Assessing regional left ventricular thickening dysfunction and dyssynchrony via personalized modeling and 3D wall thickness measurements for acute myocardial infarction. *J. Magn. Reson. Imaging* **2019**, *49*, 1006–1019, doi:10.1002/jmri.26302.
33. Matsumoto, H.; Matsuda, T.; Miyamoto, K.; Shimada, T.; Ushimaru, S.; Mikuri, M.; Yamazaki, T. Temporal change of enhancement after gadolinium injection on contrast-enhanced CMR in reperfused acute myocardial infarction. *J. Cardiol.* **2015**, *65*, 76–81, doi:10.1016/j.jjcc.2014.04.005.
34. Flett, A.S.; Hasleton, J.; Cook, C.; Hausenloy, D.; Quarta, G.; Ariti, C.; Muthurangu, V.; Moon, J.C. Evaluation of techniques for the quantification of myocardial scar of differing etiology using cardiac magnetic resonance. *JACC Cardiovasc. Imaging* **2011**, *4*, 150–156, doi:10.1016/j.jcmg.2010.11.015.
35. Kaufman, L.; Kramer, D.M.; Crooks, L.E.; Ortendahl, D.A. Measuring signal-to-noise ratios in MR imaging. *Radiology* **1989**, *173*, 265–267, doi:10.1148/radiology.173.1.2781018.
36. Bussi, S.; Coppo, A.; Botteron, C.; Fraimbault, V.; Fanizzi, A.; De Laurentiis, E.; Colombo Serra, S.; Kirchin, M.A.; Tedoldi, F.; Maisano, F. Differences in gadolinium retention after repeated injections of macrocyclic MR contrast agents to rats. *J. Magn. Reson. Imaging* **2018**, *47*, 746–752, doi:10.1002/jmri.25822.
37. Gotschy, A.; Niemann, M.; Kozerke, S.; Lüscher, T.F.; Manka, R. Cardiovascular magnetic

resonance for the assessment of coronary artery disease. *Int. J. Cardiol.* **2015**, *193*, 84–92, doi:10.1016/j.ijcard.2014.11.098.

38. Vogel-Claussen, J.; Rochitte, C.E.; Wu, K.C.; Kamel, I.R.; Foo, T.K.; Lima, J.A.C.; Bluemke, D.A. Delayed enhancement MR imaging: utility in myocardial assessment. *RadioGraphics* **2006**, *26*, 795–810, doi:10.1148/rg.263055047.

39. De Cobelli, F.; Esposito, A.; Perseghin, G.; Sallemi, C.; Belloni, E.; Ravelli, S.; Lanzani, C.; Del Maschio, A. Intraindividual comparison of gadobutrol and gadopentetate dimeglumine for detection of myocardial late enhancement in cardiac MRI. *AJR. Am. J. Roentgenol.* **2012**, *198*, 809–16, doi:10.2214/AJR.11.7118.

40. Durmus, T.; Schilling, R.; Doeblin, P.; Huppertz, A.; Hamm, B.; Taupitz, M.; Wagner, M. Gadobutrol for Magnetic Resonance Imaging of Chronic Myocardial Infarction. *Invest. Radiol.* **2011**, *47*, 1, doi:10.1097/RLI.0b013e318236e354.

41. Maravilla, K.R.; San-Juan, D.; Kim, S.J.; Elizondo-Riojas, G.; Fink, J.R.; Escobar, W.; Bag, A.; Roberts, D.R.; Hao, J.; Pitrou, C.; et al. Comparison of Gadoterate Meglumine and Gadobutrol in the MRI Diagnosis of Primary Brain Tumors: A Double-Blind Randomized Controlled Intraindividual Crossover Study (the REMIND Study). *Am. J. Neuroradiol.* **2017**, *38*, 1681–1688, doi:10.3174/ajnr.A5316.

42. Wildgruber, M.; Stadlbauer, T.; Rasper, M.; Hapfelmeier, A.; Zelger, O.; Eckstein, H.-H.; Halle, M.; Rummeny, E.J.; Huber, A.M. Single-dose gadobutrol in comparison with single-dose gadobenate dimeglumine for magnetic resonance imaging of chronic myocardial infarction at 3 T. *Invest. Radiol.* **2014**, *49*, 728–34, doi:10.1097/RLI.0000000000000076.

43. Schlosser, T.; Hunold, P.; Herborn, C.U.; Lehmkuhl, H.; Lind, A.; Massing, S.; Barkhausen, J. Myocardial Infarct: Depiction with Contrast-enhanced MR Imaging—Comparison of Gadopentetate and Gadobenate. *Radiology* **2005**, *236*, 1041–1046, doi:10.1148/radiol.2363040220.

44. Dietrich, O.; Raya, J.G.; Reeder, S.B.; Reiser, M.F.; Schoenberg, S.O. Measurement of signal-to-noise ratios in MR images: Influence of multichannel coils, parallel imaging, and reconstruction filters. *J. Magn. Reson. Imaging* **2007**, *26*, 375–385, doi:10.1002/jmri.20969.

45. Holtackers, R.J.; Chiribiri, A.; Schneider, T.; Higgins, D.M.; Botnar, R.M. Dark-blood late gadolinium enhancement without additional magnetization preparation. *J. Cardiovasc. Magn. Reson.* **2017**, *19*, 64, doi:10.1186/s12968-017-0372-4.

46. Liu, Y.; Chen, S.; Zühlke, L.; Black, G.C.; Choy, M.; Li, N.; Keavney, B.D. Global birth prevalence of congenital heart defects 1970–2017: updated systematic review and meta-analysis of 260 studies. *Int. J. Epidemiol.* **2019**, *48*, 455–463, doi:10.1093/ije/dyz009.

47. Marelli, A.J.; Ionescu-Ittu, R.; Mackie, A.S.; Guo, L.; Dendukuri, N.; Kaouache, M. Lifetime Prevalence of Congenital Heart Disease in the General Population From 2000 to 2010. *Circulation* **2014**, *130*, 749–756, doi:10.1161/CIRCULATIONAHA.113.008396.

48. Nollert, G.; Fischlein, T.; Bouterwek, S.; Böhmer, C.; Dewald, O.; Kreuzer, E.; Welz, A.; Netz, H.; Klinner, W.; Reichart, B. Long-Term Results of Total Repair of Tetralogy of Fallot in Adulthood: 35 years Follow-up in 104 Patients Corrected at the Age of 18 or Older*. *Thorac. Cardiovasc. Surg.* **1997**, *45*, 178–181, doi:10.1055/s-2007-1013719.

49. Gadiyaram, V.K.; Monti, C.B.; Sahu, A.; Filev, P.D.; Muscogiuri, G.; Secchi, F.; Sardanelli, F.; Stillman, A.E.; De Cecco, C.N. Repaired Congenital Heart Disease in Older Children and Adults. *Radiol. Clin. North Am.* **2020**, doi:10.1016/j.rcl.2019.12.004.

50. Schicchi, N.; Secinaro, A.; Muscogiuri, G.; Ciliberti, P.; Leonardi, B.; Santangelo, T.; Napolitano, C.; Agliata, G.; Basile, M.C.; Guidi, F.; et al. Multicenter review: role of cardiovascular magnetic resonance in diagnostic evaluation, pre-procedural planning and follow-up for patients with congenital heart disease. *Radiol. Med.* **2016**, *121*, 342–351, doi:10.1007/s11547-015-0608-z.

51. Geva, T. Indications for pulmonary valve replacement in repaired tetralogy of fallot: the quest continues. *Circulation* **2013**, *128*, 1855–7, doi:10.1161/CIRCULATIONAHA.113.005878.

52. Stout, K.K.; Daniels, C.J.; Aboulhosn, J.A.; Bozkurt, B.; Broberg, C.S.; Colman, J.M.; Crumb, S.R.; Dearani, J.A.; Fuller, S.; Gurvitz, M.; et al. 2018 AHA/ACC Guideline for the Management of Adults With Congenital Heart Disease: A Report of the American College of Cardiology/American Heart Association Task Force on Clinical Practice Guidelines. *Circulation* **2019**, *139*, doi:10.1161/CIR.0000000000000683.

53. Sahu, A.; Slesnick, T.C. Imaging Adults With Congenital Heart Disease Part II. *J. Thorac. Imaging* **2017**, *32*, 245–257, doi:10.1097/RTI.0000000000000274.

54. Gaydos, S.S.; Varga-Szemes, A.; Judd, R.N.; Suranyi, P.; Gregg, D. Imaging in Adult Congenital Heart Disease. *J. Thorac. Imaging* **2017**, *32*, 205–216, doi:10.1097/RTI.0000000000000282.

55. Ylitalo, P.; Pitkänen, O.M.; Lauerma, K.; Holmström, M.; Rahkonen, O.; Heikinheimo, M.; Sairanen, H.; Jokinen, E. Late gadolinium enhancement (LGE) progresses with right ventricle volume in children after repair of tetralogy of fallot. *IJC Hear. Vessel.* **2014**, *3*, 15–20, doi:10.1016/j.ijchv.2014.01.002.

56. Green, J.J.; Berger, J.S.; Kramer, C.M.; Salerno, M. Prognostic Value of Late Gadolinium Enhancement in Clinical Outcomes for Hypertrophic Cardiomyopathy. *JACC Cardiovasc. Imaging* **2012**, *5*, 370–377, doi:10.1016/j.jcmg.2011.11.021.

57. Grün, S.; Schumm, J.; Greulich, S.; Wagner, A.; Schneider, S.; Bruder, O.; Kispert, E.-M.; Hill, S.; Ong, P.; Klingel, K.; et al. Long-Term Follow-Up of Biopsy-Proven Viral Myocarditis. *J. Am. Coll. Cardiol.* **2012**, *59*, 1604–1615, doi:10.1016/j.jacc.2012.01.007.

58. Dobson, R.J.; Mordi, I.; Danton, M.H.; Walker, N.L.; Walker, H.A.; Tzemos, N. Late gadolinium enhancement and adverse outcomes in a contemporary cohort of adult survivors of tetralogy of Fallot. *Congenit. Heart Dis.* **2017**, *12*, 58–66, doi:10.1111/chd.12403.

59. Park, S.J.; On, Y.K.; Kim, J.S.; Park, S.W.; Yang, J.H.; Jun, T.G.; Kang, I.S.; Lee, H.J.; Choe, Y.H.; Huh, J. Relation of fragmented QRS complex to right ventricular fibrosis detected by late gadolinium enhancement cardiac magnetic resonance in adults with repaired tetralogy of Fallot. *Am. J.*

Cardiol. **2012**, *109*, 110–115, doi:10.1016/j.amjcard.2011.07.070.

60. Broberg, C.S.; Chugh, S.S.; Conklin, C.; Sahn, D.J.; Jerosch-Herold, M. Quantification of Diffuse Myocardial Fibrosis and Its Association With Myocardial Dysfunction in Congenital Heart Disease. *Circ. Cardiovasc. Imaging* **2010**, *3*, 727–734, doi:10.1161/CIRCIMAGING.108.842096.
61. Wald, R.R.M.; Haber, I.; Wald, R.R.M.; Valente, A.M.; Powell, A.J.; Geva, T. Effects of regional dysfunction and late gadolinium enhancement on global right ventricular function and exercise capacity in patients with repaired tetralogy of fallot. *Circulation* **2009**, *119*, 1370–1377, doi:10.1161/CIRCULATIONAHA.108.816546.
62. Babu-Narayan, S. V. Ventricular Fibrosis Suggested by Cardiovascular Magnetic Resonance in Adults With Repaired Tetralogy of Fallot and Its Relationship to Adverse Markers of Clinical Outcome. *Circulation* **2006**, *113*, 405–413, doi:10.1161/CIRCULATIONAHA.105.548727.
63. Oosterhof, T.; Mulder, B.J.M.; Vliegen, H.W.; De Roos, A. Corrected tetralogy of Fallot: Delayed enhancement in right ventricular outflow tract. *Radiology* **2005**, *237*, 868–871, doi:10.1148/radiol.2373041324.
64. Hoang, T.T.; Manso, P.H.; Edman, S.; Mercer-Rosa, L.; Mitchell, L.E.; Sewda, A.; Swartz, M.D.; Fogel, M.A.; Agopian, A.J.; Goldmuntz, E. Genetic variants of HIF1α are associated with right ventricular fibrotic load in repaired tetralogy of Fallot patients: A cardiovascular magnetic resonance study. *J. Cardiovasc. Magn. Reson.* **2019**, *21*, 1–10, doi:10.1186/s12968-019-0555-2.
65. Chen, C.A.; Dusenbery, S.M.; Valente, A.M.; Powell, A.J.; Geva, T. Myocardial ECV Fraction Assessed by CMR Is Associated with Type of Hemodynamic Load and Arrhythmia in Repaired Tetralogy of Fallot. *JACC Cardiovasc. Imaging* **2016**, *9*, 1–10, doi:10.1016/j.jcmg.2015.09.011.
66. Joynt, M.R.; Yu, S.; Dorfman, A.L.; Ghadimi Mahani, M.; Agarwal, P.P.; Lu, J.C. Differential impact of pulmonary regurgitation on patients with surgically repaired pulmonary stenosis versus tetralogy of fallot. *Am. J. Cardiol.* **2016**, *117*, 289–294, doi:10.1016/j.amjcard.2015.10.025.

67. Stirrat, J.; Rajchl, M.; Bergin, L.; Patton, D.J.; Peters, T.; White, J.A. High-resolution 3-dimensional late gadolinium enhancement scar imaging in surgically corrected Tetralogy of Fallot: Clinical feasibility of volumetric quantification and visualization. *J. Cardiovasc. Magn. Reson.* **2014**, *16*, 1–11, doi:10.1186/s12968-014-0076-y.

68. Śpiewak, M.; Małek, Ł.A.; Petryka, J.; Mazurkiewicz, Ł.; Marczak, M.; Biernacka, E.K.; Kowalski, M.; Hoffman, P.; Demkow, M.; Misḱo, J.; et al. Factors associated with biventricular dysfunction in patients with repaired tetralogy of fallot. *Kardiol. Pol.* **2014**, *72*, 631–639, doi:10.5603/KP.a2014.0049.

69. Chen, C.A.; Tseng, W.Y.I.; Wang, J.K.; Chen, S.Y.; Ni, Y.H.; Huang, K.C.; Ho, Y.L.; Chang, C.I.; Chiu, I.S.; Su, M.Y.M.; et al. Circulating biomarkers of collagen type i metabolism mark the right ventricular fibrosis and adverse markers of clinical outcome in adults with repaired tetralogy of Fallot. *Int. J. Cardiol.* **2013**, *167*, 2963–2968, doi:10.1016/j.ijcard.2012.08.059.

70. Munkhammar, P.; Carlsson, M.; Arheden, H.; Pesonen, E. Restrictive right ventricular physiology after Tetralogy of Fallot repair is associated with fibrosis of the right ventricular outflow tract visualized on cardiac magnetic resonance imaging. *Eur. Heart J. Cardiovasc. Imaging* **2013**, *14*, 978–985, doi:10.1093/ehjci/jet009.

71. Spiewak, M.; Małek, L.A.; Petryka, J.; Mazurkiewicz, L.; Marczak, M.; Biernacka, E.K.; Kowalski, M.; Hoffman, P.; Demkow, M.; Miśko, J.; et al. Determinants of left- and right-ventricular ejection fractions in patients with repaired tetralogy of Fallot: a cardiac magnetic resonance imaging study. *Pol. Arch. Med. Wewnętrznej* **2013**, *123*, 539–546, doi:10.20452/pamw.1929.

72. Wald, R.M.; Redington, A.N.; Pereira, A.; Provost, Y.L.; Paul, N.S.; Oechslin, E.N.; Silversides, C.K. Refining the assessment of pulmonary regurgitation in adults after tetralogy of Fallot repair: should we be measuring regurgitant fraction or regurgitant volume? *Eur. Heart J.* **2009**, *30*, 356–61, doi:10.1093/eurheartj/ehn595.

73. Barreiro-Pérez, M.; Curione, D.; Symons, R.; Claus, P.; Voigt, J.-U.; Bogaert, J. Left ventricular

global myocardial strain assessment comparing the reproducibility of four commercially available CMR-feature tracking algorithms. *Eur. Radiol.* **2018**, *28*, 5137–5147, doi:10.1007/s00330-018-5538-4.

74. Perk, G.; Tunick, P.A.; Kronzon, I. Non-Doppler two-dimensional strain imaging by echocardiography--from technical considerations to clinical applications. *J. Am. Soc. Echocardiogr.* **2007**, *20*, 234–43, doi:10.1016/j.echo.2006.08.023.

75. Lopez-Candales, A.; Hernandez-Suarez, D.F. Strain Imaging Echocardiography: What Imaging Cardiologists Should Know. *Curr. Cardiol. Rev.* **2017**, *13*, doi:10.2174/1573403X12666161028122649.

76. Osman, N.F.; Kerwin, W.S.; McVeigh, E.R.; Prince, J.L. Cardiac motion tracking using CINE harmonic phase (HARP) magnetic resonance imaging. *Magn. Reson. Med.* **1999**, *42*, 1048–60, doi:10.1016/j.humov.2008.02.015.Changes.

77. Cao, J.J.; Ngai, N.; Duncanson, L.; Cheng, J.; Gliganic, K.; Chen, Q. A comparison of both DENSE and feature tracking techniques with tagging for the cardiovascular magnetic resonance assessment of myocardial strain. *J. Cardiovasc. Magn. Reson.* **2018**, *20*, 26, doi:10.1186/S12968-018-0448-9.

78. Augustine, D.; Lewandowski, A.J.; Lazdam, M.; Rai, A.; Francis, J.; Myerson, S.; Noble, A.; Becher, H.; Neubauer, S.; Petersen, S.E.; et al. Global and regional left ventricular myocardial deformation measures by magnetic resonance feature tracking in healthy volunteers: comparison with tagging and relevance of gender. *J. Cardiovasc. Magn. Reson.* **2013**, *15*, 8, doi:10.1186/1532-429X-15-8.

79. Ong, G.; Brezden-Masley, C.; Dhir, V.; Deva, D.P.; Chan, K.K.W.; Chow, C.-M.; Thavendiranathan, D.; Haq, R.; Barfett, J.J.; Petrella, T.M.; et al. Myocardial strain imaging by cardiac magnetic resonance for detection of subclinical myocardial dysfunction in breast cancer patients receiving trastuzumab and chemotherapy. *Int. J. Cardiol.* **2018**, *261*, 228–233,

doi:10.1016/j.ijcard.2018.03.041.

80. Aretz, H.T.; Billingham, M.E.; Edwards, W.D.; Factor, S.M.; Fallon, J.T.; Fenoglio, J.J.; Olsen, E.G.; Schoen, F.J. Myocarditis. A histopathologic definition and classification. *Am. J. Cardiovasc. Pathol.* **1987**, *1*, 3–14.

81. Caforio, A.L.P.; Malipiero, G.; Marcolongo, R.; Iliceto, S. Myocarditis: A Clinical Overview. *Curr. Cardiol. Rep.* **2017**, *19*, 63, doi:10.1007/s11886-017-0870-x.

82. D'Ambrosio, A. The fate of acute myocarditis between spontaneous improvement and evolution to dilated cardiomyopathy: a review. *Heart* **2001**, *85*, 499–504, doi:10.1136/heart.85.5.499.

83. Weintraub, R.G.; Semsarian, C.; Macdonald, P. Dilated cardiomyopathy. *Lancet (London, England)* **2017**, *379*, 738–47, doi:10.1016/S0140-6736(16)31713-5.

84. Felker, G.M.; Hu, W.; Hare, J.M.; Hruban, R.H.; Baughman, K.L.; Kasper, E.K. The spectrum of dilated cardiomyopathy. The Johns Hopkins experience with 1,278 patients. *Medicine (Baltimore).* **1999**, *78*, 270–83, doi:10.1097/00005792-199907000-00005.

85. Basso, C.; Calabrese, F.; Corrado, D.; Thiene, G. Postmortem diagnosis in sudden cardiac death victims: macroscopic, microscopic and molecular findings. *Cardiovasc. Res.* **2001**, *50*, 290–300, doi:10.1016/S0008-6363(01)00261-9.

86. Maron, B.J.; Doerer, J.J.; Haas, T.S.; Tierney, D.M.; Mueller, F.O. Sudden deaths in young competitive athletes: analysis of 1866 deaths in the United States, 1980-2006. *Circulation* **2009**, *119*, 1085–92, doi:10.1161/CIRCULATIONAHA.108.804617.

87. Richardson, P.; McKenna, W.; Bristow, M.; Maisch, B.; Mautner, B.; O'Connell, J.; Olsen, E.; Thiene, G.; Goodwin, J.; Gyarfas, I.; et al. Report of the 1995 World Health Organization/International Society and Federation of Cardiology Task Force on the Definition and Classification of cardiomyopathies. *Circulation* **1996**, *93*, 841–2, doi:10.1161/01.CIR.93.5.841.

88. From, A.M.; Maleszewski, J.J.; Rihal, C.S. Current Status of Endomyocardial Biopsy. *Mayo Clin. Proc.* **2011**, *86*, 1095–1102, doi:10.4065/mcp.2011.0296.

89. Cooper, L.T.; Baughman, K.L.; Feldman, A.M.; Frustaci, A.; Jessup, M.; Kuhl, U.; Levine, G.N.; Narula, J.; Starling, R.C.; Towbin, J.; et al. The role of endomyocardial biopsy in the management of cardiovascular disease: a scientific statement from the American Heart Association, the American College of Cardiology, and the European Society of Cardiology. Endorsed by the Heart Failure Society of. *J. Am. Coll. Cardiol.* **2007**, *50*, 1914–31, doi:10.1016/j.jacc.2007.09.008.

90. Caforio, A.L.P.; Marcolongo, R.; Basso, C.; Iliceto, S. Clinical presentation and diagnosis of myocarditis. *Heart* **2015**, *101*, 1332–44, doi:10.1136/heartjnl-2014-306363.

91. Caforio, A.L.P.; Pankuweit, S.; Arbustini, E.; Basso, C.; Gimeno-Blanes, J.; Felix, S.B.; Fu, M.; Heli??, T.; Heymans, S.; Jahns, R.; et al. Current state of knowledge on aetiology, diagnosis, management, and therapy of myocarditis: A position statement of the European Society of Cardiology Working Group on Myocardial and Pericardial Diseases. *Eur. Heart J.* **2013**, *34*, 2636–2648, doi:10.1093/eurheartj/eht210.

92. Laissy, J.-P.; Messin, B.; Varenne, O.; Iung, B.; Karila-Cohen, D.; Schouman-Claeys, E.; Steg, P.G. MRI of Acute Myocarditis. *Chest* **2002**, *122*, 1638–1648, doi:10.1378/chest.122.5.1638.

93. Chu, G.C.W.; Flewitt, J.A.; Mikami, Y.; Vermes, E.; Friedrich, M.G. Assessment of acute myocarditis by cardiovascular MR: Diagnostic performance of shortened protocols. *Int. J. Cardiovasc. Imaging* **2013**, *29*, 1077–1083, doi:10.1007/s10554-013-0189-7.

94. Friedrich, M.G.; Sechtem, U.; Schulz-Menger, J.; Holmvang, G.; Alakija, P.; Cooper, L.T.; White, J.A.; Abdel-Aty, H.; Gutberlet, M.; Prasad, S.; et al. Cardiovascular Magnetic Resonance in Myocarditis: A JACC White Paper. *J. Am. Coll. Cardiol.* **2009**, *53*, 1475–1487, doi:10.1016/j.jacc.2009.02.007.

95. Hauer, M.P.; Uhl, M.; Allmann, K.H.; Laubenberger, J.; Zimmerhackl, L.B.; Langer, M.

Comparison of turbo inversion recovery magnitude (TIRM) with T2-weighted turbo spin-echo and T1-weighted spin-echo MR imaging in the early diagnosis of acute osteomyelitis in children. *Pediatr. Radiol.* **1998**, *28*, 846–850, doi:10.1007/s002470050479.

96. Friedrich, M.G.; Marcotte, F. How to Use Imaging Cardiac Magnetic Resonance Assessment of Myocarditis. **2016**, 833–839, doi:10.1161/CIRCIMAGING.113.000416.

97. Voigt, J.-U.; Flachskampf, F.A. Strain and strain rate. New and clinically relevant echo parameters of regional myocardial function. *Z. Kardiol.* **2004**, *93*, 249–58, doi:10.1007/s00392-004-0047-7.

98. Claus, P.; Omar, A.M.S.; Pedrizzetti, G.; Sengupta, P.P.; Nagel, E. Tissue Tracking Technology for Assessing Cardiac Mechanics. *JACC Cardiovasc. Imaging* **2015**, *8*, 1444–1460, doi:10.1016/j.jcmg.2015.11.001.

99. Taylor, R.J.; Umar, F.; Lin, E.L.S.; Ahmed, A.; Moody, W.E.; Mazur, W.; Stegemann, B.; Townend, J.N.; Steeds, R.P.; Leyva, F. Mechanical effects of left ventricular midwall fibrosis in non-ischemic cardiomyopathy. *J. Cardiovasc. Magn. Reson.* **2015**, *18*, 1, doi:10.1186/s12968-015-0221-2.

100. Uppu, S.C.; Shah, A.; Weigand, J.; Nielsen, J.C.; Ko, H.H.; Parness, I.A.; Srivastava, S. Two-Dimensional Speckle-Tracking-Derived Segmental Peak Systolic Longitudinal Strain Identifies Regional Myocardial Involvement in Patients with Myocarditis and Normal Global Left Ventricular Systolic Function. *Pediatr. Cardiol.* **2015**, *36*, 950–959, doi:10.1007/s00246-015-1105-9.

101. Schmidt, B.B.; Dick, A.; Treutlein, M.; Schiller, P.; Bunck, A.C.; Maintz, D.; Baeßler, B.; Bae??ler, B. Intra- and inter-observer reproducibility of global and regional magnetic resonance feature tracking derived strain parameters of the left and right ventricle. *Eur. J. Radiol.* **2017**, *89*, 97–105, doi:10.1016/j.ejrad.2017.01.025.

102. Schuster, A.; Morton, G.; Hussain, S.T.; Jogiya, R.; Kutty, S.; Asrress, K.N.; Makowski, M.R.;

Bigalke, B.; Perera, D.; Beerbaum, P.; et al. The intra-observer reproducibility of cardiovascular magnetic resonance myocardial feature tracking strain assessment is independent of field strength. *Eur. J. Radiol.* **2013**, *82*, 296–301, doi:10.1016/j.ejrad.2012.11.012.

103. Kytö, V.; Sipilä, J.; Rautava, P. The effects of gender and age on occurrence of clinically suspected myocarditis in adulthood. *Heart* **2013**, *99*, 1681–4, doi:10.1136/heartjnl-2013-304449.

104. Cooper, L.T. Myocarditis. *N. Engl. J. Med.* **2009**, *360*, 1526–38, doi:10.1056/NEJMra0800028.

105. Sinagra, G.; Anzini, M.; Pereira, N.L.; Bussani, R.; Finocchiaro, G.; Bartunek, J.; Merlo, M. Myocarditis in Clinical Practice. *Mayo Clin. Proc.* **2016**, *91*, 1256–66, doi:10.1016/j.mayocp.2016.05.013.

106. Ferreira, V.M.; Piechnik, S.K.; Dall'Armellina, E.; Karamitsos, T.D.; Francis, J.M.; Ntusi, N.; Holloway, C.; Choudhury, R.P.; Kardos, A.; Robson, M.D.; et al. T1 Mapping for the Diagnosis of Acute Myocarditis Using CMR. *JACC Cardiovasc. Imaging* **2013**, *6*, 1048–1058, doi:10.1016/j.jcmg.2013.03.008.

107. Dandel, M.; Hetzer, R. Echocardiographic strain and strain rate imaging--clinical applications. *Int. J. Cardiol.* **2009**, *132*, 11–24, doi:10.1016/j.ijcard.2008.06.091.

108. Tutarel, O.; Orwat, S.; Radke, R.M.; Westhoff-Bleck, M.; Vossler, C.; Schülke, C.; Baumgartner, H.; Bauersachs, J.; Röntgen, P.; Diller, G.P. Assessment of myocardial function using MRI-based feature tracking in adults after atrial repair of transposition of the great arteries: Reference values and clinical utility. *Int. J. Cardiol.* **2016**, *220*, 246–250, doi:10.1016/j.ijcard.2016.06.108.

109. André, F.; Stock, F.T.; Riffel, J.; Giannitsis, E.; Steen, H.; Scharhag, J.; Katus, H.A.; Buss, S.J. Incremental value of cardiac deformation analysis in acute myocarditis : a cardiovascular magnetic resonance imaging study. **2016**, 1093–1101, doi:10.1007/s10554-016-0878-0.

110. Taylor, R.J.; Moody, W.E.; Umar, F.; Edwards, N.C.; Taylor, T.J.; Stegemann, B.; Townend, J.N.;

Hor, K.N.; Steeds, R.P.; Mazur, W.; et al. Myocardial strain measurement with feature-tracking cardiovascular magnetic resonance: normal values. *Eur. Hear. J. – Cardiovasc. Imaging* **2015**, *16*, 871–881, doi:10.1093/ehjci/jev006.

111. Lin, K.; Collins, J.D.; Chowdhary, V.; Markl, M.; Carr, J.C. Heart deformation analysis for automated quantification of cardiac function and regional myocardial motion patterns: A proof of concept study in patients with cardiomyopathy and healthy subjects. *Eur. J. Radiol.* **2016**, *85*, 1811–1817, doi:10.1016/j.ejrad.2016.08.005.

112. Luetkens, J.A.; Homsi, R.; Dabir, D.; Kuetting, D.L.; Marx, C.; Doerner, J.; Schlesinger-Irsch, U.; Andrié, R.; Sprinkart, A.M.; Schmeel, F.C.; et al. Comprehensive Cardiac Magnetic Resonance for Short-Term Follow-Up in Acute Myocarditis. *J. Am. Heart Assoc.* **2016**, *5*, e003603, doi:10.1161/JAHA.116.003603.

113. Lee, J.W.; Jeong, Y.J.; Lee, G.; Lee, N.K. Predictive Value of Cardiac Magnetic Resonance Imaging-Derived Myocardial Strain for Poor Outcomes in Patients with Acute Myocarditis. **2017**, *18*, 643–654.

114. Yim, D.; Mertens, L.; Morgan, C.T.; Friedberg, M.K.; Grosse-Wortmann, L.; Dragulescu, A. Impact of surgical pulmonary valve replacement on ventricular mechanics in children with repaired tetralogy of Fallot. *Int. J. Cardiovasc. Imaging* **2017**, *33*, 711–720, doi:10.1007/s10554-016-1046-2.

115. Chiu, S.-N.; Wang, J.-K.; Chen, H.-C.; Lin, M.-T.; Wu, E.-T.; Chen, C.-A.; Huang, S.-C.; Chang, C.-I.; Chen, Y.-S.; Chiu, I.-S.; et al. Long-Term Survival and Unnatural Deaths of Patients With Repaired Tetralogy of Fallot in an Asian Cohort. *Circ. Cardiovasc. Qual. Outcomes* **2012**, *5*, 120–125, doi:10.1161/CIRCOUTCOMES.111.963603.

116. Secchi, F.; Chessa, M.; Petrini, M.; Monti, C.B.; Alì, M.; Cannaò, P.M.; Di Leo, G.; Sardanelli, F. Advantage of Pulmonary Regurgitation Volume Versus Pulmonary Regurgitation Fraction in a Congenital Heart Disease Mixed Population. *J. Thorac. Imaging* **2019**, *V*, 1,

doi:10.1097/RTI.0000000000000400.

117. Valente, A.M.; Cook, S.; Festa, P.; Ko, H.H.; Krishnamurthy, R.; Taylor, A.M.; Warnes, C.A.; Kreutzer, J.; Geva, T. Multimodality Imaging Guidelines for Patients with Repaired Tetralogy of Fallot: A Report from the American Society of Echocardiography. *J. Am. Soc. Echocardiogr.* **2014**, *27*, 111–141, doi:10.1016/j.echo.2013.11.009.

118. Dandel, M.; Lehmkuhl, H.; Knosalla, C.; Suramelashvili, N.; Hetzer, R. Strain and Strain Rate Imaging by Echocardiography – Basic Concepts and Clinical Applicability. *Curr. Cardiol. Rev.* **2009**, *5*, 133, doi:10.2174/157340309788166642.

119. Padiyath, A.; Gribben, P.; Abraham, J.R.; Li, L.; Rangamani, S.; Schuster, A.; Danford, D.A.; Pedrizzetti, G.; Kutty, S. Echocardiography and Cardiac Magnetic Resonance-Based Feature Tracking in the Assessment of Myocardial Mechanics in Tetralogy of Fallot: An Intermodality Comparison. *Echocardiography* **2013**, *30*, 203–210, doi:10.1111/echo.12016.

120. Maceira, A.M.; Tuset-Sanchis, L.; López-Garrido, M.; San Andres, M.; López-Lereu, M.P.; Monmeneu, J. V.; García-González, M.P.; Higueras, L. Feasibility and reproducibility of feature-tracking-based strain and strain rate measures of the left ventricle in different diseases and genders. *J. Magn. Reson. Imaging* **2018**, *47*, 1415–1425, doi:10.1002/jmri.25894.

121. Stokke, T.M.; Hasselberg, N.E.; Smedsrud, M.K.; Sarvari, S.I.; Haugaa, K.H.; Smiseth, O.A.; Edvardsen, T.; Remme, E.W. Geometry as a Confounder When Assessing Ventricular Systolic Function. *J. Am. Coll. Cardiol.* **2017**, *70*, 942–954, doi:10.1016/j.jacc.2017.06.046.

122. Potter, E.; Marwick, T.H. Assessment of Left Ventricular Function by Echocardiography. *JACC Cardiovasc. Imaging* **2018**, *11*, 260–274, doi:10.1016/j.jcmg.2017.11.017.

123. Menting, M.E.; Van Den Bosch, A.E.; McGhie, J.S.; Eindhoven, J.A.; Cuypers, J.A.A.E.; Witsenburg, M.; Geleijnse, M.L.; Helbing, W.A.; Roos-Hesselink, J.W. Assessment of ventricular function in adults with repaired Tetralogy of Fallot using myocardial deformation imaging. *Eur. Heart J. Cardiovasc. Imaging* **2015**, *16*, 1347–1357, doi:10.1093/ehjci/jev090.

124. Burkhardt, B.E.U.; Velasco Forte, M.N.; Durairaj, S.; Rafiq, I.; Valverde, I.; Tandon, A.; Simpson, J.; Hussain, T. Timely Pulmonary Valve Replacement May Allow Preservation of Left Ventricular Circumferential Strain in Patients with Tetralogy of Fallot. *Front. Pediatr.* **2017**, *5*, doi:10.3389/fped.2017.00039.

125. Tretter, J.T.; Redington, A.N. The Forgotten Ventricle? *Circ. Cardiovasc. Imaging* **2018**, *11*, doi:10.1161/CIRCIMAGING.117.007410.

126. Hamada-Harimura, Y.; Seo, Y.; Ishizu, T.; Nishi, I.; Machino-Ohtsuka, T.; Yamamoto, M.; Sugano, A.; Sato, K.; Sai, S.; Obara, K.; et al. Incremental Prognostic Value of Right Ventricular Strain in Patients With Acute Decompensated Heart Failure. *Circ. Cardiovasc. Imaging* **2018**, *11*, doi:10.1161/CIRCIMAGING.117.007249.

127. Di Leo, G.; Sardanelli, F. Statistical significance: p value, 0.05 threshold, and applications to radiomics—reasons for a conservative approach. *Eur. Radiol. Exp.* **2020**, *4*, 18, doi:10.1186/s41747-020-0145-y.

128. Liu, B.; Dardeer, A.M.; Moody, W.E.; Edwards, N.C.; Hudsmith, L.E.; Steeds, R.P. Normal values for myocardial deformation within the right heart measured by feature-tracking cardiovascular magnetic resonance imaging. *Int. J. Cardiol.* **2018**, *252*, 220–223, doi:10.1016/j.ijcard.2017.10.106.

129. Harrild, D.M.; Berul, C.I.; Cecchin, F.; Geva, T.; Gauvreau, K.; Pigula, F.; Walsh, E.P. Pulmonary Valve Replacement in Tetralogy of Fallot. *Circulation* **2009**, *119*, 445–451, doi:10.1161/CIRCULATIONAHA.108.775221.

130. Oosterhof, T.; Mulder, B.J.M.; Vliegen, H.W.; de Roos, A. Cardiovascular magnetic resonance in the follow-up of patients with corrected tetralogy of Fallot: A review. *Am. Heart J.* **2006**, *151*, 265–272, doi:10.1016/j.ahj.2005.03.058.

131. Guné, H.; Sjögren, J.; Carlsson, M.; Gustafsson, R.; Sjöberg, P.; Nozohoor, S. Right ventricular remodeling after conduit replacement in patients with corrected tetralogy of Fallot -

evaluation by cardiac magnetic resonance. *J. Cardiothorac. Surg.* **2019**, *14*, 77, doi:10.1186/s13019-019-0899-6.

132. Oosterhof, T.; Van Straten, A.; Vliegen, H.W.; Meijboom, F.J.; Van Dijk, A.P.J.J.; Spijkerboer, A.M.; Bouma, B.J.; Zwinderman, A.H.; Hazekamp, M.G.; de Roos, A.; et al. Preoperative Thresholds for Pulmonary Valve Replacement in Patients With Corrected Tetralogy of Fallot Using Cardiovascular Magnetic Resonance. *Circulation* **2007**, *116*, 545–551, doi:10.1161/CIRCULATIONAHA.106.659664.

133. Chalard, A.; Sanchez, I.; Gouton, M.; Henaine, R.; Salami, F.A.; Ninet, J.; Douek, P.C.; Di Filippo, S.; Boussel, L. Effect of Pulmonary Valve Replacement on Left Ventricular Function in Patients With Tetralogy of Fallot. *Am. J. Cardiol.* **2012**, *110*, 1828–1835, doi:10.1016/j.amjcard.2012.08.017.

134. Balasubramanian, S.; Harrild, D.M.; Kerur, B.; Marcus, E.; del Nido, P.; Geva, T.; Powell, A.J. Impact of surgical pulmonary valve replacement on ventricular strain and synchrony in patients with repaired tetralogy of Fallot: a cardiovascular magnetic resonance feature tracking study. *J. Cardiovasc. Magn. Reson.* **2018**, *20*, 37, doi:10.1186/s12968-018-0460-0.

135. DiLorenzo, M.P.; Elci, O.U.; Wang, Y.; Banerjee, A.; Sato, T.; Ky, B.; Goldmuntz, E.; Mercer-Rosa, L. Longitudinal Changes in Right Ventricular Function in Tetralogy of Fallot in the Initial Years after Surgical Repair. *J. Am. Soc. Echocardiogr.* **2018**, *31*, 816–821, doi:10.1016/j.echo.2018.02.013.

136. Hallbergson, A.; Gauvreau, K.; Powell, A.J.; Geva, T. Right Ventricular Remodeling After Pulmonary Valve Replacement: Early Gains, Late Losses. *Ann. Thorac. Surg.* **2015**, *99*, 660–666, doi:10.1016/j.athoracsur.2014.09.015.

137. Pieske, B.; Cuspidi, C.; Haßfeld, S.; Pieske-Kraigher, E.; Morris, D.A.; Baudisch, A.; Burkhardt, F.; Tadic, M.; Tschöpe, C. Right ventricular strain in heart failure: Clinical perspective. *Arch. Cardiovasc. Dis.* **2017**, *110*, 562–571, doi:10.1016/j.acvd.2017.05.002.

138. Stergiopoulos, K.; Bahrainy, S.; Strachan, P.; Kort, S. Right ventricular strain rate predicts clinical outcomes in patients with acute pulmonary embolism. *Acute Card. Care* **2011**, *13*, 181–188, doi:10.3109/17482941.2011.606468.

139. Addetia, K.; Maffessanti, F.; Dugan, K.; Wilkinson, M.; Gomberg-Maitland, M.; Mor-Avi, V.; Lang, R.; Patel, A. RIGHT VENTRICULAR LONGITUDINAL STRAIN: A SUPERIOR MEASURE OF OUTCOMES IN PATIENTS WITH PULMONARY ARTERIAL HYPERTENSION. *J. Am. Coll. Cardiol.* **2015**, *65*, A1074, doi:10.1016/S0735-1097(15)61074-9.

140. Jing, L.; Wehner, G.J.; Suever, J.D.; Charnigo, R.J.; Alhadad, S.; Stearns, E.; Mojsejenko, D.; Haggerty, C.M.; Hickey, K.; Valente, A.M.; et al. Left and right ventricular dyssynchrony and strains from cardiovascular magnetic resonance feature tracking do not predict deterioration of ventricular function in patients with repaired tetralogy of Fallot. *J. Cardiovasc. Magn. Reson.* **2016**, *18*, 49, doi:10.1186/s12968-016-0268-8.

141. Bokma, J.P.; Winter, M.M.; Oosterhof, T.; Vliegen, H.W.; van Dijk, A.P.; Hazekamp, M.G.; Koolbergen, D.R.; Groenink, M.; Mulder, B.J.M.; Bouma, B.J. Severe tricuspid regurgitation is predictive for adverse events in tetralogy of Fallot. *Heart* **2015**, *101*, 794–799, doi:10.1136/heartjnl-2014-306919.

142. Cochet, H.; Iriart, X.; Allain-Nicolaï, A.; Camaioni, C.; Sridi, S.; Nivet, H.; Fournier, E.; Dinet, M.-L.; Jalal, Z.; Laurent, F.; et al. Focal scar and diffuse myocardial fibrosis are independent imaging markers in repaired tetralogy of Fallot. *Eur. Hear. J. - Cardiovasc. Imaging* **2019**, *20*, 990–1003, doi:10.1093/ehjci/jez068.

143. Timóteo, A.T.; Branco, L.M.; Rosa, S.A.; Ramos, R.; Agapito, A.F.; Sousa, L.; Galrinho, A.; Oliveira, J.A.; Oliveira, M.M.; Ferreira, R.C. Usefulness of right ventricular and right atrial two-dimensional speckle tracking strain to predict late arrhythmic events in adult patients with repaired Tetralogy of Fallot. *Rev. Port. Cardiol. (English Ed.* **2017**, *36*, 21–29, doi:10.1016/j.repce.2016.12.004.

144. Babu-Narayan, S. V.; Kilner, P.J.; Li, W.; Moon, J.C.; Goktekin, O.; Davlouros, P.A.; Khan, M.; Ho, S.Y.; Pennell, D.J.; Gatzoulis, M.A. Ventricular Fibrosis Suggested by Cardiovascular Magnetic Resonance in Adults With Repaired Tetralogy of Fallot and Its Relationship to Adverse Markers of Clinical Outcome. *Circulation* **2006**, *113*, 405–413, doi:10.1161/CIRCULATIONAHA.105.548727.

145. Haaf, P.; Garg, P.; Messroghli, D.R.; Broadbent, D.A.; Greenwood, J.P.; Plein, S. Cardiac T1 mapping and extracellular volume (ECV) in clinical practice: a comprehensive review. *J. Cardiovasc. Magn. Reson.* **2016**, *18*, 89, doi:10.1186/s12968-016-0308-4.

146. Storz, C.; Hetterich, H.; Lorbeer, R.; Heber, S.D.; Schafnitzel, A.; Patscheider, H.; Auweter, S.; Zitzelsberger, T.; Rathmann, W.; Nikolaou, K.; et al. Myocardial tissue characterization by contrast-enhanced cardiac magnetic resonance imaging in subjects with prediabetes, diabetes, and normal controls with preserved ejection fraction from the general population. *Eur. Heart J. Cardiovasc. Imaging* **2017**, doi:10.1093/ehjci/jex190.

147. Esposito, A.; Palmisano, A.; Antunes, S.; Colantoni, C.; Rancoita, P.M.V.; Vignale, D.; Baratto, F.; Della Bella, P.; Del Maschio, A.; De Cobelli, F. Assessment of Remote Myocardium Heterogeneity in Patients with Ventricular Tachycardia Using Texture Analysis of Late Iodine Enhancement (LIE) Cardiac Computed Tomography (cCT) Images. *Mol. Imaging Biol.* **2018**, *20*, 816–825, doi:10.1007/s11307-018-1175-1.

148. Sardanelli, F.; Schiaffino, S.; Zanardo, M.; Secchi, F.; Cannaò, P.M.; Ambrogi, F.; Di Leo, G. Point estimate and reference normality interval of MRI-derived myocardial extracellular volume in healthy subjects: a systematic review and meta-analysis. *Eur. Radiol.* **2019**, *29*, 6620–6633, doi:10.1007/s00330-019-06185-w.

149. Messroghli, D.R.; Moon, J.C.; Ferreira, V.M.; Grosse-Wortmann, L.; He, T.; Kellman, P.; Mascherbauer, J.; Nezafat, R.; Salerno, M.; Schelbert, E.B.; et al. Clinical recommendations for cardiovascular magnetic resonance mapping of T1, T2, T2 and extracellular volume: A

consensus statement by the Society for Cardiovascular Magnetic Resonance (SCMR) endorsed by the European Association for Cardiovascular Imagin. *J. Cardiovasc. Magn. Reson.* **2017**, *19*, 1–24, doi:10.1186/s12968-017-0389-8.

150. Nacif, M.S.; Kawel, N.; Lee, J.J.; Chen, X.; Yao, J.; Zavodni, A.; Sibley, C.T.; Lima, J.A.C.; Liu, S.; Bluemke, D.A. Interstitial myocardial fibrosis assessed as extracellular volume fraction with low-radiation-dose cardiac CT. *Radiology* **2012**, *264*, 876–883, doi:10.1148/radiol.12112458.

151. Kammerlander, A.A.; Marzluf, B.A.; Zotter-Tufaro, C.; Aschauer, S.; Duca, F.; Bachmann, A.; Knechtelsdorfer, K.; Wiesinger, M.; Pfaffenberger, S.; Greiser, A.; et al. T1 Mapping by CMR Imaging: From Histological Validation to Clinical Implication. *JACC Cardiovasc. Imaging* **2016**, *9*, 14–23, doi:10.1016/J.JCMG.2015.11.002.

152. Ewer, M.S.; Ewer, S.M. Cardiotoxicity of anticancer treatments. *Nat. Rev. Cardiol.* **2015**, *12*, 547–558, doi:10.1038/nrcardio.2015.65.

153. Allemani, C.; Weir, H.K.; Carreira, H.; Harewood, R.; Spika, D.; Wang, X.-S.; Bannon, F.; Ahn, J. V; Johnson, C.J.; Bonaventure, A.; et al. Global surveillance of cancer survival 1995–2009: analysis of individual data for 25 676 887 patients from 279 population-based registries in 67 countries (CONCORD-2). *Lancet* **2015**, *385*, 977–1010, doi:10.1016/S0140-6736(14)62038-9.

154. Chang, H.M.; Moudgil, R.; Scarabelli, T.; Okwuosa, T.M.; Yeh, E.T.H. Cardiovascular Complications of Cancer Therapy: Best Practices in Diagnosis, Prevention, and Management: Part 1. *J. Am. Coll. Cardiol.* **2017**, *70*, 2536–2551, doi:10.1016/j.jacc.2017.09.1096.

155. Schlitt, A.; Jordan, K.; Vordermark, D.; Schwamborn, J.; Langer, T.; Thomssen, C. Cardiotoxicity and oncological treatments. *Dtsch. Arztebl. Int.* **2014**, *111*, 161–8, doi:10.3238/arztebl.2014.0161.

156. Plana, J.C.; Galderisi, M.; Barac, A.; Ewer, M.S.; Ky, B.; Scherrer-Crosbie, M.; Ganame, J.; Sebag, I.A.; Agler, D.A.; Badano, L.P.; et al. Expert consensus for multimodality imaging evaluation of

adult patients during and after cancer therapy: A report from the American Society of Echocardiography and the European Association of Cardiovascular Imaging. *Eur. Heart J. Cardiovasc. Imaging* **2014**, *15*, 1063–1093, doi:10.1093/ehjci/jeu192.

157. Cheitlin, M.D.; Armstrong, W.F.; Aurigemma, G.P.; Beller, G.A.; Bierman, F.Z.; Davis, J.L.; Douglas, P.S.; Faxon, D.P.; Gillam, L.D.; Kimball, T.R.; et al. ACC/AHA/ASE 2003 guideline update for the clinical application of echocardiography: Summary article: A report of the American College of Cardiology/American Heart Association Task Force on Practice Guidelines (ACC/AHA/ASE Committee to Update the 1997 Guid. *Circulation* 2003, *108*, 1146–1162.

158. Klocke, F.J.; Baird, M.G.; Lorell, B.H.; Bateman, T.M.; Messer, J. V.; Berman, D.S.; Gara, P.T.O.; Carabello, B.A.; Russell, R.O.; Cerqueira, M.D.; et al. ACC/AHA/ASNC Guidelines for the Clinical Use of Cardiac Radionuclide Imaging — Full text. *J. Am. Coll. Cardiol.* **2003**, *42*, 1318–1333, doi:10.1016/S0735-1097(03)01090-8.

159. Khouri, M.G.; Klein, M.R.; Velazquez, E.J.; Jones, L.W. Current and emerging modalities for detection of cardiotoxicity in cardio-oncology. *Future Cardiol.* **2015**, *11*, 471–484, doi:10.2217/fca.15.16.

160. Bandula, S.; White, S.K.; Flett, A.S.; Lawrence, D.; Pugliese, F.; Ashworth, M.T.; Punwani, S.; Taylor, S.A.; Moon, J.C. Measurement of myocardial extracellular volume fraction by using equilibrium contrast-enhanced CT: validation against histologic findings. *Radiology* **2013**, *269*, 396–403, doi:10.1148/radiol.13130130.

161. Diao, K.; Yang, Z.; Xu, H.; Liu, X.; Zhang, Q.; Shi, K.; Jiang, L.; Xie, L.; Wen, L.; Guo, Y. Histologic validation of myocardial fibrosis measured by T1 mapping: a systematic review and meta-analysis. *J. Cardiovasc. Magn. Reson.* **2017**, *18*, 92, doi:10.1186/s12968-016-0313-7.

162. Moher, D.; Liberati, A.; Tetzlaff, J.; Altman, D.G.; PRISMA Group Preferred Reporting Items for Systematic Reviews and Meta-Analyses: The PRISMA Statement. *PLoS Med.* **2009**, *6*,

e1000097, doi:10.1371/journal.pmed.1000097.

163. Neilan, T.G.; Coelho-Filho, O.R.; Shah, R. V.; Feng, J.H.; Pena-Herrera, D.; Mandry, D.; Pierre-Mongeon, F.; Heydari, B.; Francis, S.A.; Moslehi, J.; et al. Myocardial extracellular volume by cardiac magnetic resonance imaging in patients treated with anthracycline-based chemotherapy. *Am. J. Cardiol.* **2013**, *111*, 717–722, doi:10.1016/j.amjcard.2012.11.022.

164. Tham, E.B.; Haykowsky, M.J.; Chow, K.; Spavor, M.; Kaneko, S.; Khoo, N.S.; Pagano, J.J.; Mackie, A.S.; Thompson, R.B. Diffuse myocardial fibrosis by T1-mapping in children with subclinical anthracycline cardiotoxicity: Relationship to exercise capacity, cumulative dose and remodeling. *J. Cardiovasc. Magn. Reson.* **2013**, *15*, 1–11, doi:10.1186/1532-429X-15-48.

165. Harries, I.; Biglino, G.; Baritussio, A.; De Garate, E.; Dastidar, A.; Plana, J.C.; Bucciarelli-Ducci, C. Long term cardiovascular magnetic resonance phenotyping of anthracycline cardiomyopathy. *Int. J. Cardiol.* **2019**, *292*, 248–252, doi:10.1016/j.ijcard.2019.04.026.

166. Jordan, J.H.; Vasu, S.; Morgan, T.M.; D'Agostino, R.B.; Meléndez, G.C.; Hamilton, C.A.; Arai, A.E.; Liu, S.; Liu, C.-Y.; Lima, J.A.C.; et al. Anthracycline-associated T1 mapping characteristics are elevated independent of the presence of cardiovascular comorbidities in cancer survivors. *Circ. Cardiovasc. Imaging* **2016**, *9*, e004325, doi:10.1161/CIRCIMAGING.115.004325.

167. Heck, S.L.; Gulati, G.; Hoffmann, P.; Von Knobelsdorff-Brenkenhoff, F.; Storås, T.H.; Ree, A.H.; Gravdehaug, B.; Røsjø, H.; Steine, K.; Geisler, J.; et al. Effect of candesartan and metoprolol on myocardial tissue composition during anthracycline treatment: The PRADA trial. *Eur. Heart J. Cardiovasc. Imaging* **2018**, *19*, 544–552, doi:10.1093/ehjci/jex159.

168. Ferreira de Souza, T.; Quinaglia A.C. Silva, T.; Osorio Costa, F.; Shah, R.; Neilan, T.G.; Velloso, L.; Nadruz, W.; Brenelli, F.; Sposito, A.C.; Matos-Souza, J.R.; et al. Anthracycline Therapy Is Associated With Cardiomyocyte Atrophy and Preclinical Manifestations of Heart Disease. *JACC Cardiovasc. Imaging* **2018**, *11*, 1045–1055, doi:10.1016/j.jcmg.2018.05.012.

169. Heitner, S.B.; Minnier, J.; Naher, A.; Van Woerkom, R.C.; Ritts, A.; Ferencik, M.; Broberg, C.;

Medvedova, E.; Silbermann, R.; Scott, E.C. Bortezomib-based Chemotherapy for Multiple Myeloma Patients Without Comorbid Cardiovascular Disease Shows No Cardiotoxicity. *Clin. Lymphoma, Myeloma Leuk.* **2018**, *18*, 796–802, doi:10.1016/j.clml.2018.08.004.

170. Kimball, A.; Patil, S.; Koczwara, B.; Raman, K.S.; Perry, R.; Grover, S.; Selvanayagam, J. Late characterisation of cardiac effects following anthracycline and trastuzumab treatment in breast cancer patients. *Int. J. Cardiol.* **2018**, *261*, 159–161, doi:10.1016/j.ijcard.2018.03.025.

171. Muehlberg, F.; Funk, S.; Zange, L.; Knobelsdorff-Brenkenhoff, F. von; Blaszczyk, E.; Schulz, A.; Ghani, S.; Reichardt, A.; Reichardt, P.; Schulz-Menger, J. Native myocardial T1 time can predict development of subsequent anthracycline-induced cardiomyopathy. *ESC Hear. Fail.* **2018**, *5*, 620–629, doi:10.1002/ehf2.12277.

172. Takagi, H.; Ota, H.; Umezawa, R.; Kimura, T.; Kadoya, N.; Higuchi, S.; Sun, W.; Nakajima, Y.; Saito, M.; Komori, Y.; et al. Left ventricular T1 mapping during chemotherapy-radiation therapy: Serial assessment of participants with esophageal cancer. *Radiology* **2018**, *289*, 347–354, doi:10.1148/radiol.2018172076.

173. Haslbauer, J.D.; Lindner, S.; Valbuena-Lopez, S.; Zainal, H.; Zhou, H.; D'Angelo, T.; Pathan, F.; Arendt, C.A.; Bug, G.; Serve, H.; et al. CMR imaging biosignature of cardiac involvement due to cancer-related treatment by T1 and T2 mapping. *Int. J. Cardiol.* **2019**, *275*, 179–186, doi:10.1016/j.ijcard.2018.10.023.

174. de Roos, A. Onco-Cardiology: Value of Cardiac Imaging by Using CT and MRI after Radiation Therapy. *Radiology* **2018**, *289*, 355–356, doi:10.1148/radiol.2018181039.

175. Ewer, S.M. Guest Editorial: Is Cardio-oncology Ready for Algorithms? *Eur. Cardiol. Rev.* **2018**, *13*, 62, doi:10.15420/ecr.2018.13.1.GE2.

176. Cardinale, D.; Colombo, A.; Bacchiani, G.; Tedeschi, I.; Meroni, C.A.; Veglia, F.; Civelli, M.; Lamantia, G.; Colombo, N.; Curigliano, G.; et al. Early detection of anthracycline cardiotoxicity and improvement with heart failure therapy. *Circulation* **2015**, *131*, 1981–1988,

doi:10.1161/CIRCULATIONAHA.114.013777.

177. Cardinale, D. Prognostic Value of Troponin I in Cardiac Risk Stratification of Cancer Patients Undergoing High-Dose Chemotherapy. *Circulation* **2004**, *109*, 2749–2754, doi:10.1161/01.CIR.0000130926.51766.CC.

178. Morris, P.G.; Chen, C.; Steingart, R.; Fleisher, M.; Lin, N.; Moy, B.; Come, S.; Sugarman, S.; Abbruzzi, A.; Lehman, R.; et al. Troponin I and C-Reactive Protein Are Commonly Detected in Patients with Breast Cancer Treated with Dose-Dense Chemotherapy Incorporating Trastuzumab and Lapatinib. *Clin. Cancer Res.* **2011**, *17*, 3490–3499, doi:10.1158/1078-0432.CCR-10-1359.

179. D'Errico, M.P.; Grimaldi, L.; Petruzzelli, M.F.; Gianicolo, E.A.L.; Tramacere, F.; Monetti, A.; Placella, R.; Pili, G.; Andreassi, M.G.; Sicari, R.; et al. N-Terminal Pro-B–Type Natriuretic Peptide Plasma Levels as a Potential Biomarker for Cardiac Damage After Radiotherapy in Patients With Left-Sided Breast Cancer. *Int. J. Radiat. Oncol.* **2012**, *82*, e239–e246, doi:10.1016/j.ijrobp.2011.03.058.

180. Ky, B.; Putt, M.; Sawaya, H.; French, B.; Januzzi, J.L.; Sebag, I.A.; Plana, J.C.; Cohen, V.; Banchs, J.; Carver, J.R.; et al. Early Increases in Multiple Biomarkers Predict Subsequent Cardiotoxicity in Patients With Breast Cancer Treated With Doxorubicin, Taxanes, and Trastuzumab. *J. Am. Coll. Cardiol.* **2014**, *63*, 809–816, doi:10.1016/j.jacc.2013.10.061.

181. Henriksen, P.A. Anthracycline cardiotoxicity: an update on mechanisms, monitoring and prevention. *Heart* **2018**, *104*, 971–977, doi:10.1136/heartjnl-2017-312103.

182. Moon, J.C.; Messroghli, D.R.; Kellman, P.; Piechnik, S.K.; Robson, M.D.; Ugander, M.; Gatehouse, P.D.; Arai, A.E.; Friedrich, M.G.; Neubauer, S.; et al. Myocardial T1 mapping and extracellular volume quantification: a Society for Cardiovascular Magnetic Resonance (SCMR) and CMR Working Group of the European Society of Cardiology consensus statement. *J. Cardiovasc. Magn. Reson.* **2013**, *15*, 92, doi:10.1186/1532-429X-15-92.

183. Gottbrecht, M.; Kramer, C.M.; Salerno, M. Native T1 and Extracellular Volume Measurements by Cardiac MRI in Healthy Adults: A Meta-Analysis. *Radiology* **2019**, *290*, 317–326, doi:10.1148/radiol.2018180226.

184. Lenihan, D.J.; Stevens, P.L.; Massey, M.; Plana, J.C.; Araujo, D.M.; Fanale, M.A.; Fayad, L.E.; Fisch, M.J.; Yeh, E.T.H. The Utility of Point-of-Care Biomarkers to Detect Cardiotoxicity During Anthracycline Chemotherapy: A Feasibility Study. *J. Card. Fail.* **2016**, *22*, 433–438, doi:10.1016/j.cardfail.2016.04.003.

185. Jellis, C.L.; Kwon, D.H. Myocardial T1 mapping: modalities and clinical applications. *Cardiovasc. Diagn. Ther.* **2014**, *4*, 126–37, doi:10.3978/j.issn.2223-3652.2013.09.03.

186. Martinez-Naharro, A.; Kotecha, T.; Norrington, K.; Boldrini, M.; Rezk, T.; Quarta, C.; Treibel, T.A.; Whelan, C.J.; Knight, D.S.; Kellman, P.; et al. Native T1 and Extracellular Volume in Transthyretin Amyloidosis. *JACC Cardiovasc. Imaging* **2019**, *12*, 810–819, doi:10.1016/j.jcmg.2018.02.006.

187. Goetz, M.P.; Gradishar, W.J.; Anderson, B.O.; Abraham, J.; Aft, R.; Allison, K.H.; Blair, S.L.; Burstein, H.J.; Dang, C.; Elias, A.D.; et al. Breast Cancer, Version 3.2018. *J. Natl. Compr. Cancer Netw.* **2019**, *17*, 118–126, doi:10.6004/jnccn.2019.0009.

188. Ferlay, J.; Colombet, M.; Soerjomataram, I.; Dyba, T.; Randi, G.; Bettio, M.; Gavin, A.; Visser, O.; Bray, F. Cancer incidence and mortality patterns in Europe: Estimates for 40 countries and 25 major cancers in 2018. *Eur. J. Cancer* **2018**, *103*, 356–387, doi:10.1016/j.ejca.2018.07.005.

189. DeSantis, C.; Ma, J.; Bryan, L.; Jemal, A. Breast cancer statistics, 2013. *CA. Cancer J. Clin.* **2014**, *64*, 52–62, doi:10.3322/caac.21203.

190. MacKenzie, J.R. Complications of treatment of paediatric malignancies. *Eur. J. Radiol.* **2001**, *37*, 109–119, doi:10.1016/S0720-048X(00)00292-8.

191. Ryberg, M.; Nielsen, D.; Cortese, G.; Nielsen, G.; Skovsgaard, T.; Andersen, P.K. New insight into epirubicin cardiac toxicity: Competing risks analysis of 1097 breast cancer patients. *J. Natl.*

Cancer Inst. **2008**, *100*, 1058–1067, doi:10.1093/jnci/djn206.

192. Farhad, H.; Staziaki, P. V.; Addison, D.; Coelho-Filho, O.R.; Shah, R. V.; Mitchell, R.N.; Szilveszter, B.; Abbasi, S.A.; Kwong, R.Y.; Scherrer-Crosbie, M.; et al. Characterization of the changes in cardiac structure and function in mice treated with anthracyclines using serial cardiac magnetic resonance imaging. *Circ. Cardiovasc. Imaging* **2016**, *9*, e003584, doi:10.1161/CIRCIMAGING.115.003584.

193. Ades, F.; Zardavas, D.; Pinto, A.C.; Criscitiello, C.; Aftimos, P.; de Azambuja, E. Cardiotoxicity of systemic agents used in breast cancer. *The Breast* **2014**, *23*, 317–328, doi:10.1016/j.breast.2014.04.002.

194. Irwin, M.L.; Fabian, C.; McTiernan, A. Risk reduction from weight management and physical activity interventions. *Adv. Exp. Med. Biol.* **2015**, *862*, 193–212, doi:10.1007/978-3-319-16366-6_13.

195. Testore, F.; Milanese, S.; Ceste, M.; de Conciliis, E.; Parello, G.; Lanfranco, C.; Manfredi, R.; Ferrero, G.; Simoni, C.; Miglietta, L.; et al. Cardioprotective effect of dexrazoxane in patients with breast cancer treated with anthracyclines in adjuvant setting: a 10-year single institution experience. *Am. J. Cardiovasc. Drugs* **2008**, *8*, 257–263.

196. Schelbert, E.B.; Piehler, K.M.; Zareba, K.M.; Moon, J.C.; Ugander, M.; Messroghli, D.R.; Valeti, U.S.; Chang, C.C.H.; Shroff, S.G.; Diez, J.; et al. Myocardial fibrosis quantified by extracellular volume is associated with subsequent hospitalization for heart failure, death, or both across the spectrum of ejection fraction and heart failure stage. *J. Am. Heart Assoc.* **2015**, *4*, 1–14, doi:10.1161/JAHA.115.002613.

197. Miller, C.A.; Naish, J.H.; Bishop, P.; Coutts, G.; Clark, D.; Zhao, S.; Ray, S.G.; Yonan, N.; Williams, S.G.; Flett, A.S.; et al. Comprehensive validation of cardiovascular magnetic resonance techniques for the assessment of myocardial extracellular volume. *Circ. Cardiovasc. Imaging* **2013**, *6*, 373–383, doi:10.1161/CIRCIMAGING.112.000192.

198. Kuehl, H.; Veit, P.; Rosenbaum, S.J.; Bockisch, A.; Antoch, G. Can PET/CT replace separate diagnostic CT for cancer imaging? Optimizing CT protocols for imaging cancers of the chest and abdomen. *J. Nucl. Med.* **2007**, *48 Suppl 1*, 45S-57S.

199. Patnaik, J.L.; Byers, T.; DiGuiseppi, C.; Dabelea, D.; Denberg, T.D. Cardiovascular disease competes with breast cancer as the leading cause of death for older females diagnosed with breast cancer: a retrospective cohort study. *Breast Cancer Res.* **2011**, *13*, R64, doi:10.1186/bcr2901.

200. Taylor, C.; McGale, P.; Brønnum, D.; Correa, C.; Cutter, D.; Duane, F.K.; Gigante, B.; Jensen, M.-B.; Lorenzen, E.; Rahimi, K.; et al. Cardiac structure injury after radiotherapy for breast cancer: cross-sectional study with individual patient data. *J. Clin. Oncol.* **2018**, *36*, 2288–2296, doi:10.1200/JCO.2017.77.6351.

201. Chatterjee, K.; Zhang, J.; Honbo, N.; Karliner, J.S. Doxorubicin cardiomyopathy. *Cardiology* **2010**, *115*, 155–162, doi:10.1159/000265166.

202. Koo, T.K.; Li, M.Y. A guideline of selecting and reporting intraclass correlation coefficients for reliability research. *J. Chiropr. Med.* **2016**, *15*, 155–163, doi:10.1016/j.jcm.2016.02.012.

203. Evans, J. *Straightforward statistics for behavioral sciences*; Brooks/Cole Publishing: Pacific Grove, California, 1996; ISBN 0534231004 9780534231002.

204. Perez, I.E.; Taveras Alam, S.; Hernandez, G.A.; Sancassani, R. Cancer Therapy-Related Cardiac Dysfunction: An Overview for the Clinician. *Clin. Med. Insights Cardiol.* **2019**, *13*, 117954681986644, doi:10.1177/1179546819866445.

205. Song, Q.-K.; Li, J.; Huang, R.; Fan, J.-H.; Zheng, R.-S.; Zhang, B.-N.; Zhang, B.; Tang, Z.-H.; Xie, X.-M.; Yang, H.-J.; et al. Age of diagnosis of breast cancer in china: almost 10 years earlier than in the United States and the European union. *Asian Pac. J. Cancer Prev.* **2014**, *15*, 10021–10025.

206. Purushotham, A.; Shamil, E.; Cariati, M.; Agbaje, O.; Muhidin, A.; Gillett, C.; Mera, A.; Sivanadiyan, K.; Harries, M.; Sullivan, R.; et al. Age at diagnosis and distant metastasis in breast

cancer – A surprising inverse relationship. *Eur. J. Cancer* **2014**, *50*, 1697–1705, doi:10.1016/j.ejca.2014.04.002.

207. Kurita, Y.; Kitagawa, K.; Kurobe, Y.; Nakamori, S.; Nakajima, H.; Dohi, K.; Ito, M.; Sakuma, H. Estimation of myocardial extracellular volume fraction with cardiac CT in subjects without clinical coronary artery disease: a feasibility study. *J. Cardiovasc. Comput. Tomogr.* **2016**, *10*, 237–241, doi:10.1016/j.jcct.2016.02.001.

208. van Dalen, E.C.; Michiels, E.M.; Caron, H.N.; Kremer, L.C. Different anthracycline derivates for reducing cardiotoxicity in cancer patients. In *Cochrane Database of Systematic Reviews*; van Dalen, E.C., Ed.; John Wiley & Sons, Ltd: Chichester, UK, UK, 2010.

209. Ewer, M.S.; Lippman, S.M. Type II chemotherapy-related cardiac dysfunction: Time to recognize a new entity. *J. Clin. Oncol.* 2005, *23*, 2900–2902.

210. Lotrionte, M.; Biondi-Zoccai, G.; Abbate, A.; Lanzetta, G.; D'Ascenzo, F.; Malavasi, V.; Peruzzi, M.; Frati, G.; Palazzoni, G. Review and meta-analysis of incidence and clinical predictors of anthracycline cardiotoxicity. *Am. J. Cardiol.* **2013**, *112*, 1980–1984, doi:10.1016/j.amjcard.2013.08.026.

211. Bulten, B.F.; Verberne, H.J.; Bellersen, L.; Oyen, W.J.G.; Sabaté-Llobera, A.; Mavinkurve-Groothuis, A.M.C.; Kapusta, L.; van Laarhoven, H.W.M.; de Geus-Oei, L.-F. Relationship of promising methods in the detection of anthracycline-induced cardiotoxicity in breast cancer patients. *Cancer Chemother. Pharmacol.* **2015**, *76*, 957–967, doi:10.1007/s00280-015-2874-9.

212. Treibel, T.A.; Bandula, S.; Fontana, M.; White, S.K.; Gilbertson, J.A.; Herrey, A.S.; Gillmore, J.D.; Punwani, S.; Hawkins, P.N.; Taylor, S.A.; et al. Extracellular volume quantification by dynamic equilibrium cardiac computed tomography in cardiac amyloidosis. *J. Cardiovasc. Comput. Tomogr.* **2015**, *9*, 585–592, doi:10.1016/j.jcct.2015.07.001.

213. Hamdy, A.; Kitagawa, K.; Goto, Y.; Yamada, A.; Nakamura, S.; Takafuji, M.; Nagasawa, N.;

Sakuma, H. Comparison of the different imaging time points in delayed phase cardiac CT for myocardial scar assessment and extracellular volume fraction estimation in patients with old myocardial infarction. *Int. J. Cardiovasc. Imaging* **2019**, *35*, 917–926, doi:10.1007/s10554-018-1513-z.

214. Reiter, U.; Reiter, C.; Kräuter, C.; Fuchsjäger, M.; Reiter, G. Cardiac magnetic resonance T1 mapping. Part 2: Diagnostic potential and applications. *Eur. J. Radiol.* **2018**, *109*, 235–247, doi:10.1016/j.ejrad.2018.10.013.

215. McDonald, R.J.; McDonald, J.S.; Kallmes, D.F.; Jentoft, M.E.; Murray, D.L.; Thielen, K.R.; Williamson, E.E.; Eckel, L.J. Intracranial gadolinium deposition after contrast-enhanced MR imaging. *Radiology* **2015**, *275*, 772–782, doi:10.1148/radiol.15150025.

216. Kanal, K.M.; Butler, P.F.; Sengupta, D.; Bhargavan-Chatfield, M.; Coombs, L.P.; Morin, R.L. U.S. Diagnostic Reference Levels and Achievable Doses for 10 Adult CT Examinations. *Radiology* **2017**, *284*, 120–133, doi:10.1148/radiol.2017161911.

217. Cardiac computed tomography (CT) - FAQs for health professionals | IAEA Available online: https://www.iaea.org/resources/rpop/health-professionals/radiology/computed-tomography/cardiac-computed-tomography (accessed on Dec 23, 2019).

218. Thirup, P. Haematocrit. *Sport. Med.* **2003**, *33*, 231–243, doi:10.2165/00007256-200333030-00005.

219. Chen, L.; Linden, H.M.; Anderson, B.O.; Li, C.I. Trends in 5-year survival rates among breast cancer patients by hormone receptor status and stage. *Breast Cancer Res. Treat.* **2014**, *147*, 609–616, doi:10.1007/s10549-014-3112-6.

220. Monti, C.B.; Codari, M.; van Assen, M.; De Cecco, C.N.; Vliegenthart, R. Machine Learning and Deep Neural Networks Applications in Computed Tomography for Coronary Artery Disease and Myocardial Perfusion. *J. Thorac. Imaging* **2020**, *35*, S58–S65, doi:10.1097/RTI.0000000000000490.

221. Hosny, A.; Parmar, C.; Quackenbush, J.; Schwartz, L.H.; Aerts, H.J.W.L. Artificial intelligence in radiology. *Nat. Rev. Cancer* **2018**, *18*, 500–510, doi:10.1038/s41568-018-0016-5.

PUBLICATIONS

1. Petrini M, Chessa M, Monti CB, Alì M, Cannaò PM, Di Leo G, Sardanelli F, Secchi F. Pulmonary insufficiency: advantage of pulmonary regurgitation volume versus pulmonary regurgitation fraction in a congenital heart disease mixed population. To: *Journal of Thoracic Imaging*
2. Zanardo M, Cozzi A, Trimboli RM, Labaj O, Monti CB, Schiaffino S, Carbonaro LA, Sardanelli F. Technique, protocols and adverse reactions for contrast-enhanced spectral mammography (CESM): a systematic review. Insights into Imaging. 2019.
3. Gallone G, Palmisano A, Baldetti L, Monti CB, Ponticelli F, Tzanis G, Colombo A, Esposito A, Giannini F. Improved myocardial function with coronary sinus Reducer in a patient with refractory angina and heart failure with reduced ejection fraction. Can J Cardiol. 2019.
4. Monti CB, Codari M, De Cecco CN, Secchi F, Sardanelli F, Stillman AE. Novel Imaging Biomarkers: Epicardial Adipose Tissue Evaluation. Br J Radiol. 2019.
5. Alì M, Monti CB, Gold B, Lastella G, Papa S, Sardanelli F, Secchi F. Open 1.0-T versus closed 1.5-T CMR: Image quality assessment. Clin Imaging. 2020.
6. Monti CB, Zanardo M, Bosetti T, Alì M, De Benedictis E, Luporini A, Secchi F, Sardanelli F. Assessment of myocardial extracellular volume on body computed tomography in breast cancer patients treated with anthracyclines. Quant Imaging Med Surg. 2020.
7. Secchi F, Alì M, Monti CB, Greiser A, Pluchinotta FR, Carminati M, Sardanelli F. Right and left ventricle native T1 mapping in systolic phase in patients with congenital heart disease. Acta Radiol. 2020.
8. Monti CB, Alì M, Capra D, Wiedenmann F, Lastella G, Secchi F, Sardanelli F. Ultrasound semiautomatic versus manual estimation of carotid intima-media thickness: reproducibility and cardiovascular risk stratification. Med Ultrason. 2020.

9. Zanardo M, Martini C, Monti CB, Cattaneo F, Ciaralli C, Cornacchione P, Durante S. Management of patients with suspected or confirmed COVID-19, in the radiology department. Radiography (Lond). 2020.

10. Gadiyaram VK, Monti CB, Sahu A, Filev PD, Muscogiuri G, Secchi F, Sardanelli F, Stillman AE, De Cecco CN. Repaired Congenital Heart Disease in Older Children and Adults: Up-to-Date Practical Assessment and Characteristic Imaging Findings. Radiol Clin North Am. 2020.

11. Alì M, Monti CB, Melazzini L, Cardani R, Fossati B, Cavalli M, Chow K, Secchi F, Meola G, Sardanelli F. Rare Disease: Cardiac Risk Assessment with MRI in Patients with Myotonic Dystrophy Type 1. Front Neurol. 2020.

12. Monti CB, Codari M, Cozzi A, Alì M, Saggiante L, Sardanelli F, Secchi F. Image quality of late gadolinium enhancement in cardiac magnetic resonance with different doses of contrast material in patients with chronic myocardial infarction. Eur Radiol Exp. 2020.

13. Monti CB, Codari M, van Assen M, De Cecco CN, Vliegenthart R. Machine Learning and Deep Neural Networks Applications in Computed Tomography for Coronary Artery Disease and Myocardial Perfusion. J Thorac Imaging. 2020.

14. De Cecco CN, Monti CB. Use of Early T1 Mapping for MRI in Acute Myocarditis. Radiology. 2020.

15. Palmisano A, Piccoli M, Monti CB, Canu T, Cirillo F, Napolitano A, Perani L, Signorelli P, Vignale D, Anastasia L, Esposito A. Single-shot morpho-functional and structural characterization of the left-ventricle in a mouse model of acute ischemia-reperfusion injury with an optimized 3D IntraGate cine FLASH sequence at 7T MR. Magn Reson Imaging. 2020.

16. Alì M, Monti CB, Secchi F, Spairani R, Speciani M, Di Leo G, Sardanelli F. Fast thoracic MRI as an alternative to chest x-ray: A retrospective evaluation of 287 patients. Clin Imaging. 2020.

17. Randelli F, Nocerino EA, Nicosia L, Alì M, Monti CB, Sardanelli F, Aliprandi A. Image quality of hip MR arthrography with intra-articular injection of hyaluronic acid versus gadolinium-based contrast agent in patients with femoroacetabular impingement. Skeletal Radiol. 2020.

18. Zanardo M, Sardanelli F, Rainford L, Monti CB, Murray JG, Secchi F, Cradock A. Technique and protocols for cardiothoracic time-resolved contrast-enhanced magnetic resonance angiography sequences: a systematic review. Clin Radiol. 2020

19. Monti CB, Secchi F, Capra D, Guarnieri G, Lastella G, Barbaro U, Carminati M, Sardanelli F. Right ventricular strain in repaired Tetralogy of Fallot with regards to pulmonary valve replacement. Eur J Radiol. 2020.

20. Spagnolo P, Giglio M, Di Marco D, Cannaò PM, Agricola E, Dell Bella PE, Monti CB, Sardanelli F. Diagnosis of left atrial appendage thrombus in patients with atrial fibrillation: delayed contrast-enhanced cardiac CT. Eur Radiol. 2020.

21. Secchi F, Monti CB, Alì M, Carbone FS, Cannaò PM, Sardanelli F. Diagnostic value of global cardiac strain in patients with myocarditis. J Comput Assist Tomogr. 2020.

Papers under revision

1. Monti CB, Zanardo M, Cozzi A, Schiaffino S, Spagnolo P, Secchi F, De Cecco CN, Sardanelli F. Dual-energy CT performance in acute pulmonary embolism: a meta-analysis.

2. Monti CB, van Assen M, Stillman AE, Lee SJ, Hoelzer P, Fung GSK, Secchi F, Sardanelli F, De Cecco CN. Convolutional neural network algorithm for automatic thoracic aorta sizing: performance testing in a heterogeneous population with multivendor CT datasets.

3. Secchi F, Monti CB, Asteria C, Malavazos A, Capra D, Alì M, Giassi C, Francesconi S, Giovannelli A, Morricone L, Sardanelli F. Quantification of epicardial adipose tissue in obese patients using an open-bore MRI scanner.

4. Secchi F, Lastella G, Monti CB, Barbaro U, Capra D, Zanardo M, Sardanelli F. Late gadolinium enhancement in patients with Tetralogy of Fallot: a systematic review.

5. Castiglioni I, Ippolito D, Interlenghi M, Monti CB, Salvatore C, Schiaffino S, Polidori A, Gandola D, Messa C, Sardanelli F. Artificial intelligence applied on chest x-ray can aid in the diagnosis of COVID-19: a first experience from Lombardy, Italy.

6. Trimboli RM, Codari M, Cozzi A, Monti CB, Capra D, Nenna C, Spinelli D, Di Leo G, Baselli G, Sardanelli F. Semiquantitative score of breast arterial calcifications on mammography (BAC-SS): intra- and inter-reader reproducibility.

7. Salvatore C, Interlenghi M, Monti CB, Ippolito D, Capra D, Schiaffino S, Polidori A, Gandola D, Castiglioni I, Messa C, Sardanelli F. Artificial intelligence applied to chest x-ray for differential diagnosis of COVID-19 pneumonia.

OTHER PhD ACTIVITIES

Conference abstracts

1. Monti CB, Alì M, Secchi F, Carbone FS, Cannaò PM, Sardanelli F. Ruolo diagnostico dei parametri di strain cardiaco in pazienti con miocardite. Convegno nazionale sezione cardioradiologia SIRM. December 14–15, Rome
2. Monti CB, Alì M, Secchi F, Carbone FS, Cannaò PM, Sardanelli F. strain. Diagnostic value of global cardiac strain in patients with myocarditis. ECR 2018 European Congress of Radiology, February 28–March 4, 2018, Vienna, Austria
3. Monti CB, Alì M, Secchi F, Carbone FS, Cannaò PM, Sardanelli F. strain. Diagnostic value of global cardiac strain in patients with myocarditis. San Raffaele Scientific Retreat, March 16–18, 2018, Baveno, Italy
4. Monti CB, Alì M, Secchi F, Carbone FS, Cannaò PM, Sardanelli F. Ruolo diagnostico dei parametri di strain cardiaco in pazienti con miocardite. ISMRM Italian Chapter, May 10–11, 2018, Padova, Italy
5. Monti CB, Zanardo M, Schiaffino S, Di Leo G, Secchi F, Sardanelli F. Myocardial CT-derived Extracellular Volume (ECV): A Systematic Review and Meta-analysis. ESTI/ESCR 2018 Joint Meeting of ESTI and ESCR, May 24–26, 2018, Geneva, Switzerland
6. Monti CB, Secchi F, Petrini M, Alì M, Ziouziou A, Sardanelli F. Volume rigurgitante polmonare versus frazione rigurgitante polmonare nelle cardiopatie congenite. 48° Congresso Nazionale della Società Italiana di Radiologia Medica (SIRM). October 8–11 2018, Genova
7. Monti CB, Secchi F, Alì M, Carbone FS, Sardanelli F. Ruolo diagnostico dello strain globale nella miocardite. 48° Congresso Nazionale della Società Italiana di Radiologia Medica (SIRM). October 8–11 2018, Genova

8. Monti CB, Secchi F, Alì M, Carbone FS, Sardanelli F. Diagnostic Value of Global Cardiac Strain in Patients with Myocarditis. RSNA 2018, 104th annual meeting of the Radiological Society of North America. November 25–30 2018, Chicago
9. Monti CB, Palmisano A, Piccoli M, Canu T, Signorelli P, Perani L, Anastasia L, Esposito A. Comprehensive morpho-functional and structural characterization of the left ventricle in a mouse model of acute ischemia/reperfusion injury with a single CMR 3D flash intragate cine sequence. San Raffaele Scientific Retreat. March 14–16 2019, Baveno
10. Monti CB, Secchi F, Saggiante L, Alì M, Sardanelli F. Late gadolinium enhancement in cardiac magnetic resonance with different doses of contrast material in patients with chronic myocardial infarction. ISMRM Italian Chapter. March 28–29 2019, Milano
11. Monti CB, Saggiante L, Alì M, Cozzi A, Codari M, Sardanelli F, Secchi F. Image quality of late gadolinium enhancement in cardiac magnetic resonance with different doses of contrast material in patients with chronic myocardial infarction. ESCR 2019. October 24–26 2019, Antwerp
12. Monti CB, Zanardo M, Bosetti T, Alì M, De Benedictis E, Luporini A, Sardanelli F, Secchi F. Assessment of myocardial extracellular volume on routine body computed tomography in breast cancer patients treated with anthracyclines. RSNA 2019, 105th annual meeting of the Radiological Society of North America. December 1–6 2019, Chicago
13. Monti CB, Secchi F, Capra D, Guarnieri G, Lastella G, Barbaro U, Carminati M, Sardanelli F. Right ventricular strain variations in repaired Tetralogy of Fallot patients with regards to pulmonary valve replacement. ESCR 2020. October 15–16 2020. Online edition.

PhD fellowship

Emory University - Department of Radiology, Division of Cardiothoracic Imaging

Supervisor: Prof. Carlo De Cecco

May 2019 - December 2019

Reviewer activities

1. European Radiology Experimental
2. European Journal of Radiology
3. Journal of Cardiovascular Computed Tomography
4. Journal of Magnetic Resonance Imaging
5. International Journal of Cardiovascular Imaging
6. The British Journal of Radiology

Learning activities

1. Preclinical and Clinical High-Resolution Ultrasound and PhotoAcoustic Workshop, April 10, 2018, Ospedale San Raffaele, Milano
2. Right Ventricular Strain Analysis Webinar, June 14, 2018
3. HIPAA and Research - Online, Emory University, May 09, 2019
4. HIPAA Security - Online, Emory University, May 09, 2019
5. HIPAA@Emory - Online, Emory University, May 09, 2019
6. Responsible Conduct of Research - Human Subject Research Track, CITI, Emory University, May 21, 2019
7. Basic/Refresher Course Human Subjects Projection - Biomedical Focus, CITI, Emory University, May 21, 2019

Transferable skills

1. Open access-open data and publication. Università degli Studi di Milano. Duration: 4 hours.
2. Research evaluation: bibliometrics and peer-review. Università degli Studi di Milano. Duration: 4 hours.
3. Research integrity: biomedical sciences. Epigeum Online Course System. Duration: 6 hours.
4. Experimental design: the good, the bad and the ugly. University of Oxford. Duration: 8 hours.

5. Protecting and enhancing the value of research results on market. Università degli Studi di Milano. Duration: 4 hours
6. Communication on new media, part 1 and part 2. Università degli Studi di Milano (Microsoft Teams). Duration: 4 hours.
7. Value enhancement through business creation. Università degli Studi di Milano (Microsoft Teams). Duration: 4 hours.
8. CV writing and recruitment techniques. Università degli Studi di Milano (Microsoft Teams). Duration: 6.30 hours.
9. Sustainability and Innovation. Università degli Studi di Milano (Microsoft Teams). Duration: 3 hours.
10. Data protection and scientific research activity. Università degli Studi di Milano (Microsoft Teams). Duration: 3 hours.

PhD Courses

1. Poster e presentazioni orali: come presentare i vostri risultati in modo efficace e accattivante
2. Strumenti di base per la ricerca: tecniche e metodi matematico/statistici, e loro programmazione
3. Fondamentali tecniche e metodi matematico/statistici e loro programmazione informatica
4. Anatomia sistematica, topografica e funzionale della testa nell'uomo
5. Cellule staminali pluripotenti indotte come modello di malattia e applicazione di terapia genica
6. Circa diem: dalle basi molecolari alle implicazioni della periodicità circadiana dei fenomeni biologici

Teaching activities

1. Elective: Radiologia in emergenza e urgenza. Bachelor's Degree in Medical Radiology Techniques for Imaging and Radiotherapy, Università degli Studi di Milano
2. Elective: Metodologia della ricerca per le professioni sanitarie. Master's degree in Technical and Diagnostic Healthcare Science, Università degli Studi di Milano
3. FASTER: Metodologia della ricerca clinica per tecnici sanitari di radiologia medica, Corso residenziale

Thesis tutoring

As Co-advisor:

1. Assessment of myocardial extracellular volume on routine body CT in breast cancer patients treated with anthracyclines (Tommaso Bosetti)
2. Epicardial adipose tissue on cardiac magnetic resonance and computed tomography: correlation with metabolic syndrome (Maria del Mar Galimberti Ortiz)
3. Feasibility of fractional flow reserve (FFR) derived from computed tomography angiography and comparison with invasive FFR (Alberto Senatieri)
4. Routine computed tomography-derived myocardial extracellular volume: a marker of cardiotoxicity in esophageal cancer patients undergoing radiotherapy (Davide Capra)
5. Epicardial adipose tissue, a novel biomarker for cardiovascular risk: CT pericoronary attenuation values with regards to coronary stenosis (Carlo Parietti)

Others:

1. Pulmonary regurgitation volume versus pulmonary regurgitation fraction in congenital heart disease (Asmaa Ziouziou)
2. Reproducibility of myocardial strain by cardiac magnetic resonance (Matteo Regazzetti)
3. Aortic annulus deformation and aortic valve calcifications in patients referred for transcatheter aortic valve implantation: a dynamic CT study (Luca Bonomo)

4. Late gadolinium enhancement in cardiac magnetic resonance with different doses of contrast material in patients with chronic myocardial infarction (Lorenzo Saggiante)
5. Ultrasound semiautomatic versus manual estimation of carotid intima-media thickness: reproducibility and cardiovascular risk stratification (Federico Wiedenmann)
6. Safe follow-up after endovascular aortic repair (EVAR) with non-contrast magnetic resonance imaging (NCMRI): the SAFEVAR study (Slobodan Raden)
7. Contrast-enhanced MR angiography in patients with congenital heart disease: image quality using two different doses of a contrast agent (Gaston Fabian Dellaferrera)
8. Biventricular cardiac strain in patients with Tetralogy of Fallot: a cardiac magnetic resonance study (Gianluca Guarnieri)
9. Diagnosis of left atrial appendage thrombus in patients with atrial fibrillation: delayed contrast-enhanced cardiac CT (Valeria Fagiani)
10. Comparison of different adipose tissues CT attenuation values among epicardial, paracardiac, and subcutaneous fat (Giorgia Florini)
11. Ventricular functional parameters assessed with compressed sensing CMR in patients with congenital heart diseases (Marco Gabriello)

LIST OF FIGURES

LIST OF TABLES